LARIAT PEPTIDE INHIBITORS OF ABL KINASE

A Thesis Submitted to the College of

Graduate Studies and Research

in Partial Fulfillment of the Requirements

for the Degree of Master of Science

in the Department of Biochemistry

University of Saskatchewan

Saskatoon

By

Bharathikumar Vellalore Maruthachalam

PERMISSION TO USE

In presenting this thesis in partial fulfillment of the requirements for a Postgraduate degree from the University of Saskatchewan, I agree that the Libraries of this University may make it freely available for inspection. I further agree that permission for copying of this thesis in any manner, in whole or in part, for scholarly purposes may be granted by the professor or professors who supervised my thesis work or, in their absence, by the Head of the Department or the Dean of the College in which my thesis work was done. It is understood that any copying or publication or use of this thesis or parts thereof for financial gain shall not be allowed without my written permission. It is also understood that due recognition shall be given to me and to the University of Saskatchewan in any scholarly use which may be made of any material in my thesis.

Requests for permission to copy or to make other use of material in this thesis in whole or part should be addressed to:

Head of the Department of Biochemistry
University of Saskatchewan
Saskatoon, Saskatchewan, S7N 5E5

ABSTRACT

A majority of kinase inhibitors predominantly occupy the highly conserved adenine-binding pocket located in the kinase catalytic cleft, and therefore the target selectivity of these molecules is a major concern. In order to design highly specific next-generation drugs, it is essential to exploit the less-conserved binding pockets, which lie adjacent to the adenine-binding pocket. Small peptides that can function as adenosine triphosphate (ATP) competitive inhibitors would prove useful in identifying and validating new druggable surfaces in the kinase catalytic cleft. These peptides, being larger than small molecules, have the potential to target the ATP binding pocket as well as surfaces that lie adjacent to this pocket. Such peptides recognizing novel binding pockets can assist the drug discovery process in several ways.

In this thesis, we describe the isolation and characterization of a novel class of cyclic peptides, referred to as lariats, against Abl kinase, a drug target important in chronic myeloid leukemia and other disorders. Using a yeast two-hybrid approach, we first isolated two related lariats, named A1 and A2, from a pool of five million lariats, which interact with the catalytic domain of Abl kinase. *In vitro* studies indicated that the synthetic A1 lariat competitively inhibits ATP binding by targeting the catalytic cleft that lies between the N- and C- lobes of the kinase catalytic domain. To obtain tighter-binding variants of the A1 lariat, we developed an affinity maturation protocol consisting of two steps. In the first step, we defined acceptable and tolerable substitutions at each position of the A1 lariat using site-saturation mutagenesis (SSM). In the second step, we designed specific mutations to the A1 lariat based on the SSM results and evolved higher affinity variants. Synthetic and recombinant higher affinity lariats exhibited a strong inhibition of Abl kinase activity *in vitro* and Bcr-Abl kinase activity *in vivo*, respectively, illustrating the potential of lariats as chemical genetic tools. Resistance mutation profiling showed that the lariats are not affected by the activating mutations located in the activation loop of kinase, and instead bind preferentially to the kinase active conformation. Selectivity analysis indicated that the lariats do not recognize Src family kinases, which share a high structural similarity with Abl kinase in their active conformation. These findings, coupled with preliminary results from modeling studies, strongly suggest that the lariats have identified novel allosteric drug-binding pockets in the kinase catalytic cleft.

ACKNOWLEDGEMENTS

I have been fortunate to have Dr. Ron Geyer as my mentor. I am deeply grateful to him for providing me a dynamic and challenging project, for allowing me to pursue some of my ideas, and for having confidence in my work. His kindness, guidance and support have been integral in the completion of this work.

I owe an immense debt of gratitude to my graduate committee members, Dr. Warrington, Dr. Lee, Dr. Roesler and Dr. Khandelwal, for their invaluable contribution towards shaping my budding scientific career.

I extend my sincere thanks to Dr. John F. DeCoteau and Dr. Yu Luo for providing facilities and support to perform cell biological and structural studies, respectively.

I would also like to thank past/present lab members, Dr. Kris Barreto, Dr. Theodora Zlateva, Dr. Landon Pastushok and Karen Mochoruk, for all the help provided to me in various forms.

TABLE OF CONTENTS

LIST OF TABLES

LIST OF FIGURES

LIST OF ABBREVIATIONS

8- oxo-dGTP	8-oxo-7,8-dihydro-deoxyguanosine-triphosphate
A- pocket	Adenine binding pocket
A- segment	Activation segment
Abl	Abelson kinase
AD	Transcription activation domain
Ade2	Phosphoribosylamino-imidazole-carboxylase
ADH	Alcohol dehydrogenase promoter
Akt	Protein kinase B
Alk	Anaplastic lymphoma receptor
AML	Acute myeloid leukemia
Amp	Ampicillin
ATM	Ataxia telangiectasia mutated kinase
ATP	Adenosine triphosphate
b-Raf/ c-Raf	Serine/threonine kinases encoded by *RAF* proto-oncogenes
BC	Breast carcinoma
Bcr	Breakpoint cluster region
bp	Base pairs
BP (I-IV)	Binding pockets in the back catalytic cleft of kinases (I-IV)
c-Kit	Mast/stem cell growth factor receptor
c-Met	Hepatocyte growth factor receptor
c-Ret	Tyrosine kinase encoded by the *RET* proto-oncogene
c-Yes	Tyrosine kinase encoded by the *YES1* proto-oncogene
CAMK	Calcium/calmodulin-dependent protein kinase
Cdk	Cyclin dependent kinase
CEP110	Centrosome-associated protein 110 kDa
CFU	Colony forming unit
CK2a1	Casein kinase II alpha 1
CML	Chronic myeloid leukemia
CMML	Chronic myelomonocytic leukemia
CSF1R	Colony stimulating factor 1 receptor
CSM	Complete synthetic media
DBD	DNA binding domain
ddH_2O	Sterile double distilled water
DFG motif	Aspartate-Phenylalanine-Glycine motif
DFSP	Dermatofibrosarcoma protuberans
DMSO	Dimethyl sulfoxide
DNA	Deoxyribonucleic acid
dPTP	2'-deoxy-P-nucleoside-5'-triphosphate
DTT	1,4-Dithiothreitol
E. coli	*Escherichia coli*
EDTA	Ethylenediaminetetraacetic acid
EGFR	Epidermal growth factor receptor
Erk	Extracellular-signal regulated kinase
FCC	Frozen competent cell solution

FDA	Food and Drug Administration
FGFR	Fibroblast growth factor receptor
Flt 3/4	Fms-related tyrosine kinase 3/4
GAL1/2	Galactose 1/2 promoter
GIST	Gastrointestinal stromal tumors
HA	Hemagglutinin tag
Hck	Hemopoietic cell kinase
HER-2/ErbB2	Human epidermal growth factor Receptor 2
HTS	High-throughput screening
I_C	Intein C-terminal domain
IC_{50}	Half maximal inhibitory concentration
IGF1R	Insulin-like growth factor 1 receptor
I_N	Intein N-terminal domain
IPTG	Isopropyl β-D-1-thiogalactopyranoside
IR	Infrared
Jak2	Janus kinase 2
Kan	Kanamycin
kDa	Kilo Dalton
K_i	Inhibitory constant
K_m	Michaelis-Menton constant
LacZ	Beta-galactosidase
LB	Lysogeny broth
Leu2	Beta-isopropylmalate dehydrogenase
LexAop	LexA operator
LK	Lipid kinase
LTR	5’ Long terminal repeat
MAPK	Mitogen-activated protein kinase
MCS	Multiple cloning site
MDM2	Ubiquitin ligase mouse double minute 2-protein
Mek1/2	Mitogen-activated protein kinase kinase 1/2
Mst4	A serine/threonine protein kinase
mTOR	Mammalian target of rapamycin kinase
Mylk2	Myosin light chain kinase 2
NADH	Nicotinamide adenine dinucleotide
NES	Nuclear export signal
NLS	Nuclear localization signal
NMR	Nuclear magnetic resonance
NSCLC	Non-small-cell lung carcinoma
NTA	Nitrilotriacetic acid
P- pocket	Triphosphate binding pocket
PBS	Phosphate buffered saline
PBT	Phosphate buffered saline tween 20
PC	Pancreatic carcinoma
PCR	Polymerase chain reaction
PDGFR	Platelet-derived growth factor receptor
PGK	phosphoglycerate kinase promoter

PI3K	Phosphoinositide 3-kinase
PKC	Protein kinase C
Plk	Polo-like kinase
PTEN	Phosphatase and tensin homolog protein
R- pocket	Ribose binding pocket
RCC	Renal cell carcinoma
RNA	Ribonucleic acid
RNAi	Ribonucleic acid interference
Rsk1	Ribosomal protein S6 kinase
S. cerevisiae	*Saccharomyces cerevisiae*
S6K	Ribosomal protein S6 kinase
SD H-	Synthetic dextrose His^- media
SD H-W-	Synthetic dextrose His^- Trp^- media
SD	Standard deviation
SD W-	Synthetic dextrose Trp^- media
SDS-PAGE	Sodium dodecyl sulfate polyacrylamide gel electrophoresis
SGR H-W-L- A- Xgal+	Synthetic galactose raffinose His^- Trp^- Leu^- Ade^- $Xgal^+$ media
SGR H-W-L-	Synthetic galactose- raffinose His^- Trp^- Leu^- media
SH1/SH2/SH3	Src homology 1/2/3 domains
SK1	Sphingosine kinase 1
Src kinase/family	Sarcoma kinase/ Sarcoma family kinases
SSM	Site saturation mutagenesis
Ssp	*Synechocystis species*
Stat	Signal transducer and activator of transcription protein
T-ALL	T-cell acute lymphoblastic leukemia
Taok1	Serine/threonine-protein kinase encoded by the *TAOK1* gene
Taq	*Thermus aquaticus*
TB	Terrific broth
TEL	Translocated Ets leukemia protein
TEMED	Tetramethylethylenediamine
TEV	Tobacco etch virus
TK	Tyrosine kinase group
TKL	Tyrosine kinase like group
Tris	Tris(hydroxymethyl)aminomethane
Tween 20	Polyoxyethylene (20) sorbitan monolaurate
Txk	Tyrosine kinase encoded by the *TXK* gene
VEGFR	Vascular endothelial growth factor receptor
V_{max}	Maximum reaction rate
X-gal	Bromo-chloro-indolyl-galactopyranoside
Y2H	Yeast two-hybrid
YFP	Yellow fluorescent protein
YopH	*Yersinia pestis* tyrosine phosphatase
YPDA	Yeast peptone dextrose adenine (yeast rich media)
ZNF198	Zinc finger protein 198

1. Introduction

Protein kinases are implicated in more than 400 human diseases, directly or indirectly, and hence considered to be the most important group of drug targets in drug discovery programs (Melnikova and Golden, 2004). Currently, a large number of small molecule kinase inhibitors are in various phases of development and in clinical trials, with 11 approved for clinical use by U. S. Food and Drug Administration (FDA) (Krishnamurthy and Maly, 2010). The vast majority of kinase inhibitors predominantly occupy the highly conserved adenine-binding pocket located in the kinase catalytic cleft, and therefore the target selectivity of these molecules is a major concern. In order to design highly specific next-generation drugs, it is essential to exploit the less-conserved binding pockets, which lie adjacent to the adenine-binding pocket (Noble *et al*., 2004; Zhang *et al*., 2009).

Various computational and experimental approaches (Coleman *et al*., 2006; Landon *et al*., 2007; Brenke *et al*., 2009; Ivetac *et al*., 2010) can be used to identify and characterize allosteric drug binding pockets in the kinase catalytic cleft. However, conventionally, the search for allosteric pockets has involved high-throughput screening (HTS) of small molecule libraries against purified kinase domains, followed by intensive kinetic and structural characterization. Although this method is attractive, only a small fraction of selected compounds recognize novel binding pockets. Small molecules, often attracted to the active site that is rich in functional groups, do not extend into the adjacent binding sites due to their small size. In addition, this HTS approach requires a huge investment of time and money, and therefore is primarily an enterprise for industry (Hardy and Wells, 2004; Sperandio *et al*., 2008).

In recent years, peptide-based affinity reagents are increasingly used to identify new druggable surfaces on targets. Indeed, there are a number of peptide inhibitors that target a range of kinases (Bogoyevitch *et al*., 2005; Eldar-Finkelman and Eisenstein, 2009). A majority of these inhibitors are synthetic linear peptides, which are either isolated from a library of chemically synthesized peptides or rationally designed to mimic the recognition sequences of specific kinase-binding proteins. There are a few recombinant constrained peptides, called peptide aptamers, which are isolated from genetically encoded peptide libraries (Kolonin and Finley, 1998; Buerger *et al*., 2003; Kunz *et al*., 2006; Martel *et al*., 2006; Miller *et al*., 2007). In many cases, these synthetic or recombinant peptides function as competitive inhibitors by

binding to the substrate peptide-binding region of kinases. In a few cases, these peptides inhibit protein-protein interactions by targeting the regulatory domains of kinases.

To date, there are no peptide inhibitors that target the adenosine triphosphate (ATP) binding site of kinases. Small peptides that can function as ATP competitive inhibitors would prove useful in identifying and validating new druggable surfaces in the kinase catalytic cleft. These peptides, being larger than small molecules, have the potential to target the ATP binding pocket as well as surfaces that lie adjacent to this pocket. Such peptides recognizing novel binding pockets can be made useful in several ways: (i) structure of the kinase domain in complex with the peptide could be solved, which would provide information for the rational design of small molecule drugs; (ii) small molecules that disrupt kinase-peptide interactions could be identified by performing peptide displacement screens (Bardou *et al*., 2009), which in turn would serve as lead structures for drug development; and (iii) novel pharmacophores of the peptide could be grafted onto an existing small molecule using peptidomimetics (Vagner *et al*., 2008), to design a next generation drug that recognizes additional binding pockets.

In this thesis, we describe the isolation and characterization of a novel class of cyclic peptides, referred to as lariats, that bind to the catalytic cleft of Abelson (Abl) kinase, a drug target important in chronic myeloid leukemia (CML) and other disorders (Advani and Pendergast, 2002; Hantschel and Superti-Furga, 2004).

2. Literature Review

2.1 Molecular recognition of protein kinases by small molecules

2.1.1 Protein kinases as drug targets

Protein kinases are phosphotransferases, which catalyze the transfer of γ-phosphate from ATP to the hydroxyl group of defined tyrosine, serine, and threonine residues in various protein substrates. Phosphorylated proteins initiate a cascade of reactions downstream, playing essential roles in cell-signaling pathways. As phosphorylation acts as a biological control process in modulating a wide range of cellular events, abnormal phosphorylation is often a cause or consequence of diseased states (Johnson and Lewis, 2001; Parang and Sun, 2005). The human genome encodes 518 putative kinases, of which 164 kinases are implicated in cancer and 80 kinases are implicated in other non-malignant disorders, making the kinome a rich source of therapeutic targets (Manning *et al*., 2002; Cohen, 2002; Greenman *et al*., 2007). Few well-studied kinase targets that are intimately involved in cancer are listed in Table 2.1 (Blume-Jensen and Hunter, 2001; Futreal *et al*., 2004; Perez-de-Castro *et al*., 2007; Zhang *et al*., 2009).

Kinase targets implicated in cancer are grouped into three classes. The first class contains kinases that acquire transforming capacity upon mutation and deregulation (Zhang *et al*., 2009). These kinases are primary targets for cancer intervention (Weinstein *et al*., 2006). Among the primary targets, Abl kinase is a classic example. Abl kinase has been implicated in processes of cell division, cell differentiation, actin dynamics, cell migration, and oxidative stress and DNA-damage responses (Pendergast, 2002; Smith and Mayer, 2002). Tight temporal and spatial control of Abl kinase activity is essential for normal cell function, growth and development. Aberrant Abl kinase activity leads to different forms of leukemia in humans (Hantschel and Superti-Furga, 2004). In CML and a subset of acute lymphocytic leukemia (ALL), a reciprocal translocation between chromosomes 22 and 9 {t(9;22)(q34;q11)}, in which sequences of the first exon of *ABL1* gene are replaced by sequences from the *BCR* (Breakpoint Cluster Region) gene, results in expression of the Bcr–Abl fusion protein (Daley *et al*., 1990). In the fusion protein, Abl lacks the N-terminal region that carries a myristoyl modification. Lacking this modification, Bcr-Abl becomes constitutively active, as the myristoyl group is a negative regulator of native Abl kinase activity (Nagar *et al*., 2003; Hantschel *et al*., 2003). The Bcr coiled-coil domain, located in the N-terminus of the Bcr moiety, also favors constitutive

Table 2.1: Examples of protein kinases implicated in human cancer (Table modified with permission from Macmillan Publishers Ltd: Nature Reviews in Cancer, (Zhang *et al*., 2009)).

Kinase	**Oncogenic Alteration**	**Tumor/Cancer Types**
Abl	Translocation (BCR-)	CML
Src	Overexpression, C-terminal truncation	Lung, colon, breast & prostate
Jak-2	Translocation (TEL-), point mutations	CML, T-ALL
c-Yes, Akt, Aurora, Cdks, mTOR, Plk, S6K, PKC	Overexpression	Multiple
ATM	Point mutations	Ataxia telangiectasia
b-Raf	Point mutations	Colon, thyroid, melanoma
PI3K	Overexpression and point mutations	Prostate, colorectal, breast
SK1	Overexpression	Breast
EGFR	Extracellular domain deletions and point mutations	Breast, lung, glioma
HER-2/ErbB2	Overexpression	Breast, ovarian, colon, lung, gastric
IGF-IR	Overexpression	Colorectal, pancreatic, breast, ovarian
PDGFR-α	Overexpression and translocation	Glioma, ovarian
PDGFR-β	Translocation (TEL-)	CMML, glioma, DFSP
c-Kit	Point mutations	GIST, seminoma
Flt-4, Flt3	Internal tandem duplication	AML
FGFR1	Translocations (BCR-, FOP-, ZNF198-, CEP110-)	Myeloproliferative disorders
FGFR3	Translocations & point mutations	Multiple myeloma
FGFR4	Overexpression	Breast, ovarian
c-Ret, c-Met, Alk	Translocations & point mutations	Multiple

activation by inducing dimerisation of the fusion protein (McWhirter *et al*., 1993; Zhang *et al*., 2001). Critical signals emanate downstream of the Bcr-Abl fusion protein and lead to oncogenic transformation of haematopoietic stem cells (Samanta *et al*., 2010) (Figure 2.1).

A second class of kinase targets is required for sustaining rapid proliferation and/or survival of cancer cells. These kinases, however, are not oncogenic and are rarely mutated in cancer (Zhang *et al*., 2009). Examples of this class include (i) mitogen-activated protein kinase kinase 1/2 (Mek1/2), ribosomal S6 kinase (Rsk), and mammalian target of rapamycin (mTOR) kinase, which are located downstream of transforming oncogenes in signaling pathways (Hu *et al*., 2004; Faivre *et al*., 2006; Wang *et al*., 2007); (ii) cyclin-dependent kinases (Cdk) and polo-like kinases (Plk), which are important regulators of the cell cycle; and (iii) aurora kinases, which play a crucial role during mitosis and cytokinesis (Malumbres and Barbacid, 2007).

A third class of kinase targets is required for different stages of tumor formation. These kinases are overexpressed in the tumor or in surrounding tissues (Zhang *et al*., 2009). Examples of this class include (i) vascular endothelial growth factor receptor (VEGFR) and fibroblast growth factor receptor (FGFR), which are essential in tumor angiogenesis (Kerbel, 2008); (ii) neurotrophic growth factor receptor, which may be required for tumor cell metastasis (Geiger and Peeper, 2007); and (iii) M2 splice isoform of pyruvate kinase, which is important for cancer metabolism and tumor growth (Christofk *et al*., 2008).

Protein kinases are also targets for treatment of non-malignant disorders such as cardiac hypertrophy, pulmonary hypertension, lung fibrosis, rheumatoid disorders, atherosclerosis, in-stent restenosis, glomerulonephritis, cystic fibrosis, asthma, chronic obstructive pulmonary disease, gastritis, psoriasis, sepsis, and macular degeneration (Grimminger *et al*., 2010).

2.1.2 Protein kinase inhibitors

On the market in the United States, there are currently 11 FDA approved small molecule inhibitors that target a range of kinases (Table 2.2). Nine out of these 11 inhibitors target the ATP-binding pocket of kinases, and two molecules inhibit protein-protein interactions (Force and Kolaja, 2011). Three ATP competitive inhibitors (imatinib, dasatinib and nilotinib) are used to treat leukemias (Wei *et al*., 2010). Their modes of action are discussed in detail later. In addition to the FDA approved drugs, there are many ATP-competitive and a few allosteric inhibitors in various phases of development and clinical trials.

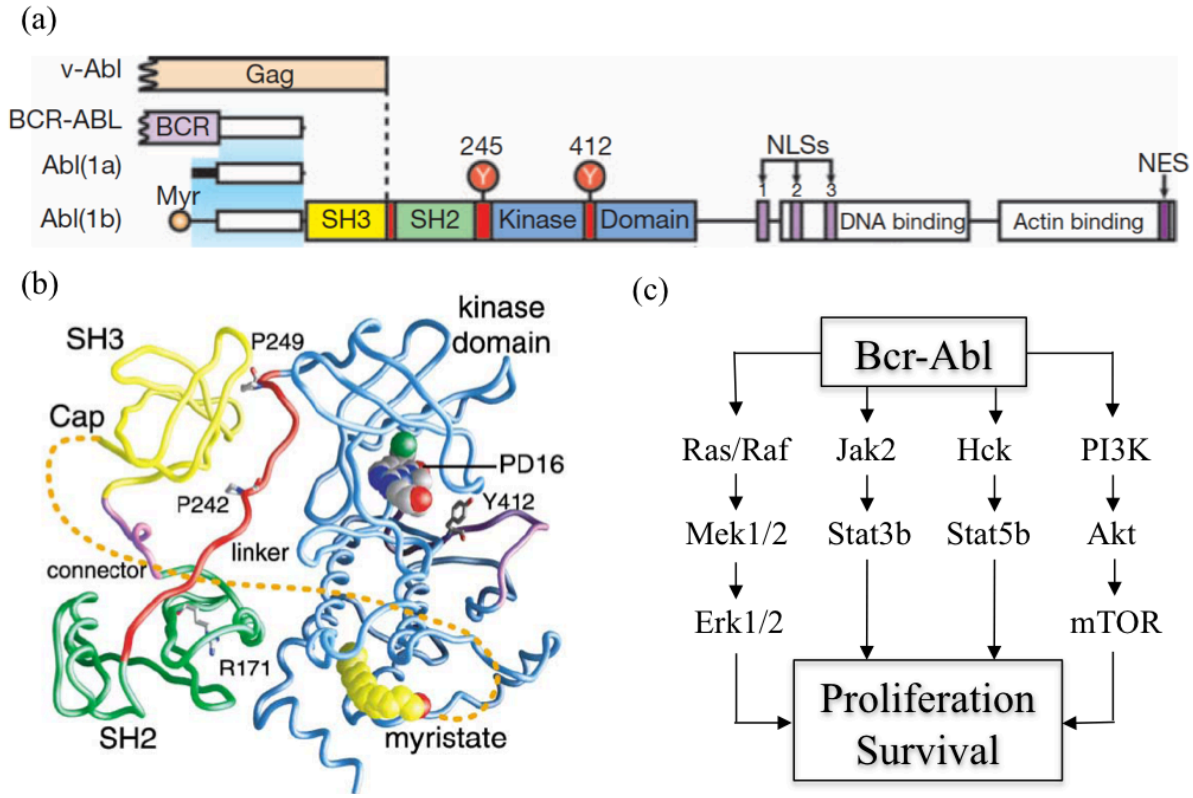

Figure 2.1: (a) Primary structure of Abl kinase and its variants: Abl kinase contains SH3, SH2, kinase (SH1), DNA binding and actin binding domains. NLS and NES represent nuclear localization signal and nuclear export signal, respectively. Abl(1b) but not Abl(1a) is myristoylated. Bcr-Abl and v-Abl are two N-terminal mutants of Abl kinase. In the clinically important Bcr-Abl fusion protein, Abl lacks the N-terminal region that carries a myristoyl modification (Cap sequence). In the Gag-Abl fusion protein, Abl lacks the Cap sequence and the SH3 domain. **(b) Tertiary structure of Abl SH3-SH2-SH1:** Backbone worm representation of myristoylated Abl SH3-SH2-SH1 in complex with PD16 inhibitor is shown. Dotted line represents the Cap sequence region. Some important residues and secondary structure elements are indicated. The myristoyl moiety binds to a hydrophobic pocket in the C-lobe of the kinase domain, which is important for establishing the latent conformation of Abl. **(c) Oncogenic signaling of Bcr-Abl:** Bcr-Abl protein expression leads to the activation of multiple downstream signalling events such as Ras/Raf/Mek/Erk, Jak2/Stat3b, Hck/Stat5b and PI3K/PTEN/Akt/mTOR pathways, which contribute to growth and survival. Figure 2.1(a) reprinted with permission from Macmillan Publishers Ltd: Nature Cell Biology, (Wang, 2004). Figure 2.1(b) reprinted with permission from Elsevier: Cell, (Hantschel *et al*., 2003).

Table 2.2: Eleven FDA approved protein kinase inhibitors and their targets (Table modified with permission from Macmillan Publishers Ltd: Nature Reviews Drug Discovery, (Force and Kolaja, 2011)).

Drug	Brand name	Company	Launc--hed in	Primary target(s)	Disease
Imatinib	Gleevec	Novartis	2001	Abl, PDGFR, c-Kit	CML etc.,
Gefitinib	Iressa	AstraZeneca	2003	EGFR	NSCLC
Erlotinib	Tarceva	Roche/Genentech	2004	EGFR	NSCLC, PC etc.,
Sorafenib	Nexavar	Bayer	2005	B-Raf, VEGFR, PDGFR, Flt3, c-Kit	RCC, LC
Sunitinib	Sutent	Pfizer	2006	VEGFR, PDGFR, CSF1R, Flt3, c-Kit	RCC, GIST
Dasatinib	Sprycel	Bristol-Myers Squibb	2006	Abl, c-Kit, PDGFR, Src	CML
Temsirolimus	Torisel	Pfizer	2007	mTOR	RCC
Nilotinib	Tasigna	Novartis	2007	Abl, PDGFR, c-Kit	CML
Lapatinib	Tykerb	GlaxoSmithKline	2007	EGFR	BC
Everolimus	Afinitor	Novartis	2009	mTOR	RCC
Pazopanib	Votrient	GlaxoSmithKline	2009	VEGFR, PDGFR, c-Kit	RCC

Allosteric inhibitors bind outside the ATP-binding pocket and modulate the kinase activity in an allosteric manner. Well-studied allosteric inhibitors include: (i) GNF2 and GNF5, which bind to the myristate-binding pocket of Abl kinase (Adrian *et al*., 2006; Zhang *et al*., 2010) (ii) ON012380 and ON44580, which bind to the substrate-binding pocket of Abl kinase and Janus kinase 2 (Jak2), respectively (Gumireddy *et al*., 2005; Jatiani *et al*., 2010) (iii) PD318088, which inhibits Mek1/2 by occupying an allosteric site adjacent to the ATP binding pocket (Ohren *et al*., 2004); (iv) protein kinase B inhibitors, which target the pleckstrin homology domain (Lindsley *et al*., 2005); and (v) BMS-345541, which inhibits nuclear factor-κB kinase by binding to an allosteric site on the enzyme (McIntyre *et al*., 2003).

Apart from the inhibitors mentioned here, there are also: (i) covalent inhibitors, which are capable of forming an irreversible, covalent bond to the kinase active site (Cohen *et al*., 2005; Kwak *et al*., 2005); (ii) bisubstrate analog inhibitors, which are designed to mimic two natural ligands that simultaneously associate with ATP and peptide binding sites of kinases (Parang and Cole, 2002); (iii) SH2 domain inhibitors, which antagonize SH2 domain dependent protein-protein interactions (Vu, 2000; Muller, 2000; Wojcik *et al*., 2010); and (iv) humanized monoclonal antibodies, which are generated against growth factors and their receptors [e.g. bevacizumab that targets vascular endothelial growth factor for treatment of metastatic colorectal cancer (Fuh *et al*., 2006), and trastuzumab that targets the exracellular domain of epidermal growth factor receptor 2 (HER-2/ErbB2) for treatment of breast cancer (Cho *et al*., 2003)].

2.1.3 Structural features of the catalytic domain of kinases

All kinases have a conserved catalytic domain consisting of ~ 300 residues (Johnson, 2009). In addition to the catalytic domain, kinases contain several other domains. However, only the catalytic domain structure is discussed here, since all the kinase inhibitors used in the clinic bind to this domain. The catalytic domain of kinases folds into two lobes, a smaller N-terminal lobe (N-lobe) and a larger C-terminal lobe (C-lobe) (Figure 2.2). The two lobes are connected with a linker that contains a hinge and a convex shaped motif (E_0). The active site is present in the interlobal cleft (Liao, 2007a). The N-lobe consists of five β strands (β1 – β5), and one α helix (αC). The glycine-rich loop (G-loop), between β1 and β2, is an important structural element in the N-lobe (Hubbard and Till, 2000; Huse and Kuriyan, 2002). The C-lobe is mainly α helical and contains only four short β strands (β6 – β9). This stable helical subdomain serves as a tethering surface for protein/peptide substrates, and also houses a myristic acid binding pocket. Important structural elements in the C-lobe include a catalytic loop, an activation segment (A-segment) and one α helix (αF). The catalytic loop is present between β6 and β7 and has most of the catalytic machinery. The A-segment consists of DFG motif, β9, activation loop (A-loop), and P + 1 loop (Huse and Kuriyan, 2002; Nolen *et al*., 2004). The hydrophobic F helix is the organizing element for the entire kinase core. Motifs in the C-lobe are anchored firmly through hydrophobic contacts to the F- helix (Taylor and Kornev, 2011).

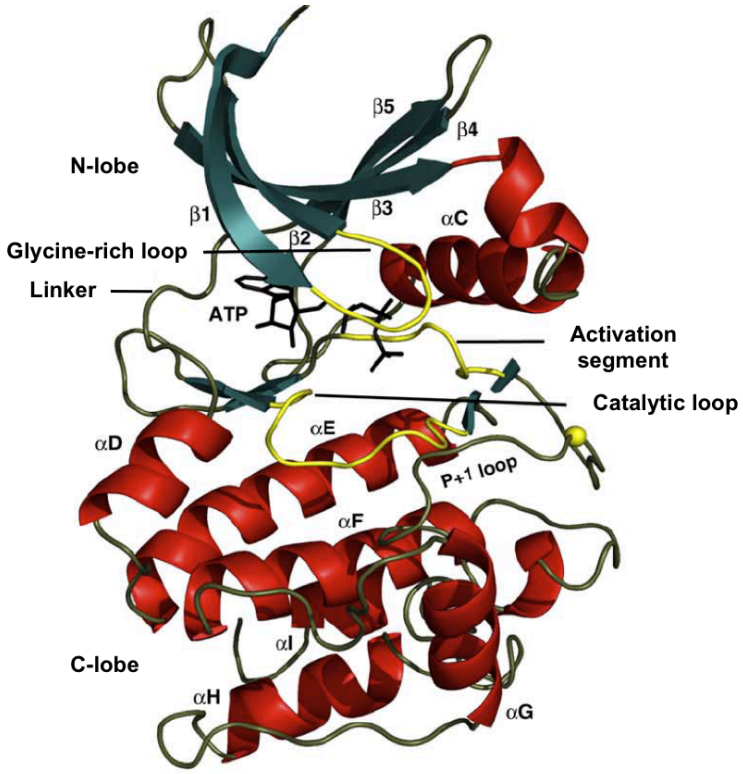

Figure 2.2. Conserved structure of kinase catalytic domain: Ribbon representation of kinase core in complex with ATP is shown. Important secondary structure elements are indicated. See section 2.1.3 for details. Figure reprinted with permission from Elsevier: Trends in Biochemical Sciences, (Taylor and Kornev, 2011).

2.1.4 Structure and activation of the kinase catalytic cleft

The catalytic cleft is formed between the N- and C- lobes (Figure 2.3). The basic structural features of the cleft include nine β strands (β1-β5 in the N-lobe and β6-β9 in the C-lobe), two α helices (αC in the N-lobe and αE in the C-lobe), two loops (G-loop and the catalytic loop), and the A-segment. Five β strands (β1-β5) and the G-loop form the ceiling of the cleft. The C-terminus of αE, N-terminus of the catalytic loop, β7, β8 and the DFG motif constitute the basement of the cleft (Liao, 2007a; Liao and Andrews, 2007).

The catalytic cleft is composed of two regions: (i) the front cleft that contains predominantly the ATP-binding site; and (ii) the back cleft that contains elements important for regulation of kinase catalysis. The two regions are bordered by β3, β8 and the DFG motif. Two residues (K271 in β3 and T315 in β5) form an internal gate between the front and the back clefts (Huse and Kuriyan, 2002; Nolen *et al*., 2004). Here, the crystal structure of active Abl kinase is used for discussion. The T315 residue is referred to as the gatekeeper. The gatekeeper

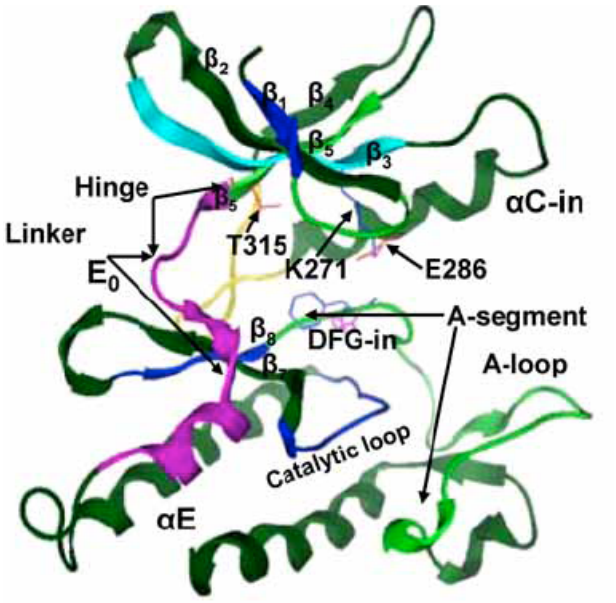

Figure 2.3. Basic structural features of the kinase catalytic cleft: Ribbon representation of Abl kinase catalytic cleft (PDB code: 2G2I) in active conformation is shown. Important residues and secondary structure elements are indicated. See section 2.1.4 for details. Figure reprinted with permission from Bentham Science Publishers Ltd: Current Topics in Medicinal Chemistry, (Liao and Andrews, 2007).

residue controls the access to the back cleft. A small amino acid (threonine or alanine) at this position allows access to the back cleft, while a bulky gatekeeper (phenylalanine, leucine or methionine) blocks the access to the back cleft (Liu *et al*., 1998; Bishop, 2004). Another component of the gate, the β3 lysine, also plays an important role in the catalysis. The lysine couples the non-transferable α and β phosphates of the ATP to the helix αC by forming an ion pair with the catalytic glutamate residue (E286 in Abl) located nearly at the centre of αC. The lysine–glutamate salt bridge is highly conserved through the entire kinase family (Hanks and Hunter, 1995; Wu et al., 2003).

Depending on the conformational state of the kinase and the presence of a ligand, the G-loop, the A-segment, and the αC helix can adopt various conformations. In the fully active state (Figure 2.4), the A-segment adopts an open conformation and provides a platform for substrate binding. The A-segment in the open conformation is also called the DFG-in conformation, where the side chain of D381 in the DFG motif is directed into the ATP binding site, and the aromatic ring of F382 is positioned in the back cleft. In the DFG-in state, D381 chelates Mg^{2+} that orients the γ-phosphate of ATP for transfer, and the aromatic ring of F382 contacts the αC

helix to promote αC-in conformation. The αC-in conformation, characterized by an inward shift of the αC helix with its E286 pointing towards the cleft, facilitates the formation of the lysine–glutamate salt bridge mentioned earlier. Overall, an active kinase requires the DFG-in and the αC-in conformations for catalysis. For a stable active kinase conformation, phosphorylation of a critical residue in the A-segment by an upstream kinase is required (Huse and Kuriyan, 2002; Nolen *et al*., 2004, Levinson *et al*., 2006).

The inactive kinases are characterized by DFG-out and/or αC-out conformations. In the DFG-out state, the A-segment adopts a closed conformation and interferes with substrate binding. The aromatic ring of F382 is positioned in the ATP binding site and the side chain of D381 occupies the back cleft. In the αC-out state, there is an outward shift of the αC helix, which makes E286 point out of the catalytic cleft (Huse and Kuriyan, 2002; Nolen *et al*., 2004, Levinson *et al*., 2006). Two different inactive conformations of Abl kinase (Abl/c-Kit–like inactive state [DFG-out, αC-in] and Src/Cdk–like inactive state [DFG-in, αC-out]) are shown in Figure 2.4.

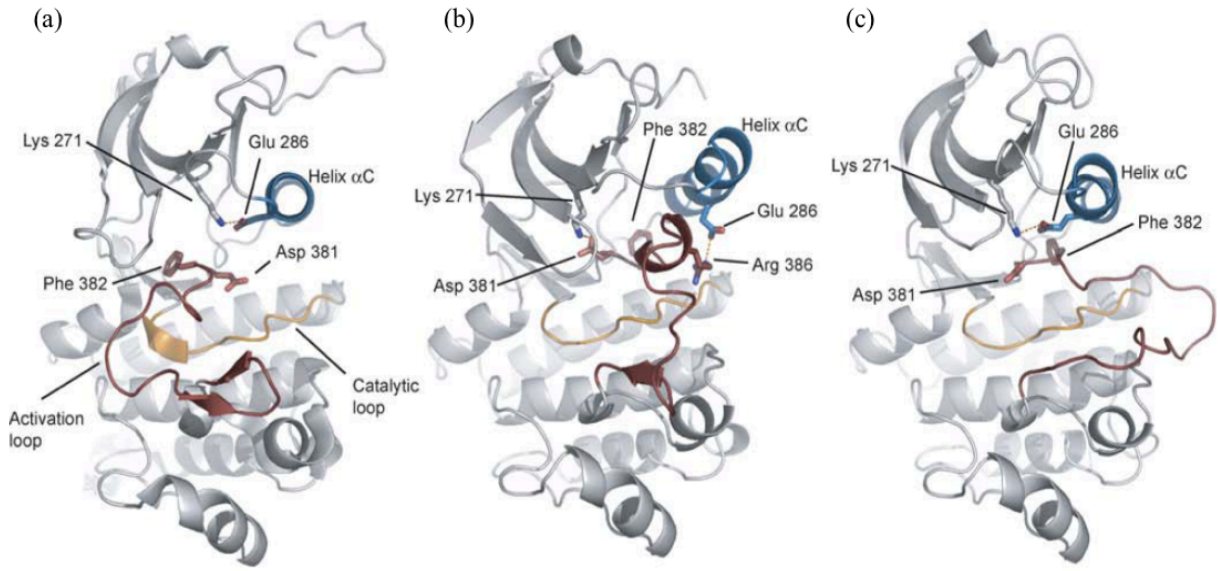

Figure 2.4. Multiple states of Abl kinase: Ribbon representations of three key Abl catalytic domain conformations are shown. **(a)** Abl/c-Kit–like inactive conformation (DFG-out, αC-in); **(b)** Src/Cdk–like inactive conformation (DFG-in, αC-out); and **(c)** active conformation (DFG-in, αC-in). Src/Cdk–like inactive state is one of the intermediate conformations adopted by Abl kinase during the activation process. Important residues and secondary structure elements are indicated in the figure. PDB codes: 1OPJ (for A), 2G1T (for B), and 2G2I (for C). Figure reprinted from PLOS Biology (Levinson *et al*., 2006) under Creative Commons Attribution License.

2.1.5 Binding pockets in the catalytic cleft

Though the following section is based mainly upon published articles (Noble *et al*., 2004; Liu and Gray, 2006; Liao, 2007a; Liao, 2007b; Liao and Andrews, 2007; Johnson, 2009), personal observations gained from detailed structure, sequence and binding-site analyses are also incorporated. Human Abl 1b numbering is used throughout the discussion. The front cleft contains four binding pockets (denoted A, R, P and K pockets) and two entrance regions (denoted E_0 and E_1). The hydrophobic adenine-binding pocket (A-pocket) provides a major scaffold for ATP/inhibitor binding. This pocket is covered by five hydrophobic residues (L248 in β1, V256 in β2, A269 in β3, V299 in the loop between αC and β4, and L370 in β6) and rimmed with gatekeeper (T315 in β5) and hinge residues (E316, F317, and M318 in the loop between β5 and αD). The first and the third hinge residues form hydrogen bonds (H-bond) with adenine (Brown *et al*., 1999) or ATP competitive small molecules (Cherry *et al*., 2004). Although the A-pocket is highly conserved in the kinase family, the gatekeeper and a few other residues have specific features in this pocket, which are used to gain selectivity in the design of inhibitors. For example, the smaller alanine (A269 in Abl) conserved in many kinases (Manning *et al*., 2002) is replaced by a bulkier residue (V66) in casein kinase II. In addition, the entrance region E_0 lining the A-pocket varies in sequence and conformation, thereby providing opportunities for selective drug design (Fabbro *et al*., 2002). This E_0 region often serves as an entrance for the binding of ATP competitive small molecules.

The ribose-binding pocket (R pocket) is covered by three hydrophobic residues (L248, V256, and L370 (shared with the A-pocket)), first two residues (backbone) in the G-loop (G249 and G250), two residues in the loop between β5 and αD (G321 and N322), D325 in αD, and R367 in the catalytic loop. The entrance region E_1 that lies adjacent to the R-pocket is hydrophilic and solvent-exposed. The triphosphate-binding pocket (P pocket) is lined with the G-loop from the top, three residues in the catalytic loop (D363, A365 and N368), K271 in β3, and D381 in the DFG motif. The P pocket is highly flexible, hydrophilic and solvent-exposed. Therefore, this pocket is believed to be less important for improving the affinity of the inhibitor (Fabbro *et al*., 2002). However, the P pocket could be utilized to improve the selectivity and physicochemical properties of the inhibitor (Kontopidis *et al*., 2006). With the exception of few highly selective inhibitors, the majority of ATP competitive small molecules do not exploit the R and P pockets (Zhang *et al*., 2009). The K pocket, a relatively small, non-ATP contact region

is located in the deep front pocket and is covered by four residues (K271, T315, A380, and D381).

Two binding pockets (denoted BPI and BPII) have been identified in the back cleft of kinases in the active conformation. Upon adopting the inactive conformation (DFG-out), the back cleft of kinases is enlarged and therefore four binding sites (denoted BPI – BPIV) have been identified. Residues that cover the binding pockets in the back cleft of Abl kinase are given in Table 2.3. Topological distribution of the binding pockets in the catalytic cleft with active (DFG-in, αC-in) and inactive (DFG-out, αC-in) conformations is shown in Figure 2.5. In order to achieve high selectivity and affinity, inhibitors are rationally designed to target many binding sites in the front and the back clefts of kinases.

2.1.6 Binding modes of kinase inhibitors

Based on the mode of binding, the inhibitors that bind within the catalytic cleft are classified into three types: type I, type II, and allosteric kinase inhibitors. Type I and type II kinase inhibitors are ATP competitive and bind predominantly to the A-pocket. Typically, all type I/II inhibitors form one to three H-bonds with the hinge residues. Allosteric inhibitors (type III) bind outside the ATP binding pocket and are non-ATP competitive (Okram *et al*., 2006; Liu and Gray, 2006; Zhang *et al*., 2009).

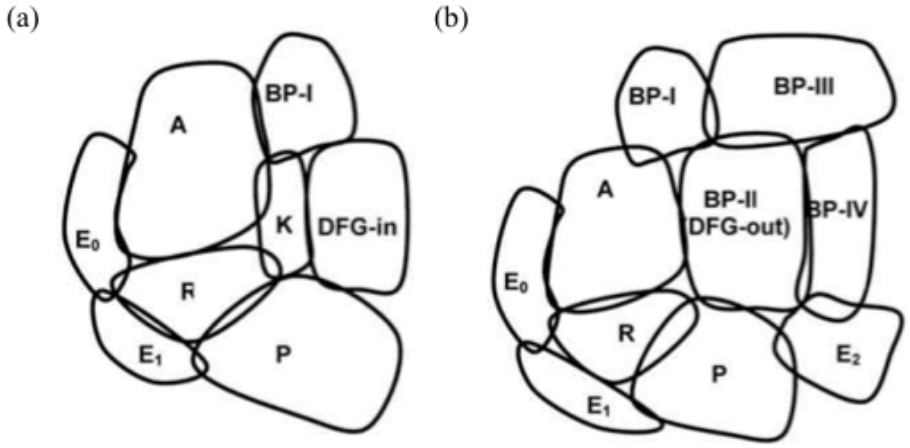

Figure 2.5. Topological distribution of binding pockets in the kinase catalytic cleft: (a) with active (DFG-in, αC-in); and **(b)** with inactive (DFG-out, αC-in) conformations. Adenine (A), ribose (R), phosphate (P), and K pockets are located in the front catalytic cleft. Binding pockets I, II (DFG-in or DFG-out), III, and IV are located in the back catalytic cleft. E_0, E_1, and E_2 denote various entrance regions that surround the cleft. Figure reprinted with permission from Bentham Science Publishers Ltd: Current Topics in Medicinal Chemistry, (Liao, 2007b).

Table 2.3: Residues lining the binding pockets located in the back cleft of Abl kinase

Pocket	Cleft conformation	Residues
BPI	Active (DFG-in, αC-in) Inactive (DFG-in, αC-out) (DFG-out, αC-in)	A269 (in β3) K271 (catalytic lysine in β3) M290 (in αC) I313, I314 (in β5) T315 (gatekeeper in β5)
BPII	Active (DFG-in, αC-in)	E286 (catalytic Glutamate in αC) M290 (in αC) V299, E300, L301 (in loop between αC and β4) T315 (gatekeeper in β5) A380 (in β8) D381, F382, G383 (DFG motif in activation loop)
BPII	Inactive (DFG-in, αC-out)	M290 (in αC) V299, E300, L301 (in loop between αC and β4) T315 (gatekeeper in β5) A380 (in β8) D381, F382, G383 (DFG motif in activation loop)
BPIII	Inactive (DFG-out, αC-in)	V289 (in αC) I293, L298 (in loop between αC and β4) L354 (in αE) H361 (in catalytic loop) A380 (in β7)
BPIV	Inactive (DFG-out, αC-in)	V289 (in αC) L354 (in αE) F359, I360, H361 (in catalytic loop) D381 (in DFG motif)

Type I inhibitors can bind to kinases in both the active and inactive conformations, but so far all type I inhibitors have been co-crystallized with kinases in the active conformation. Examples of this class include dasatinib, erlotinib, sunitinib, and VX-680. In addition to the A-pocket, type I inhibitors can also occupy R, P, BPI, and BPII pockets. Type II inhibitors require a specific inactive conformation of the kinase for binding. Examples of this class include imatinib, nilotinib, lapatanib, and sorafenib. In addition to the A-pocket, type II inhibitors can also occupy R, P, BPI, BPII, BPIII, and BPIV pockets (Liu and Gray, 2006; Liao, 2007a; Liao and Andrews, 2007; Johnson, 2009; Zhang *et al*., 2009). Specific conformations of the activation loop and the αC helix targeted by these inhibitors are given in Table 2.4.

Allosteric inhibitors that bind within the catalytic cleft target a region adjacent to the ATP binding site. They exploit very specific and unique binding sites in the back cleft. Examples of this class include Mek1/2 inhibitor PD318088 (Ohren *et al*., 2004) and its derivatives PD184352 and PD325901. PD318088 recognizes two binding pockets in the Mek1 back cleft (BPII and $BPIII^{I}$) but does not bind to the A, R, and P pockets in the front cleft (Liao, 2007a). $BPIII^{I}$ is a new hydrophobic half-opened binding pocket, which is different from the BPIII pocket. PD318088 binds to the target through the E_2 entrance at the αC side. Binding modes of type I, type II and allosteric inhibitors are illustrated in Figure 2.6.

Table 2.4: Conformational preferences for the binding of kinase inhibitors

Inhibitor	Type	Targeted Conformation		
		Catalytic cleft	Activation loop	αC helix
Dasatinib	I	Active	DFG-in	αC-in
VX-680	I	Active	DFG-in	αC-in
Erlotinib	I	Active	DFG-in	αC-in
Sunitinib	I	Active	DFG-in	αC-in
Imatinib	II	Inactive	DFG-out	αC-in
Nilotinib	II	Inactive	DFG-out	αC-in
Lapatanib	II	Inactive	DFG-in	αC-out
Sorafenib	II	Inactive	DFG-out	αC-in
PD318088	III	Inactive	DFG-out	αC-out

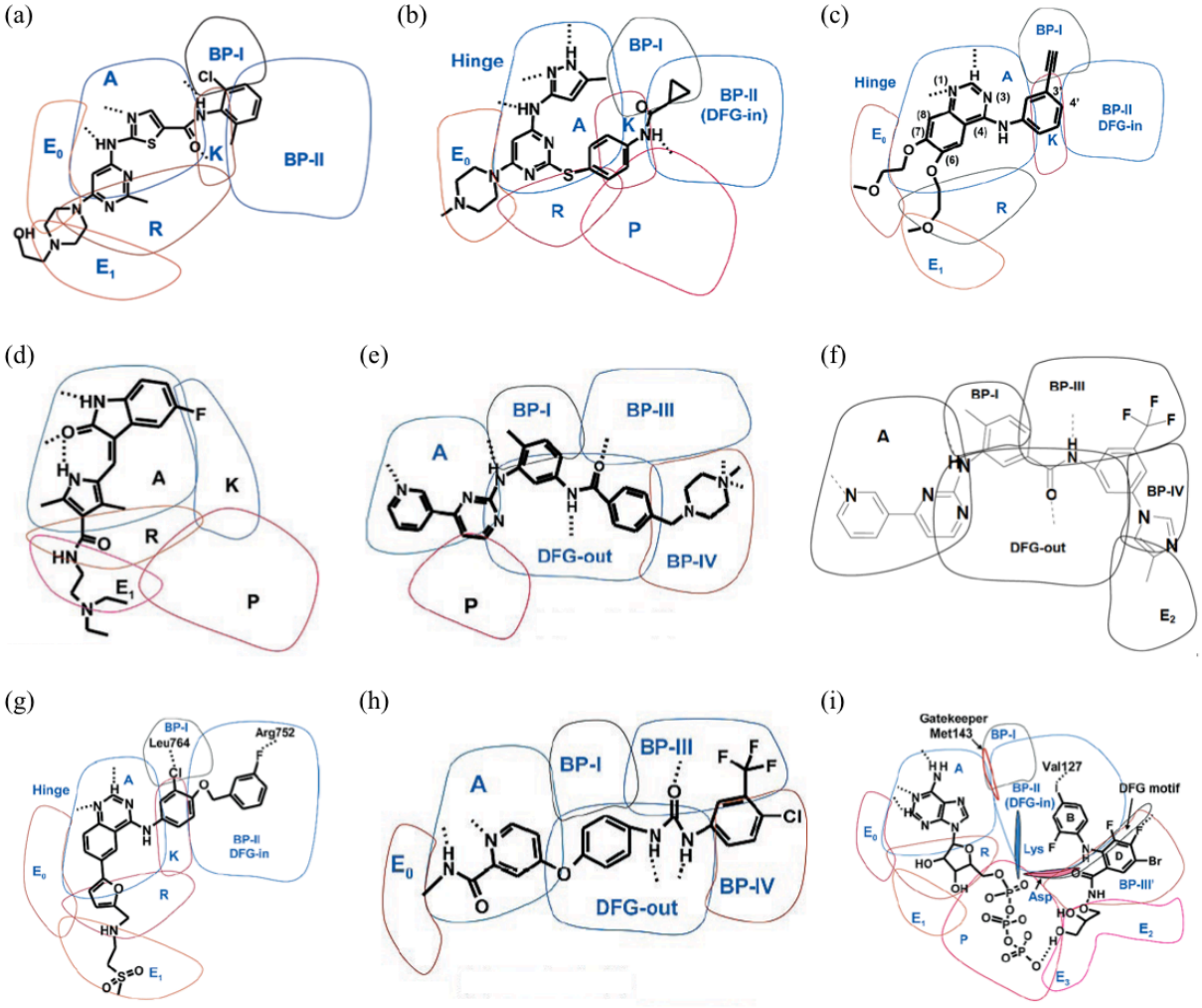

Figure 2.6. Binding modes of kinase inhibitors in the catalytic cleft: Type I inhibitors - **(a)** dasatinib in active Abl; **(b)** VX-680 in active Abl; **(c)** erlotinib in active EGFR; and **(d)** sunitinib in active FGFR. Type II inhibitors - **(e)** imatinib in inactive Abl; **(f)** nilotinib in inactive Abl; **(g)** lapatinib in inactive EGFR; and **(h)** sorafenib in inactive B-Raf. Type III inhibitor – **(i)** PD318088 in inactive Mek1. ATP binding is shown in (i) for reference. Adenine (A), ribose (R), phosphate (P), and K pockets are located in the front catalytic cleft. Binding pockets I, II, III, III[I], and IV are located in the back catalytic cleft. E_0, E_1, E_2, and E_2 denote various entrance regions that surround the cleft. Figures 2.6 (a-e) and (g-i) reprinted with permission from American Chemical Society: Journal of Medicinal Chemistry, (Liao, 2007a). Figure 2.6 (f) reprinted with permission from Bentham Science Publishers Ltd: Current Topics in Medicinal Chemistry, (Liao and Andrews, 2007).

2.1.7 Selectivity and resistance profiles of kinase inhibitors

In order to minimize the side effects of kinase inhibitors in patients, selective inhibition of only a few kinases is essential. Type I, type II and allosteric inhibitors have varying degrees of selectivity (Karaman et al., 2008). As the catalytic cleft of all kinases exhibit a similar conformation in the active state (Figure 2.7a), inhibitors that target the active form of kinases (type I) exhibit poor kinase selectivity. In contrast, inhibitors that target the specific inactive conformation of kinase (type II) achieve a high degree of selectivity relative to type I inhibitors. This is because structures of inactive forms of kinases are much more varied and specific for a particular kinase (Figure 2.7b) (Liu and Gray, 2006; Johnson, 2009). For example, imatinib recognizes a specific Abl/c-Kit like inactive conformation in Abl kinase and does not bind to Src kinase, which adopts a different Src/Cdk like inactive conformation. Abl and Src kinases look very similar in their active state and therefore dasatinib, a type I inhibitor binds to both kinases. Allosteric or type III inhibitors exhibit the highest degree of selectivity because they bind outside the conserved A-pocket and recognize unique binding pockets in the back cleft (Zhang *et al*., 2009).

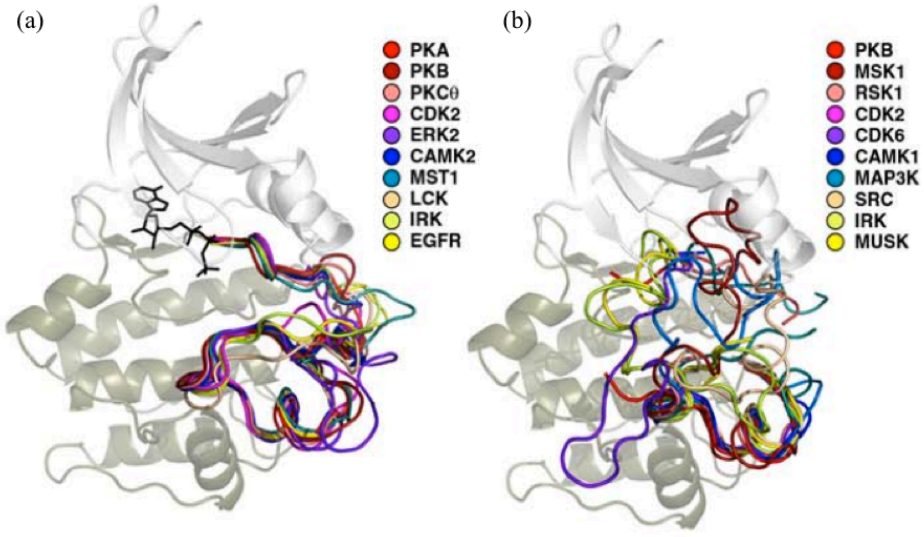

Figure 2.7. Conformation of the activation segment in different kinases present in active and inactive states: (a) Since there is a need for catalysis, activation segments of kinases have a highly conserved conformation in their active state; and **(b)** Geometry of the activation segment changes significantly and is not structurally conserved upon inactivation. Figure reprinted with permission from Elsevier: Trends in Biochemical Sciences, (Taylor and Kornev, 2011).

In addition to selectivity, drug-resistant mutations in patients have become a significant issue in kinase-targeted anticancer therapy. A number of resistant mutations have been detected in the catalytic and regulatory domains of kinases. The majority of the resistant mutations can be grouped into two classes: (i) mutations within the catalytic cleft, which directly impair drug binding by loss of bonded/steric interactions; and (ii) allosteric drug-resistant mutations, which indirectly impair drug binding by shifting the conformation of the kinase towards the active form. Allosteric drug-resistant mutations emerge as a result of targeting a specific inactive conformation of the kinase, which imposes a strong selective pressure for cells to acquire mutations that activate kinases and impair drug binding (Krishnamurthy and Maly, 2010).

Comprehensive analysis of the selectivity and resistance profiles of kinase inhibitors has revealed that the two different profiles are related to one another (Figure 2.8). As shown in the case of Abl kinase (Figure 2.4), kinases can adopt multiple conformations. The specificity of these structures is increased from the active to the inactive conformation. Therefore, type II inhibitors targeting a specific inactive conformation of the kinase have narrow selectivity profiles. However, these inhibitors are affected by a large number of allosteric activating mutations leading to broad resistant mutation profiles. On the other hand, type I inhibitors targeting less specific (active) or multiple conformations of the kinase possess broad selectivity and narrow resistant mutation profiles (Liao, 2007b).

2.2. Lariat peptide technology

In order to perform reverse analysis with cyclic peptides using genetic assays, we developed a new technology (Barreto *et al*., 2009) that generates lariat cyclic peptides against any protein of interest. Lariat peptides are lactone-cyclized peptides, which consist of a "noose" region with a covalently attached transcription activation domain. Lariats with known sequences or lariat peptide libraries are generated by engineering specific mutations to the intein cyclic peptide producing system (Scott *et al*., 1999), which halts the cyclic peptide reaction at an intermediate step and produces a lariat (Figure 2.9). The transcription activation domain is incorporated into the lariat in order to facilitate the screening of a combinatorial lariat peptide library against a known target using the yeast two-hybrid (Y2H) interaction trap (Figure 2.10). Using this technology, we have isolated lariats against different classes of proteins and characterized them *in vitro* and *in vivo*.

(a) Imatinib

(b) Dasatinib

(c)

	IC_{50} (nM)	
	Imatinib	Dasatinib
WT Abl	280	0.6
M244V	220	0.8
G250E	1,650	0.3
Q252H	nd	nd
Y253F	4,300	0.4
Y253H	>5,000	1.8
E255K	>5,000	0.2
E255V	3700	0.6
F311L	800	0.9
T315I	>5,000	>10,000
F317L	800	0.9
M351T	440	0.1
F359V	900	0.5
V379I	950	0.7
L387M	825	0.5
H396P	2,000	0.5
H396R	1,400	0.8
Src	>5,000	0.8
Lyn	>5,000	2.8

Figure 2.8. Selectivity and resistant mutation profiles of a kinase inhibitor are correlated with each other: (a) kinome interaction map for imatinib, a type II inhibitor; **(b)** kinome interaction map for dasatinib, a type I inhibitor; and **(c)** resistant mutation profiles of imatinib and dasatinib. Type II inhibitors have narrow selectivity and broad resistant mutation profiles. Type I inhibitors have broad selectivity and narrow resistant mutation profiles. Figures 2.8(a) and 2.8(b) reprinted with permission from Macmillan Publishers Ltd: Nature Biotechnology, (Karaman *et al*., 2008). Table (2.8c) modified and redrawn from O'Hare *et al*., 2005.

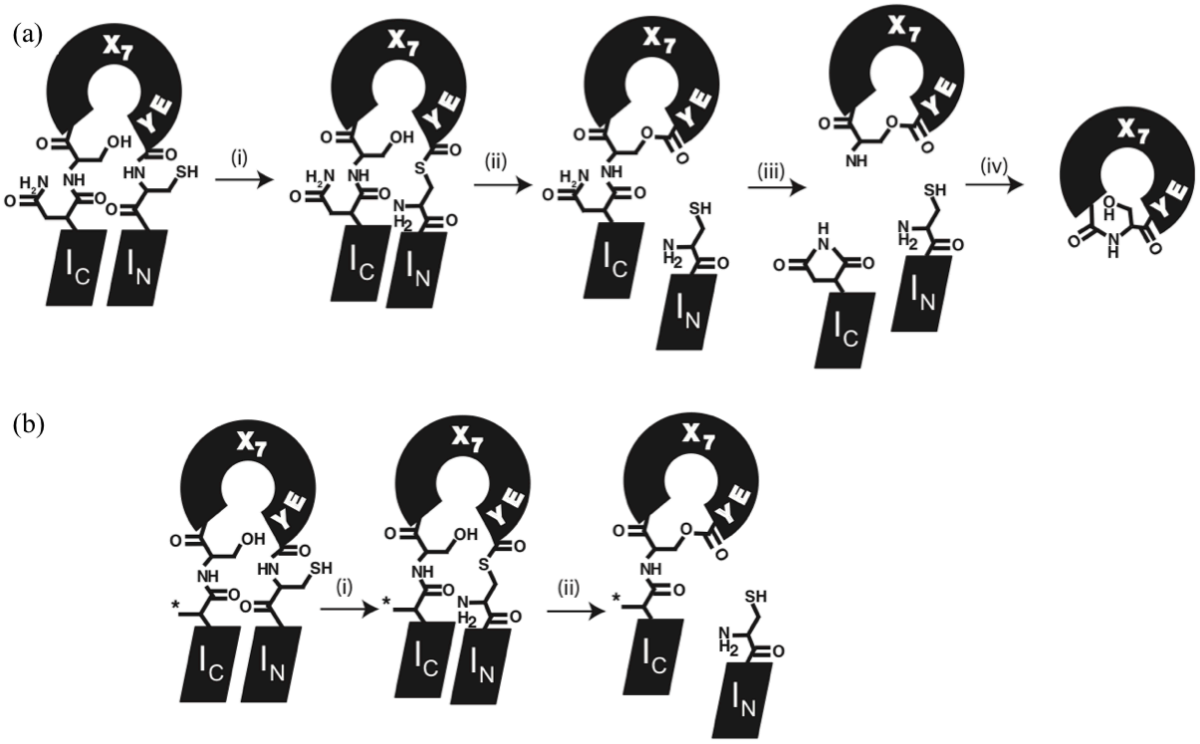

Figure 2.9. Schematic of intein processing: (a) Intein mediated cyclic peptide production: Inteins are naturally occurring proteins, which catalyze a self-splicing reaction by removing themselves from the precursor protein. This reaction results in the ligation of exteins and produces the mature protein. In order to catalyze a cyclization reaction using inteins, the order of the intein domains are permutated by protein engineering (I_N-extein-I_C to I_C-extein-I_N), which enables the head to tail cyclization of the extein. I_N and I_C represent N-terminal and C-terminal domains of intein. The cyclization reaction proceeds in four steps: (i) Unprocessed intein undergoes an N-to-S acyl shift using the I_{N+1} Cys at the peptide-I_N junction; (ii) Transesterification reaction involving I_{C+1} Ser at the I_C-peptide junction and the thioester formed in step (i), which releases the I_N domain and produces the lariat intermediate; (iii) I_{C-1} Asn undergoes a side chain cyclization, which releases the I_C domain and generates a lactone-cyclized peptide; and (iv) Lactone-cyclized peptide undergoes a thermodynamically favored O-to-N acyl shift to produce a lactam-cyclized peptide. **(b) Intein mediated lariat peptide production:** Lariat peptides are produced by mutating the Asn at position I_{C-1} to Ala (*), which inhibits asparagine cyclization and stops the reaction at the lariat intermediate. The lariat is useful for applications such as yeast two-hybrid screening, allowing a transcription activation domain to be attached to the N-terminus of the lariat (I_C domain). In this way libraries of genetically encoded cyclic peptides can be screened for an interaction with a target protein. X_7-EY represents the peptide "noose" region, which codes for a seven random amino acids, followed by Glu and Tyr. Figure reprinted with permission from Elsevier: Chemistry and Biology, (Barreto *et al*., 2009).

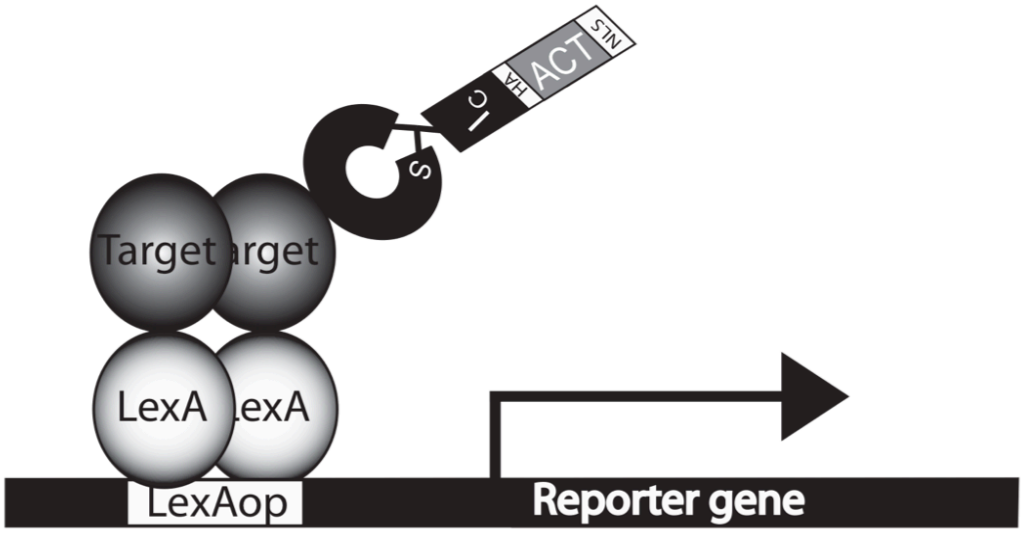

Figure 2.10. Lariat yeast two-hybrid interaction trap: The LexA operator (LexAop) is upstream of stably integrated *LEU2, ADE2, and LacZ* reporter genes. Plasmid pEG202 expresses LexA-target protein fusion, which binds to the LexA operator. Plasmid pIN01 expresses members of the lariat library that contain the peptide "noose" region and the I_C domain fused to an N terminus haemagglutinin (HA) tag, a transcription activation domain (ACT), and a nuclear localization sequence (NLS). Lariats that interact with the target protein bring the transcription activation domain near the transcription start sites of the reporter genes and activate transcription. The identity of the interacting lariat is determined by sequencing the genetic material that encodes the lariat (Figure modified from Barreto, 2010).

In addition to the validation of new druggable surfaces on the targets, the lariat peptide technology can serve many purposes and has multiple advantages: (i) Lariats inhibit their protein targets directly and function as *trans* dominant inhibitors. They block specific interactions with a protein while leaving other interactions unperturbed. This is in contrast to other reagents like antisense RNA/DNA, ribozymes, and RNAi that block transcription and translation of their target; (ii) Lariats are easily and rapidly generated against any target in a cost effective manner. Thus, they are easier to generate than small molecules or antibodies; (iii) Lariats are constrained by a lactone bond, allowing them to be used in reducing intracellular environments. This is in contrast to disulfide bond-constrained peptides, which are not stable under reducing conditions and must be screened using *in vitro* selection strategies such as phage display; (iv) Lariats are amenable to chemical synthesis and synthetic lariats are well suited for biophysical and structural studies. This is in contrast to peptide aptamers that cannot be chemically synthesized but are only over-expressed and purified; (v) The transcription

activation domain of lariats can be replaced by other chemical moieties such as affinity tags, fluorescent molecules, localization sequences, membrane permeable peptides, etc., which give them advantages over ‘‘head-to-tail’’ cyclized peptides that have no free end to attach moieties. Together, these properties make lariats ideal reagents for performing forward and reverse analysis of cellular processes or protein function (Barreto *et al*., 2009).

3. Objective and Specific Aims

A number of drug discovery programs have demonstrated that the ATP binding pocket of kinases are remarkably adaptable for the design of inhibitors. Despite the substantial achievements in this field, design of novel inhibitors with high degrees of specificity remains a major challenge. As the vast majority of inhibitors predominantly occupy the highly conserved adenine-binding pocket, it becomes essential to exploit the less conserved adjacent pockets, in order to design highly specific next-generation drugs. Lariat peptides, 7-10 amino acids in length, provide an avenue to identify and validate new druggable surfaces located in the kinase catalytic cleft, as they are larger than small molecule drugs. This additional size provides added functionality that could be used to bind the ATP binding pocket as well as surfaces adjacent to this pocket. Further, lariats have the potential to easily generate useful structure-activity relationship data for rational drug design, in a rapid and cost-effective manner. Taking advantage of our established lariat peptide technology, the **objective** of this thesis is to isolate and characterize ATP competitive lariats of Abl kinase, a drug target important in chronic myelogenous leukemia and other disorders. To achieve this objective, the following aims were devised.

Specific Aim 1: Isolate lariat peptide inhibitors of Abl SH1 from the combinatorial *Ssp*-*Ssp* R7 lariat library and characterize their mechanism of action.

Specific Aim 2: Delineate important residues of the lariat and generate tighter-binding variants of the lariat.

Specific Aim 3: Characterize the activity of Abl SH1-interacting lariats *in vitro* and *in vivo*, and evaluate their selectivity and resistant mutation profiles.

4. Materials and Methods

4.1 General Information

4.1.1 Strains

Table 4.1: *E. coli* strains and genotypes

Strain	Genotype	Source/Reference
XL1-Blue	*recA1 endA1 gyrA96 thi-1 hsdR17 supE44 relA1 lac (F′ proAB lacI^{q}ZΔM15 Tn10 (Tet^r))*	Stratagene
MC1061	*F$^-$ araD139 Δ(araA-leu)7697 galE15 galK16 Δ(lac)X74 rpsL (Str^r) hsdR2 ($r_K^- m_K^+$) mcrA mcrB1*	Wertman *et al.*, 1986
ER2925	*ara-14 leuB6 fhuA31 lacY1 tsx78 glnV44 galK2 galT22 mcrA dcm-6 hisG4 rfbD1 R(zgb210::Tn10)TetS endA1 rpsL136 dam13::Tn9 xylA-5 mtl-1 thi-1 mcrB1 hsdR2*	New England Biolabs
BL21 (DE3)	*F$^-$ ompT gal dcm lon hsdS$_B$ ($r_B^- m_B^-$) λ(DE3 [lacI lacUV5-T7 gene 1 ind1 sam7 nin5])*	Novagen

Table 4.2: *S. cerevisiae* strains and genotypes

Strain	Genotype	Reference
EY93	MATa *ura2 his3 trp1 leu2 ade2::URA3*	Barreto *et al*., 2009
EY111	MATα *his3 trp1 ura3*::LexA8op-*LacZ ade2::URA3*-LexA8op-*ADE2 leu2::*LexA6op-*LEU2*	Barreto *et al*., 2009

4.1.2 Antibodies

Table 4.3: Primary and secondary antibodies and their suppliers

Antibody	Supplier
Mouse Anti HA antibody	Santa Cruz Biotechnology Inc.
Rabbit Anti FLAG antibody	Sigma-Aldrich
Rabbit Anti Hck antibody	Santa Cruz Biotechnology Inc.
Rabbit Anti p-Hck (Y411) antibody	Santa Cruz Biotechnology Inc.
Rabbit Anti c-Abl antibody	Cell Signaling Technology
Rabbit Anti p-c-Abl (Y412) antibody	Cell Signaling Technology
Goat Anti-Mouse LI-COR IR dye (680 and 800CW)	LI-COR Biosciences
Goat Anti-Rabbit LI-COR IR dye (680 and 800CW)	LI-COR Biosciences

4.1.3 Synthetic Peptides

Linear and lariat peptides were synthesized by Genscript and Peptide Protein Research, respectively. Linear peptides were acetylated at their N-terminus and amidated at their C-terminus. Lariat versions were created by cyclizing the side chain of serine and the C-terminal carboxylic acid via an ester bond. Lariat peptides were acetylated at their N-terminus. Sequences of the synthetic peptides can be found in sections 5.1.3 and 5.3.2.

4.1.4 Oligonucleotides

Oligonucleotides were synthesized by Integrated DNA Technologies. Their sequences in 5' to 3' orientation are given in the following table. Serial numbers are used to reference the oligonucleotides in the text. P1, P2, Seq and Temp represent forward primer, reverse primer, sequencing primer and template, respectively. Oligonucleotides are represented by one letter nucleotide codes, where N = (A, C, T, G) and K = (G, T).

Table 4.4: Oligonucleotide sequences

S.No	Name	Sequence
1	pEG202 Seq P1	GGG CTG GCG GTT GGG GTT ATT C
2	pEG202 Seq P2	CAT GCC GGT AGA GGT GTG GTC AA
3	pJG4-5 Seq P1	GGA CAG GAG ATG CCG ATG GA
4	pJG4-5 Seq P2	GCA AGG TAG ACA AGC CGA CAA C
5	Inactive A1 Temp	ATT GCT CAC GCT TCT GGT TGG CAG CGG CTG CCT TTT GAA TAC GCT TTG TCT TTC GGT ACT
6	Inactive A2 Temp	ATT GCT CAC GCT TCT GGG TGG CAT CGT CTT AGT GAG GAA TAC GCT TTG TCT TTC GGT ACT
7	Linear A1 Temp	ATT GCT CAC GCT TCT GGT TGG CAG CGG CTG CCT TTT GAA TAC TAA CTC GAG AAG CTT TGG
8	Linear A2 Temp	ATT GCT CAC GCT TCT GGG TGG CAT CGT CTT AGT GAG GAA TAC TAA CTC GAG AAG CTT TGG
9	*Ssp*-I_C Ins Amp P1	GAT ATT GGT TTG CCA CAA GAT CAC AAC TTC TTG TTG GCT AAC GGT GCT ATT GCT CAC GCT
10	*Ssp*-I_N Ins Amp P2	ATC TTA CCA ATT GGC AAT GGA CCG TAT TCA ACA GTC AAA ATT TCA GTA CCG AAA GAC AA
11	Linear Ins Amp P2	CAA CCT TGA TTG GAG ACT TGA CCA AAC CTC TGG CGA AGA AGT CCA AAG CTT CTC GAG TTA
12	Lariat A1 Temp	ATT GCT CAC GCT TCT GGT TGG CAG CGG CTG CCT TTT GAA TAC TGT TTG TCT TTC GGT ACT
13	A1/G1 Random Temp	ATT GCT CAC GCT TCT NNK TGG CAG CGG CTG CCT TTT GAA TAC TGT TTG TCT TTC GGT ACT
14	A1/W2 Random Temp	ATT GCT CAC GCT TCT GGT NNK CAG CGG CTG CCT TTT GAA TAC TGT TTG TCT TTC GGT ACT

15	A1/Q3 Random Temp	ATT GCT CAC GCT TCT GGT TGG NNK CGG CTG CCT TTT GAA TAC TGT TTG TCT TTC GGT ACT
16	A1/R4 Random Temp	ATT GCT CAC GCT TCT GGT TGG CAG NNK CTG CCT TTT GAA TAC TGT TTG TCT TTC GGT ACT
17	A1/L5 Random Temp	ATT GCT CAC GCT TCT GGT TGG CAG CGG NNK CCT TTT GAA TAC TGT TTG TCT TTC GGT ACT
18	A1/P6 Random Temp	ATT GCT CAC GCT TCT GGT TGG CAG CGG CTG NNK TTT GAA TAC TGT TTG TCT TTC GGT ACT
19	A1/F7 Random Temp	ATT GCT CAC GCT TCT GGT TGG CAG CGG CTG CCT NNK GAA TAC TGT TTG TCT TTC GGT ACT
20	A1/E8 Random Temp	ATT GCT CAC GCT TCT GGT TGG CAG CGG CTG CCT TTT NNK TAC TGT TTG TCT TTC GGT ACT
21	A1/Y9 Random Temp	ATT GCT CAC GCT TCT GGT TGG CAG CGG CTG CCT TTT GAA NNK TGT TTG TCT TTC GGT ACT
22	*Ssp*-I_C Ins Amp New P1	ATT GGT TTG CCA CAA GAT CAC AAC TTC TTG TTG GCT AAC GGT GCT ATT GCT CAC GCT TCT
23	*Ssp*-I_N Lar Ins Amp P2	CTT ACC AAT TGG CAA TGG ACC GTA TTC AAC AGT CAA AAT TTC AGT ACC GAA AGA CAA ACA
24	TG1 Lariat Temp	ATT GCT CAC GCT TCT GGT TGG CAG ACG CTG GAT TTT GAA TAC TGC TTG TCT TTC GGT ACT
25	TG2 Lariat Temp	ATT GCT CAC GCT TCT GGT TGG CAG ACG CTG CCT TGG GAA TAC TGC TTG TCT TTC GGT ACT
26	TG3 Lariat Temp	ATT GCT CAC GCT TCT GGT TGG CAG ACG CTG CCT TAT GAA TAC TGC TTG TCT TTC GGT ACT
27	TG4 Lariat Temp	ATT GCT CAC GCT TCT GGT TGG CAG ACG CTG CCT TTT AAT TAC TGC TTG TCT TTC GGT ACT
28	TG5 Lariat Temp	ATT GCT CAC GCT TCT GGT TGG CAG CGG CTG GAT TGG GAA TAC TGC TTG TCT TTC GGT ACT
29	TG6 Lariat Temp	ATT GCT CAC GCT TCT GGT TGG CAG CGG CTG GAT TAT GAA TAC TGC TTG TCT TTC GGT ACT
30	TG7 Lariat Temp	ATT GCT CAC GCT TCT GGT TGG CAG CGG CTG GAT TTT AAT TAC TGC TTG TCT TTC GGT ACT
31	TG8 Lariat Temp	ATT GCT CAC GCT TCT GGT TGG CAG CGG CTG CCT TGG AAT TAC TGC TTG TCT TTC GGT ACT
32	TG9 Lariat Temp	ATT GCT CAC GCT TCT GGT TGG CAG CGG CTG CCT TAT AAT TAC TGC TTG TCT TTC GGT ACT
33	TG10 Lariat Temp	ATT GCT CAC GCT TCT GGT TGG CAG ACG CTG GAT TGG GAA TAC TGC TTG TCT TTC GGT ACT
34	TG11 Lariat Temp	ATT GCT CAC GCT TCT GGT TGG CAG ACG CTG GAT TAT GAA TAC TGC TTG TCT TTC GGT ACT
35	TG12 Lariat Temp	ATT GCT CAC GCT TCT GGT TGG CAG ACG CTG GAT TTT AAT TAC TGC TTG TCT TTC GGT ACT
36	TG13 Lariat Temp	ATT GCT CAC GCT TCT GGT TGG CAG CGG CTG GAT TGG AAT TAC TGC TTG TCT TTC GGT ACT
37	TG14 Lariat Temp	ATT GCT CAC GCT TCT GGT TGG CAG CGG CTG GAT TAT AAT TAC TGC TTG TCT TTC GGT ACT

38	TG15 Lariat Temp	ATT GCT CAC GCT TCT GGT TGG CAG ACG CTG CCT TGG AAT TAC TGC TTG TCT TTC GGT ACT
39	TG16 Lariat Temp	ATT GCT CAC GCT TCT GGT TGG CAG ACG CTG CCT TAT AAT TAC TGC TTG TCT TTC GGT ACT
40	TG17 Lariat Temp	ATT GCT CAC GCT TCT GGT TGG CAG ACG CTG GAT TGG AAT TAC TGC TTG TCT TTC GGT ACT
41	TG18 Lariat Temp	ATT GCT CAC GCT TCT GGT TGG CAG ACG CTG GAT TAT AAT TAC TGC TTG TCT TTC GGT ACT
42	ΔE8 A1 Lariat Temp	ATT GCT CAC GCT TCT GGT TGG CAG CGG CTG CCT TTT TAC TGC TTG TCT TTC GGT ACT
43	ΔN8 TG17 Lariat Temp	ATT GCT CAC GCT TCT GGT TGG CAG ACG CTG GAT TGG TAC TGC TTG TCT TTC GGT ACT
44	ΔN8 TG18 Lariat Temp	ATT GCT CAC GCT TCT GGT TGG CAG ACG CTG GAT TAT TAC TGC TTG TCT TTC GGT ACT
45	Inactive TG17 Temp	ATT GCT CAC GCT TCT GGT TGG CAG ACG CTG GAT TGG AAT TAC GCT TTG TCT TTC GGT ACT
46	Inactive TG18 Temp	ATT GCT CAC GCT TCT GGT TGG CAG ACG CTG GAT TAT AAT TAC GCT TTG TCT TTC GGT ACT
47	Linear TG17 Temp	ATT GCT CAC GCT TCT GGT TGG CAG ACG CTG GAT TGG AAT TAC TAA CTC GAG AAG CTT TGG
48	Linear TG18 Temp	ATT GCT CAC GCT TCT GGT TGG CAG ACG CTG GAT TAT AAT TAC TAA CTC GAG AAG CTT TGG
49	pMSCV *Ssp*-I_C P1	GG GAATTC ATG TAC CCA TAC GAT GTT CCA GAT TAC GCT ATG GTT AAG GTT ATT GGT AGA
50	pMSCV *Ssp*-I_N P2	GG CTCGAG TTA CTT ATC ATC ATC ATC CTT GTA ATC CTT AAT AGT ACC AGC ATC CAA CAA
51	pMSCV Seq P1	CCC TTG AAC CTC CTC GTT CGA CC
52	pMSCV Seq P2	GAG ACG TGC TAC TTC CAT TTG TC
53	Abl T315I P1	AG CCC CCG TTC TAT ATC ATC ATT GAG TTC ATG ACC
54	Abl T315I P2	GGT CAT GAA CTC AAT GAT GAT ATA GAA CGG GGG CT
55	Abl Y253F P1	TG GGC GGG GGC CAG TTC GGG GAG G
56	Abl Y253F P2	C CTC CCC GAA CTG GCC CCC GCC CA
57	Abl E355G P1	A GCC ATG GAG TAC CTG GGG AAG AAA AAC TTC ATC C
58	Abl E355G P2	G GAT GAA GTT TTT CTT CCC CAG GTA CTC CAT GGC T
59	Abl H396R P1	C ACC TAC ACA GCC CGT GCT GGA GCC AAG T
60	Abl H396R P2	A CTT GGC TCC AGC ACG GGC TGT GTA GGT G
61	Abl H396P P1	C ACC TAC ACA GCC CCT GCT GGA GCC AAG T
62	Abl H396P P2	A CTT GGC TCC AGC AGG GGC TGT GTA GGT G

4.1.5 Plasmids

Five plasmids were used in this study. pEG202 and pIN01 plasmids were used for Y2H assays. pET28a and pCDFDuet-1 plasmids were used to coexpress proteins in *E. coli*. pMSCV-YFP plasmid was used to express intein peptides in mammalian cells. Plasmid maps and details are given in Figures 4.1 to 4.5. The following plasmid maps were created using PlasMapper (Dong *et al*., 2004).

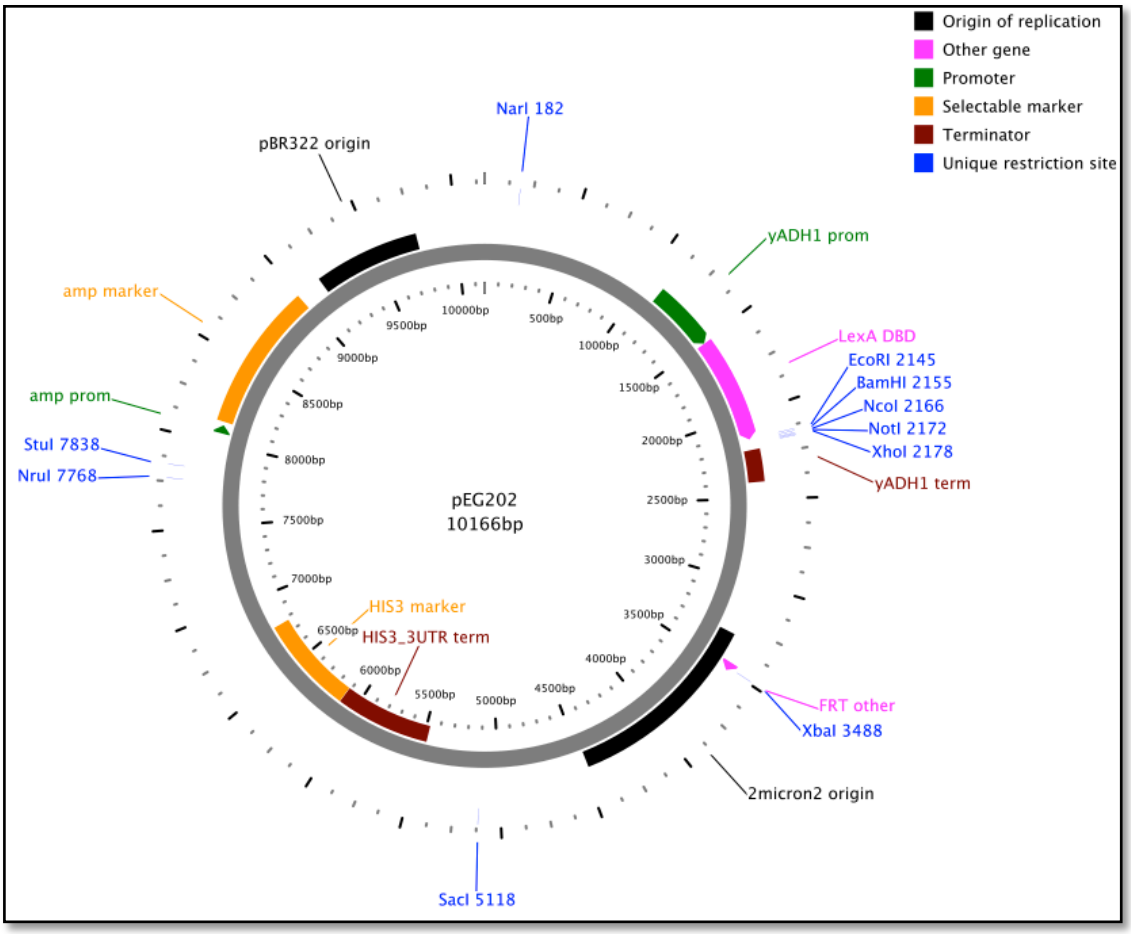

Figure 4.1. pEG202 plasmid: pEG202 (GenBank accession U89960) was used as a bait plasmid in the lariat Y2H interaction trap. Targets were cloned between the *EcoR*I and *Xho*I restriction sites using homologous recombination. Cloned targets were expressed constitutively as a fusion to the LexA DNA binding domain (DBD) in EY111. The plasmid has yeast alcohol dehydrogenase promoter (yADH1 prom) and yeast alcohol dehydrogenase terminator (yADH1 term) to promote and terminate transcription, respectively. The yeast 2µ origin enables autonomous replication of the plasmids in *S. cerevisiae.* An auxotrophic selectable marker (*HIS3* gene) is used to select and maintain the vectors in yeast cells. The pBR322 origin allows for replication in *E. coli* and the ampicillin-resistance gene (amp marker) allows for selection in *E. coli*.

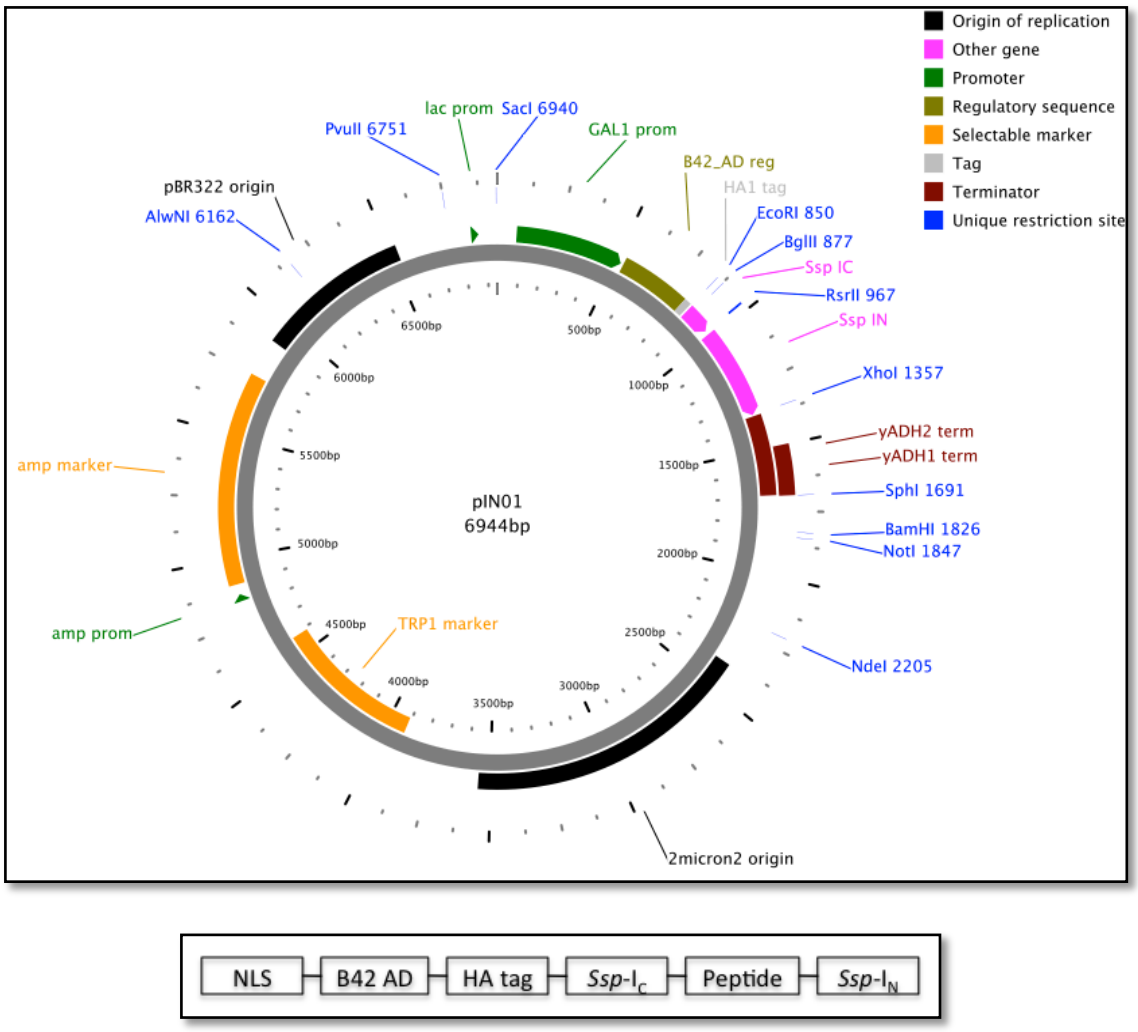

Figure 4.2. pIN01 plasmid (top) and the construct expressed from the plasmid (bottom): pIN01 was used as a prey plasmid in the lariat Y2H interaction trap. The plasmid contains *Ssp*-I_C and *Ssp*-I_N domains separated by *Rsr*II restriction site. The intein domains are cloned as C-terminal fusions to the Y2H machinery present in the plasmid backbone. The *Rsr*II site is used to clone peptide libraries into the plasmid. The galactose promoter (GAL1 prom) is used to drive the expression of intein peptides fused to the Y2H machinery. The construct expressed from the plasmid is shown in the bottom figure, where NLS, B42 AD and HA tag refer to nuclear localization sequence, B42 activation domain, and haemagglutinin tag, respectively. The plasmid has yeast alcohol dehydrogenase terminator (yADH1/2 term) to terminate transcription. The yeast 2µ origin enables autonomous replication of the plasmids in *S. cerevisiae.* An auxotrophic selectable marker (*TRP1* gene) is used to select and maintain the vectors in yeast cells. The pBR322 origin allows for replication in *E. coli* and the ampicillin-resistance gene (amp marker) allows for selection in *E. coli*.

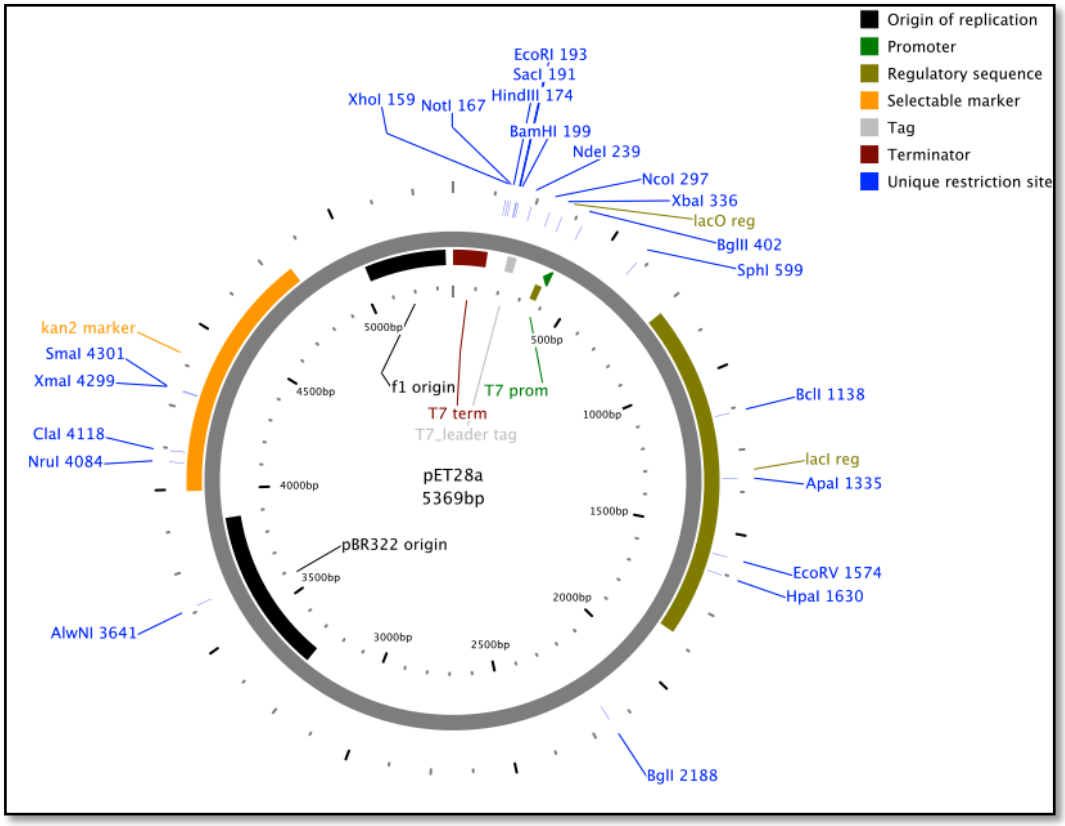

Figure 4.3. pET28a plasmid: pET28a is an *E. coli* expression plasmid. Generally, the proteins are expressed with a N-terminal His tag-thrombin-T7 tag sequence and/or a C-terminal His tag sequence using this plasmid. Protein expression is controlled with an IPTG inducible promoter (T7 promoter). T7 terminator is used to terminate transcription. The pBR322 origin enables the replication of plasmids in *E. coli*. The kanamycin-resistance gene (kan2 marker) is used to select and maintain the vectors in the host. We used this plasmid to express human Abl SH3-SH2-SH1 construct (residues 64-515 c-Abl 1b numbering) in *E. coli*. The construct was subcloned between the *Nde*I and *Xho*I restriction sites in the vector modified to yield a tobacco etch virus (TEV) protease cleavable N-terminal His tag. The modified pET28a-Abl SH3-SH2-SH1 plasmid was kindly provided by Dr. John Kuriyan.

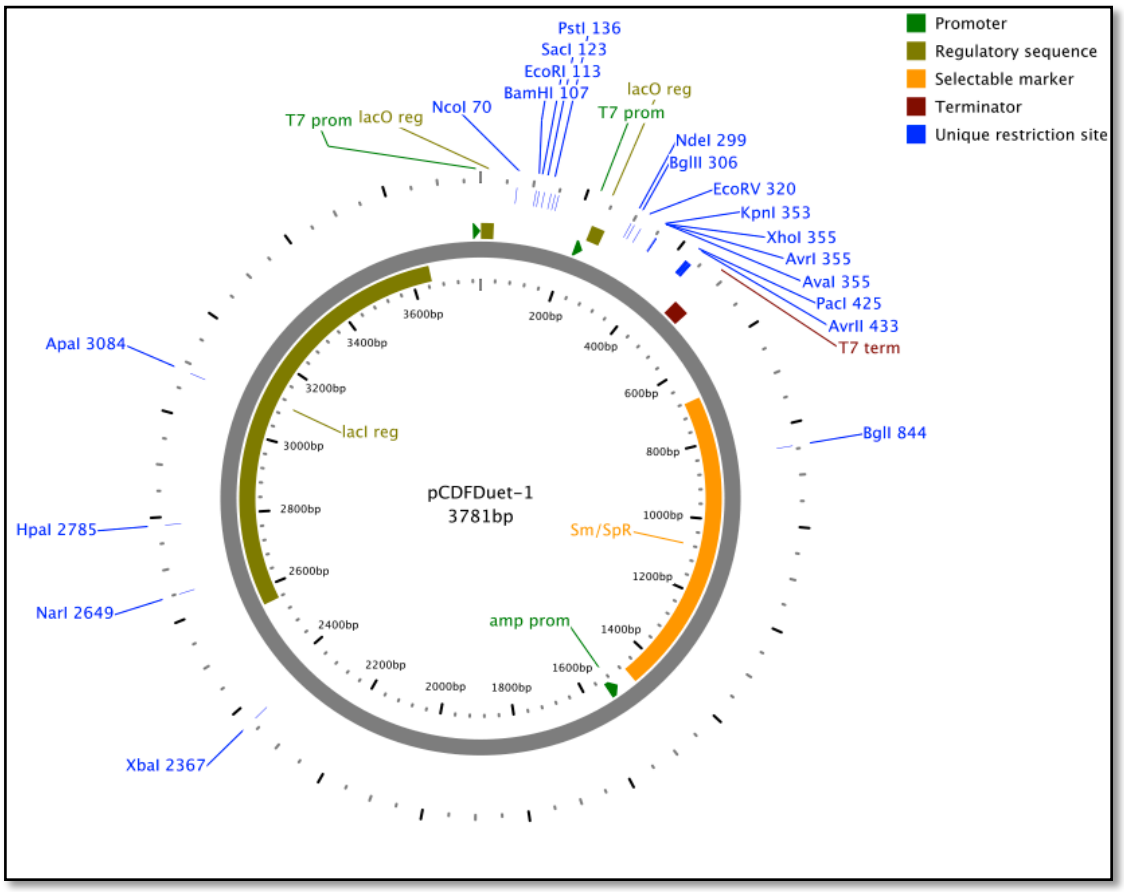

Figure 4.4. pCDFDuet-1 plasmid: pCDFDuet-1 is an *E. coli* expression plasmid designed for the coexpression of two proteins. The vector contains two T7 promoters and two multiple cloning sites (MCS). The T7 promoter is an IPTG inducible promoter. The T7 terminator is used to terminate transcription. There is a His tag sequence at the N-terminus of the MCS1 and a S-tag sequence at the C-terminus of the MCS2. CloDF13-derived CDF replicon enables the replication of plasmids in *E. coli*. The spectinomycin/streptomycin-resistance gene (Sm/SpR) is used to select and maintain the vectors in the host. We used this vector to coexpress *Yersinia pestis* tyrosine phosphatase (YopH) in *E. coli* with Abl kinase. YopH was subcloned between the *Nco*I (N-terminus to His tag and MCS1) and *Avr*II (MCS2) restriction sites in the plasmid to express an untagged YopH construct. His tagged Abl kinase was expressed from the pET28a vector (Figure 4.3). This YopH coexpression maintains the over-expressed tyrosine kinases in the dephosphorylated state and helps to overcome the toxic effects of protein tyrosine kinase activity in *E. coli*. The pCDFDuet-1-YopH plasmid was kindly provided by Dr. John Kuriyan.

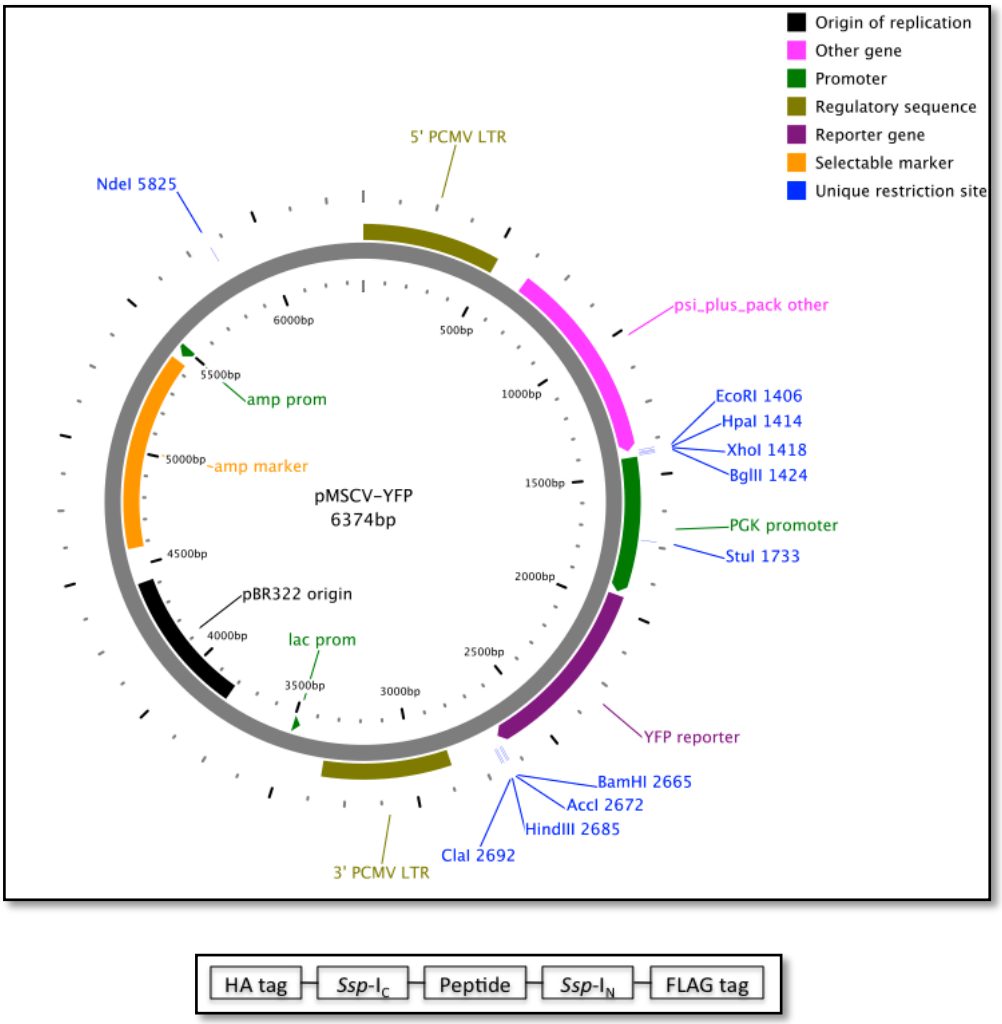

Figure 4.5. pMSCV-YFP plasmid (top) and the gene of interest subcloned into the plasmid (bottom): pMSCV is a murine stem cell virus vector. Generally, pMSCV is used to produce high-titer, replication-incompetent, infectious retrovirus particles in packaging cell lines. These particles can infect target cells and transmit the gene of interest to them. Upon transfection, pMSCV can transiently or stably express a transcript containing the extended viral packaging signal Ψ+, a gene of interest, and the yellow fluorescent protein (YFP) marker. To achieve high-level gene expression in mammalian cells and hematopoietic/embryonic stem cells, the vector harbors a specifically designed 5' long terminal repeat (LTR) derived from the murine stem cell PCMV virus. The murine phosphoglycerate kinase (PGK) promoter controls expression of the YFP marker. The pBR322 origin allows for replication in *E. coli* and the ampicillin-resistance gene (amp marker) allows for selection in *E. coli*. The intein peptides with appropriate tags for detection at N- and C- termini (bottom figure) were directionally subcloned into the pMSCV vector using the *EcoR*I and *Xho*I restriction sites. The MSCV-YFP plasmid was kindly provided by Dr. Craig Jordan.

4.2 General Molecular Biology Protocols

4.2.1 Agarose gel electrophoresis

To visualize DNA or to determine the size of DNA, samples (PCR products/plasmids) were mixed with 6x loading dye (50% (v/v) glycerol, 0.2 M EDTA pH 8.3, 0.05% (w/v) bromophenol blue) to achieve a final dye concentration of 1x. The samples were resolved in an agarose gel consisting of 0.5 to 2% (w/v) ultrapure agarose in 1x TAE Buffer (40 mM Tris-acetate, 1 mM EDTA, pH 8.0) and 0.5 μg/mL ethidium bromide. Gels were run at a constant voltage between 150-200 V for 20 to 40 minutes in 1x TAE Buffer and photographed using a UV light transilluminator (Bio-Rad).

4.2.2 DNA Purification

PCR products and restriction enzyme digested plasmids were purified using PCR clean-up kit (Qiagen/Bio-Basic) and gel purification kit (Qiagen/Bio-Basic), respectively, according to manufacturer's instructions.

4.2.3 Site directed mutagenesis

Mutations were generated in the pEG202-Abl SH1 plasmid using Quikchange II XL site directed mutagenesis kit (Stratagene) as per manufacturer's directions. All mutations were confirmed by sequence analysis. Mutagenic primers (oligonucleotides 53-62) and sequencing primers (oligonucleotides 1 and 2) are listed in Table 4.4.

4.2.4 DNA sequencing

Samples (plasmids/PCR products) were sent to the Plant Biotechnology Institute, National Research Council of Canada for sequencing.

4.2.5 SDS- PAGE and Western analysis

Samples for SDS-PAGE were prepared by suspending the proteins or *E. coli* cells in 4x SDS loading dye (240 mM Tris-HCl pH 6.8, 20% (v/v) glycerol, 8% (w/v) SDS, 16% (v/v) 2-mercaptoethanol, 0.01% (w/v) bromophenol blue). Samples from yeast cells were prepared in the same way except that the cells were first suspended in 200 μL of 0.1 M NaOH and incubated for 5 min at room temperature. Prior to loading, all samples were boiled for 5 min and cooled.

SDS-PAGE was performed as described by Laemmli (Laemmli, 1970) using a Mini-Protean 3 electrophoresis unit (Bio-Rad). Briefly, sample fractions were resolved on a 4-12% polyacrylamide gel in 1x running buffer (25 mM Tris-HCl pH 8.3, 190 mM glycine, 0.1% (w/v) SDS) at a constant voltage of 200 V for 45 min. A 4% stacking gel contained 0.125 M Tris-HCl pH 6.8, 0.1% SDS, 4% degassed acrylamide:bis-acrylamide (37.5:1), 0.1% (v/v) TEMED, and 0.05% (w/v) ammonium persulphate. A 12% resolving gel contained 0.375 M Tris-HCl pH 8.8, 0.1% SDS, 12% degassed acrylamide:bis-acrylamide (37.5:1), 0.05% (v/v) TEMED, and 0.05% (w/v) ammonium persulphate.

To visualize total proteins by Coomassie-staining, SDS-PAGE gels were incubated in staining solution (0.12% (w/v) Coomassie Brilliant Blue R-250, 50% methanol, 10% acetic acid) for 2 hours, and washed with destaining solution (40% methanol, 10% acetic acid) for several hours to overnight. Destained gels were visualized and photographed using a Gel-Doc imager (Bio-Rad).

To visualize specific proteins by Western analysis, proteins were transferred from SDS-PAGE gels to nitrocellulose membranes (Bio-Rad) using a semi-dry electrophoretic transfer cell (Trans-Blot). Transfer was performed at a constant voltage of 15 V for 20 min in the presence of transblot buffer (48 mM Tris-HCl pH 8.3, 39 mM glycine, 20% (v/v) methanol, 0.04% (w/v) SDS). Membranes were blocked with Odyssey blocking buffer (LI-COR Biosciences) for 1 hour at room temperature, and incubated overnight with primary antibody (diluted in Odyssey blocking buffer) at 4 °C. Membranes were washed 3 times with PBT (PBS with 0.1% Tween-20) and incubated with a fluorescently labeled secondary antibody (diluted in Odyssey blocking buffer) for 1 hour at room temperature. Membranes were washed two times with PBT, and one time with PBS. The blots were visualized and quantified using an Odyssey infrared imager (LI-COR Biosciences).

4.3 General *E. coli* Protocols

4.3.1 Propagation of *E. coli*

Standard procedures were used to culture and propagate *E. coli* (Elbing and Brent, 2002). Lysogeny broth (LB) was prepared with 1% (w/v) tryptone, 0.5% (w/v) yeast extract, 85.6 mM NaCl, and 1 mM NaOH in ddH_2O. Solid media contained 2% (w/v) agar. Ampicillin

was used at 100 μg/mL concentration. Kanamycin, spectinomycin and chloramphenicol were used at 50 μg/mL concentration.

4.3.2 Preparation of plasmid DNA from *E. coli*

Plasmid mini-preparation kits (Qiagen/Bio-Basic) and maxi-preparation kits (Qiagen) were used as described by the manufacturer.

4.3.3 *E. coli* transformation

Electrocompetent cells were prepared as described by Ausubel *et al*., 1988. Briefly, a fresh bacterial colony was transferred into 5 mL of LB media and grown overnight at 37 °C. The culture was diluted in 500 mL LB to an OD_{600} of 0.1–0.2 and allowed to reach an OD_{600} of 0.6–0.8. The cells were harvested and washed twice with 250 mL of ice cold ddH_2O by centrifugation at 4,000 x g for 20 min at 4 °C. The cells were washed finally with 20 mL of ice cold ddH_2O by centrifugation at 4,200 x g for 10 min at 4 °C. The cells were resuspended in one pellet volume of ice-cold 10% (v/v) glycerol and aliquots of 50 μL were stored at −80 °C.

Electrocompetent cells were transformed with plasmids by electroporation. Briefly, 1 μL of plasmid (50-150 ng/μL) was mixed with 50 μL of electrocompetent cells, and the mixture was transferred into an electroporation cuvette. The cuvette was subjected to a short electric pulse (field strength = 12.5 kV/cm) using a gene pulser (Bio-Rad). The cells were recovered immediately, transferred into 1 mL of pre-warmed LB media and incubated for 30 min at 37 °C. The cells were harvested and plated onto LB agar plates containing the appropriate antibiotic.

4.4 General Yeast Protocols

4.4.1 Propagation of yeast

Standard procedures were used to culture and propagate *S. cerevisiae* (Geyer and Brent, 2000). Rich media (YPDA) was prepared with 1% (w/v) yeast extract, 2% (w/v) peptone, 80 mg/L adenine, and 2% (w/v) dextrose. Complete synthetic media (CSM) was prepared with 0.67% (w/v) yeast nitrogen base without amino acids, appropriate CSM supplement mix, and either 2% (w/v) dextrose or a combination of 2% (w/v) galactose and 1% (w/v) raffinose. X-gal media was supplemented with 0.008% X-gal (dissolved in 100% dimethylformamide) and 1× BU salts (25 mM sodium phosphate buffer pH 7.0). Solid media contained 2% agar.

4.4.2 Preparation of plasmid DNA from yeast

Plasmids were isolated from yeast using the "smash and grab" procedure (Hoffman and Winston, 1987). Briefly, a yeast colony was transferred into 2 mL of appropriate synthetic amino acid dropout media and grown overnight at 30 °C. The culture was centrifuged at 18,000 x g for 30 seconds. The cells were resuspended in 200 µL breaking buffer (2% (v/v) Triton X-100, 1% (v/v) SDS, 100 mM NaCl, 10 mM Tris-HCl pH 8.0, 1 mM EDTA) followed by the addition of 300 µg glass beads and 200 µL phenol-chloroform-isoamylalcohol (25:24:1, v/v/v). The mixture was vortexed vigorously for 2 min and centrifuged at 18,000 x g for 5 min. 50 µL of the aqueous layer was collected and stored at – 20 °C.

4.4.3 Yeast transformation

Yeast competent cells were prepared according to the procedure described by Gietz and Schiestl in 2007. Briefly, a fresh yeast colony was transferred into 5 mL of appropriate media and grown overnight at 30 °C. The culture was diluted in 500 mL of appropriate media to an OD_{600} of 0.1–0.2 and allowed to reach an OD_{600} of 0.6–0.8. The cells were harvested and washed once with 250 mL of sterile ddH_2O by centrifugation at 3,000 x g for 5 min at 20 °C. The cells were resuspended in 5 ml of sterile frozen competent cell (FCC) solution (5% v/v glycerol, 10% v/v DMSO) and aliquots of 50 µL were stored at −80 °C.

Yeast competent cells were transformed with plasmids using the lithium acetate transformation procedure (Gietz and Schiestl, 2007). Cell samples (50 µL FCC aliquots) were thawed at 37 °C for 30 seconds and centrifuged at 13,000 x g for 2 min at 20 °C. The FCC solution (supernatant) was removed and the pellet was overlaid with 260 µL of 50% (w/v) polyethylene glycol 3350, 36 µL of 1 M LiOAc, 50 µL of 2 mg/mL single-stranded DNA, 0.1-1 µg plasmid (digested/undigested) and PCR insert (optional). The mixture was vortexed vigorously to resuspend the pellet, incubated for 30 min at 30 °C and heat shocked for 15 min at 42 °C. The sample was centrifuged at 13,000 x g for 30 seconds and the supernatant was removed. The pellet was resuspended in 100 µL ddH_2O and plated onto appropriate media.

4.5 Manipulation of the pIN01 plasmid

We manipulated pIN01 to derive plasmids that express desired inactive, lariat and linear peptides, and to construct random and focused libraries in yeast. A brief description about pIN01 is given in section 4.1.5.

4.5.1 Construction of inactive intein plasmids

To construct plasmids that express A1, A2, TG17 and TG18 inactive intein constructs, we PCR amplified oligonucleotides 5, 6, 45 and 46, respectively, using oligonucleotides 9 and 10 as primers. PCR reactions were performed in a 50 µL volume containing 1X PCR buffer (60 mM Tris-SO_4 (pH 8.9), 18 mM $(NH_4)_2SO_4$), 2 mM $MgSO_4$, 200 µM dNTPs, 0.4 µM forward primer, 0.4 µM reverse primer, 4 nM oligonucleotide template, and 1 Unit Platinum® Taq DNA Polymerase High Fidelity. The reaction mixtures were subjected to ten amplification cycles consisting of a denaturing step at 94 °C for 30 seconds, an annealing step at 50 °C for 30 seconds, and an extension step at 68 °C for 15 seconds. pIN01 was digested with *Rsr*II (New England Biolabs) according to manufacturer's directions and the digested plasmid was gel-purified. PCR products were cloned into *Rsr*II-cut, gel-purified pIN01 using *in vivo* homologous recombination (Ma *et al*., 1987; Hua *et al.*, 1997) in EY93. Lithium acetate transformations were performed as described earlier, with each transformation containing 30 µL of PCR product and 0.25 µg of *Rsr*II-cut, gel-purified pIN01. Resulting plasmids were isolated from yeast, transformed into *E. coli*, amplified, purified, and sequenced (using oligonucleotides 3 and 4).

4.5.2 Construction of linear peptide plasmids

To construct plasmids that express A1, A2, TG17 and TG18 linear peptides, we PCR amplified oligonucleotides 7, 8, 47 and 48, respectively, using oligonucleotides 9 and 11 as primers. PCR reactions were performed as described in section 4.5.1. pIN01 was digested with *Rsr*II and *Xho*I (New England Biolabs) according to manufacturer's directions, the two fragments were separated by gel electrophoresis, and the larger fragment was gel purified. PCR products were cloned into the gel-purified pIN01 fragment using *in vivo* homologous recombination (Ma *et al*., 1987; Hua *et al.*, 1997) in EY93. Lithium acetate transformations were performed as described earlier, with each transformation containing 30 µL of PCR product and 0.25 µg of purified pIN01 fragment. Resulting plasmids were isolated from yeast, transformed into *E. coli*, amplified, purified, and sequenced (using oligonucleotides 3 and 4).

4.5.3 Construction of site saturation libraries

To construct nine site saturation libraries corresponding to nine residues (GWQRLPFEY) of the A1 lariat, we sequentially randomized each residue of the lariat starting

from glycine to tryptophan, using oligonucleotides numbered from 13 to 21, respectively. Oligonucleotides 13 to 21 were PCR amplified using oligonucleotides 22 and 23 as primers. PCR products were cloned into *Rsr*II-cut, gel-purified pIN01 using *in vivo* homologous recombination (Ma *et al*., 1987; Hua *et al.*, 1997) in EY93. PCR reactions and cloning of PCR products into the library vector were performed as described in section 4.5.1.

4.5.4 Construction of third-generation constructs

To construct plasmids that express third-generation lariat constructs named from TG1 to TG18 (18 different constructs), we PCR amplified oligonucleotides numbered from 24 to 41, respectively, using oligonucleotides 22 and 23 as primers. PCR products were cloned into *Rsr*II-cut, gel-purified pIN01 using *in vivo* homologous recombination (Ma *et al*., 1987; Hua *et al.*, 1997) in EY93. PCR reactions and cloning of PCR products into pIN01 were performed as described in section 4.5.1.

To construct plasmids that express ΔE8-A1, ΔN8-TG17 and ΔN8-TG18 lariat constructs, we PCR amplified oligonucleotides 42, 43 and 44, respectively, using oligonucleotides 22 and 23 as primers. PCR products were cloned into *Rsr*II-cut, gel-purified pIN01 using *in vivo* homologous recombination (Ma *et al*., 1987; Hua *et al.*, 1997) in EY93. PCR reactions and cloning of PCR products into pIN01 were performed as described in section 4.5.1.

4.6 Yeast two-hybrid protocols

4.6.1 Y2H Screening

Y2H screens were conducted using the lariat Y2H interaction trap (Barreto *et al*., 2009). Targets were cloned as a fusion to LexA DNA binding domain in the Y2H bait vector pEG202 and expressed in the MATα strain EY111. EY111::pEG202 was cultured in SD H-media to an OD_{600} of 0.6–0.8. The combinatorial lariat libraries were constructed in the Y2H prey vector pIN01 and harbored in the MATa strain EY93. EY93::pIN-01 cells were scraped off the SD W- plates using a sterile glass microscope slide and grown in SD W- media to an OD_{600} of 0.6–0.8. Prior to mating, viability and processing of the library members were analyzed. EY93::pIN-01 cells were mixed with EY111::pEG202 cells at a ratio of 1:20, pelleted by centrifugation, resuspended in YPDA media and spread on YPDA plates. Plates were incubated at 30 °C for

24 hours. Mated cells were scraped off the plates, washed with PBS, resuspended in glycerol freeze down solution (25 mM Tris-HCl pH 8.0, 65% (v/v) glycerol, 0.1 M $MgSO_4$) and stored at – 80 °C. A sample of the library was thawed and serial dilutions were plated onto SD H-, SD W-, SD H-W-, SGR H-W-L- and SGR H-W-A- Xgal+ plates to calculate the mating efficiency of the yeast cells and to determine the optimal cell density for performing Y2H screens. Once the optimal conditions were determined, an aliquot of the mated cells was thawed, suspended in SGR H-W- media, incubated at 30 °C for six hours, and plated onto SGR H-W-L- and SGR H-W-A- Xgal+ selection plates. These plates were incubated at 30 °C for three to five days. Colonies (positive hits) were picked off the selection plates, grown overnight in SD H-W- media, harvested by centrifugation, resuspended in glycerol freeze down solution and stored at – 80 °C.

4.6.2 Rechecking Y2H interactions

Using the "smash and grab" technique, plasmids were isolated from the positive hits. The noose region in the prey plasmids was amplified by PCR using oligonucleotides 9 and 10 as primers. PCR reactions were performed as described in section 4.5.1. PCR products were recloned into *Rsr*II-cut, gel-purified pIN01 using *in vivo* homologous recombination (Ma *et al*., 1987; Hua *et al.*, 1997) in EY93. Lithium acetate transformations were performed as described earlier, with each transformation containing 30 µL of PCR product and 0.25 µg of gel-purified pIN01 fragment. Three to five individual colonies from each yeast transformation were selected and mated to EY111 cells containing the appropriate target. Diploids were selected on SD H-W- plates and plated onto SGR H-W-L- and SGR H-W-A- Xgal+ plates to estimate the strength of interactions. Plasmids were isolated from positive colonies, which conferred strong and specific interactions. The intein peptide in the prey plasmids was amplified by PCR using oligonucleotides 3 and 4 as primers. PCR reactions were performed in a 50 µL volume containing 1X PCR buffer (60 mM Tris-SO_4 (pH 8.9), 18 mM $(NH_4)_2SO_4$), 2 mM $MgSO_4$, 200 µM dNTPs, 0.4 µM forward primer, 0.4 µM reverse primer, 50 ng plasmid DNA, and 1 Unit Platinum® Taq DNA Polymerase High Fidelity. The reaction mixtures were subjected to a 5 min initial denaturation step at 94 °C followed by 25 cycles of amplification. Each cycle contained a denaturing step at 94 °C for 30 seconds, an annealing step at 50 °C for 30 seconds,

and an extension step at 68 °C for 60 seconds. PCR products were cleaned up and sequenced (using oligonucleotides 3 and 4) to determine the sequence of the interacting lariat.

4.6.3 Beta-Galactosidase assay

Yeast cells containing bait and prey plasmids were grown overnight in SGR H-W- media. The culture was diluted to an OD_{600} of 0.1–0.2 and allowed to reach an OD_{600} of 0.6–0.8. 1.2 mL of the culture was centrifuged at 18,000 x g for 5 min. The pellet was resuspended in 1 mL of Z buffer without 2-mercaptoethanol (0.06 M $Na_2HPO_4.7H_2O$, 0.04 M $NaH_2PO_4.H_2O$, 0.01 M KCl, 0.001 M $MgSO_4$) and centrifuged again as in the previous step. The resulting pellet was resuspended in 150 µL of Z buffer with 2-mercaptoethanol (0.06 M $Na_2HPO_4.7H_2O$, 0.04 M $NaH_2PO_4.H_2O$, 0.01 M KCl, 0.001 M $MgSO_4$, 0.05 M 2-mercaptoethanol), 50 µL of chloroform and 20 µL of 0.1% SDS, and this mixture was vortexed vigorously. 700 µL of *ortho*-nitrophenyl-β-galactopyranoside (1 mg/mL in Z buffer with 2-mercaptoethanol) was added to the mixture and the reaction was started. The reaction was incubated at 30 °C until a color change was observed from white to medium yellow. The reaction was stopped by adding 500 µL of 1 M Na_2CO_3 and then centrifuged at 18,000 x g for 10 min. OD_{420} of the supernatant was measured using a microplate reader (Spectramax M5) and the β-galactosidase activity was calculated in Miller units according to the formula: Miller unit = (A_{420}) (1000) / (time) (volume) (A_{600}), where time is reaction time in minutes and volume is reaction volume in mL.

4.7 *In vitro* studies

To perform *in vitro* kinase assays, binding and structural studies, we expressed and purified His-tagged human c-Abl SH3-SH2-SH1 (residues 64-515 Abl1b numbering) construct using a bacterial expression system as described previously (Seeliger *et al*., 2005). Briefly, pET28a-Abl SH3-SH2-SH1 and pCDFDuet-1-YopH vectors (plasmid maps and details in section 4.1.5) were transformed into BL21C+ *E. coli* cells. *Yersinia pestis* tyrosine phosphatase (YopH) was co-expressed in order to maintain the tyrosine kinases in the dephosphorylated state. Positive transformants were grown to OD_{600} of 1.2 in expression media (TB with 50 µg/mL kanamycin and 50 µg/mL spectinomycin) at 37 °C. The expression of recombinant proteins was induced with 0.25 mM IPTG for 16 hours at 18 °C. Cells were harvested and

lysed by French press in buffer A (50 mM Tris-HCl pH 8.0, 500 mM NaCl, 10% (v/v) glycerol, 2 mM DTT, 10 mM imidazole, 1 % (v/v) protease inhibitor cocktail (Sigma-Aldrich)). Cleared lysates were mixed gently with Ni-NTA slurry (Qiagen) for 30 min at 4 °C. The mixture was loaded into a column and the column was washed 3 times with buffer B (50 mM Tris-HCl pH 8.0, 500 mM NaCl, 10% (v/v) glycerol, 1 mM DTT, 10 mM imidazole). Kinase fractions were eluted with buffer C (buffer B plus 40 mM imidazole) and dialyzed against 20 volumes of buffer D (20 mM Tris-HCl pH 8.0, 100 mM NaCl, 10% (v/v) glycerol, 1 mM DTT) with a 13-kDa molecular weight cutoff membrane for 16 hours at 4 °C. The dialyzed protein was diluted and loaded onto an anion exchange column (Hitrap Q FF, GE Life Sciences) equilibrated with buffer E (20 mM Tris-HCl pH 8.0, 10% (v/v) glycerol, 1 mM DTT). Proteins were eluted with a linear gradient of 0–35% buffer F (buffer E plus 1 M NaCl). Kinase fractions were pooled, concentrated and loaded onto a gel-filtration column (Sephacryl S-100, GE Life Sciences) equilibrated with buffer G (50 mM Tris-HCl pH 8.0, 100 mM NaCl, 10% (v/v) glycerol, 1 mM DTT). Proteins were eluted from the column using the same buffer (G). The major peak containing Abl Kinase was pooled, concentrated and stored at – 80 °C.

Kinetic analysis of Abl kinase inhibition by synthetic peptides was carried out using a continuous spectroscopic kinase assay (Boerner *et al*., 1995). This assay couples the phosphorylation of substrate peptide and production of ADP to the oxidation of NADH through phosphoenolpyruvate, pyruvate kinase, and lactate dehydrogenase (Barker *et al*., 1995). The reaction mixture contained 100 mM Tris-HCl pH 8.0, 10 mM $MgCl_2$, 75 U pyruvate kinase (Sigma-Aldrich), 105 U lactate dehydrogenase (Sigma-Aldrich), 1 mM phosphoenolpyruvate (Sigma-Aldrich), 846 μM NADH (Sigma-Aldrich), 60 nM Abl kinase, and fixed or varied concentrations of ATP, Abl peptide substrate (EAIYAAPFAKKK; Genscript) and inhibitory peptide in a total volume of 75 μL. Reaction mixtures for dose response assays contained a fixed concentration of ATP (2.2 mM) and Abl peptide substrate (350 μM). The assays were performed in 96-well plates and initiated with the addition of Abl kinase. Absorbance data were collected every 30 s at 340 nm with a microplate reader (SpectraMax M5). To calculate Abl kinase activity, initial rates of change in A_{340} were drawn from the slopes of A_{340} curves and equated to the moles of NADH oxidized per unit time using the extinction coefficient of NADH (6.2×10^3). To determine IC_{50} of inhibitory peptides, the values from individual samples were analyzed and plotted as a function of drug concentration. K_i value was calculated

from the IC_{50} value and concentration of ATP in the assay (2.2 mM) according to the Cheng-Prusoff relationship: $K_i = IC_{50} / (1 + \{[ATP]/K_m\})$ where K_m is the Michaelis Menton constant for ATP, which was determined to be 70 μM for the Abl Kinase. To determine kinetic parameters (K_m and V_{max}), the values from individual samples were analyzed and fit to the Michaelis–Menten equation using Prism (GraphPad).

Fluorescence analysis of binding of ligands to the Abl myristoyl pocket was carried out using a F2500 fluorescence spectrophotometer (Hitachi). GNF2, a myristate competitive small molecule inhibitor of Abl kinase (Adrian *et al*., 2006), fluoresces at 407 nm upon binding to the protein. Increasing amounts of ligands (A1 lariat or myristic acid) were titrated to the Abl-GNF2 complex (0.18 μM Abl+0.3 μM GNF2 in 20 mM Tris-HCl pH 8.0, 10% (v/v) glycerol, 100 mM NaCl, 1 mM DTT), and the ability of the ligands to displace GNF2 from the Abl myristoyl pocket was examined by monitoring the fluorescence at 407 nm. All titrations were carried out in a quartz cuvette (Starna cells) at 20 ± 2 °C. A wavelength of 295 nm was used for excitation and the emission was recorded between 310 and 550 nm. A slit of 2.5 nm was used for excitation and emission. The decrease in fluorescence at 407 nm was fit to the one-site competition binding equation for determining the IC_{50} value.

Kinase selectivity analysis was carried out using an ATP site-dependent *in vitro* competition-binding assay (Kinex™ Protein Kinase Microarray-200). The assay evaluated the selectivity of the synthetic TG17 lariat against a panel of 200 distinct kinases, which included 36 AGC kinases, 30 calmodulin dependent protein kinases (CAMK), 29 CMGC kinases, 20 STE kinases, 61 tyrosine kinases (TK), nine tyrosine kinase-like (TKL) proteins, two lipid kinases (LK), and 13 other kinases. Briefly, the lariat was incubated with a biotinylated ATP probe on the protein kinase microarray. If the lariat binds to the kinase and directly or indirectly occludes the ATP binding pocket, then fewer probes can covalently bind to the ATP site. If the lariat does not bind to the kinase, there is no reduction in the binding of probes to the ATP site. The results were read out by quantifying the amount of ATP probe bound to the kinases using fluorescently labeled streptavidin conjugates. To obtain relative binding scores (RBS), binding data were fit to the following equation: $RBS = \{(1-F_P)\ [D]\ F_D\}/\ (F_P-F_D)$, where F_P is the fraction of the probe bound to the kinase, F_D is the fraction of the lariat bound to the kinase, and [D] is the lariat concentration (10 μM). Kinases that had a relative binding score of less than 50% of the DMSO control were predicted as non-binders.

4.8 Cell biological studies

Cell biological studies were conducted with K562 cells (erythrocytic cell type, triploid, multiple t(9;22) translocations, b3-a2 Bcr-Abl fusion). K562 (CCL243) was obtained from ATCC and cultured in IMDM (Iscove's Modified Dulbecco's Media) supplemented with 10% fetal calf serum, 100 IU/ml penicillin and 100 mg/ml streptomycin. Cells were grown at 37 °C with 5% CO_2.

To express intein peptides in K562 cells, we first subcloned the intein peptides into the pMSCV vector (plasmid map and details in Figure 4.5). The intein peptides were PCR amplified from Y2H prey plasmids using oligonucleotides 49 and 50 as primers. PCR reactions were performed as described in section 4.6.2. PCR products were digested with *EcoR*I and *Xho*I (New England Biolabs) and cloned into pMSCV using standard restriction enzyme based cloning procedures (Ausubel *et al*., 1997). Resulting plasmids were sequence verified using oligonucleotides 51 and 52 as primers.

Transient transfections of pMSCV vectors into K562 cells were carried out using the cell line nucleofector system (Amaxa Biosystems) according to manufacturer's directions. Briefly, 1×10^6 cells were suspended in 100 μL nucleofector solution, mixed with 5 μL of plasmid DNA (1 μg/μL in TE buffer) and subjected to nucleofection using the program T-016. Analysis of transfection efficiency was carried out by flow cytometry. To assess cell viability, cells were stained with trypan blue reagent and counted using a hemocytometer. For Western analysis, K562 cells were harvested 24 hours post-nucleofection, washed twice with PBS, and lysed in SDS-PAGE loading buffer (62.5 mM Tris-HCl pH 6.8, 10% (v/v) glycerol, 2.3% (w/v) SDS, 5% (v/v) 2- mercaptoethanol, 0.002% (w/v) bromophenol blue). Lysates were subjected to SDS-PAGE and immunoblotting as described in section 4.2.5.

5. Results and Discussion

Since there are no ATP competitive peptide inhibitors of protein kinases, and considering that such inhibitors could identify new allosteric drug-binding pockets in the kinase catalytic cleft, we started a project to isolate and characterize a novel class of cyclic peptides, referred to as lariats, against Abl kinase, a drug target important in CML and other disorders. Several aspects prompted us to employ the lariat peptide system as a screening method for the identification of peptide inhibitors of kinases. First, lariats possess a lactone constraint. Constrained peptides bind to targets with higher affinity than their linear counterparts (Koivunen *et al*., 1994; McConnell *et al*., 1994; Colas *et al*., 1996). In addition, without exposed N and C termini, constrained peptides are not open to degradation by cellular exoproteases (Horswill and Bencovic, 2005). Second, lariats are easily and rapidly generated against any target in a cost-effective manner. This is in contrast to isolating linear/cyclic peptides from synthetic peptide libraries, which incur huge investment of time and money (Horswill and Bencovic, 2005). Third, lariat screens are conducted in eukaryotic cells. This circumvents the problems associated with the large-scale purification of target proteins. Furthermore, this approach should select for peptides that are stable and functional under intracellular conditions. In contrast, phage display requires pure targets to conduct screens, and a substantial proportion of molecules selected from phage display turn out to be either unstable or non-functional in eukaryotic cells (Cattaneo and Biocca, 1999; Hoppe-Seyler *et al*., 2001). Fourth, lariats are amenable to chemical synthesis, and synthetic lariats are well suited for *in vitro* studies. This property of lariats makes them advantageous over peptide aptamers and other scaffolded peptides, which are only over-expressed and purified (Borghouts and Weiss, 2009). Fifth, lariats are easily extended to cell biological and animal studies. Once the DNA sequences of interacting lariats are identified by genetic selection, the genes coding for intein peptides are transferred from the Y2H vector to appropriate mammalian vectors, and delivered into cells through transfection or viral infection. Sixth, chemical moieties such as affinity tags, fluorescent molecules, localization sequences and membrane permeable peptides can be easily attached to the N-terminus of synthetic/recombinant lariats. This property of lariats gives them advantages over "head-to-tail" cyclized peptides that have no free end to attach moieties (Barreto *et al*., 2009).

5.1 Isolation and mechanism of action of Abl SH1-interacting lariats

5.1.1 Library screening

To identify lariats interacting with the Abl SH1 domain, we first cloned the target (human Abl1b residues 210-496) as a fusion to the LexA DNA binding domain in the Y2H bait vector pEG202 and expressed it in the MATα strain EY111. As prey constructs, we used members of the combinatorial *Ssp-Ssp* R7 lariat library expressed in the MATa strain EY93.

The *Ssp-Ssp* R7 library was constructed using the pIN01 plasmid. This plasmid codes for the I_C and I_N domains of the *Synechocystis sp. PCC6803* (*Ssp)* DnaE intein with specific mutations for lariat production, in addition to other domains required for Y2H assays, replication, and selection. The random region of the peptide library was cloned between the permutated intein domains for facilitating the formation of lariat peptides. With seven random positions, the *Ssp-Ssp* R7 library displays the amino acid sequence SX_7EY in the noose region of the lariat. Serine was included at the I_C-peptide junction to catalyze a transesterification reaction that releases the I_N domain and produces the lariat (Scott *et al.*, 2001). Glutamic acid and tyrosine were included in the noose region to facilitate lariat formation (Naumann *et al.*, 2005). Random amino acids were generated using the degenerate NNK codon, which encodes 32 triplets that code for 20 different amino acids and one stop codon. The NNK codon was used for randomization in order to maximize the diversity of amino acids with a minimum number of stop and redundant codons (Wong *et al*., 2006).

The *Ssp-Ssp* R7 library contains ~20 million members. Sequencing analysis showed that ~31% of library members contain correct sequences. Western blot analysis showed that ~70% of library members with correct sequences process to form the lariat. In total, ~25% of the library is capable of producing a lariat (Barreto *et al*., 2009). To ensure a 95% probability of screening a library with ~20 million members, we mated 20 copies of the library in the strain EY93 to the strain EY111, which expresses the target and contains the Y2H reporter genes. The diploids were screened for positive interactions based on the activation of *LEU2, ADE2,* and *LacZ* reporter genes using the lariat Y2H interaction trap. Two unique lariat sequences were isolated in the screen: A1 (SGWQRLPFEY) and A2 (SGWHRLSEEY), which interact with Abl SH1 but not with control proteins or other Bcr-Abl domains. Within the random region, the lariats have four residues in common: G1, W2, R4, and L5. One or more of these residues could play an important role in contributing to Abl SH1-lariat interactions.

5.1.2 *In vitro* studies with the synthetic A1 lariat

We chose one of the two lariats, A1, for further characterization. To determine the mechanism of Abl kinase inhibition by the A1 lariat, we performed *in vitro* kinetic and binding experiments using the purified His-tagged human c-Abl kinase (residues 64-515 Abl1b numbering) and the synthetic A1 lariat. A truncated version of the A1 lariat was synthesized with an alanine at the N-terminus "tail" replacing the Ic domain in the A1 lariat. The lariat version of the peptide was created by cyclizing the side chain of serine and the C-terminal carboxylic acid via an ester bond (A-[SGWQRLPFEY]).

Kinetic analysis was carried out using a continuous spectroscopic kinase assay (Boerner *et al*., 1995). This assay couples the phosphorylation of substrate peptide and production of ADP to the oxidation of NADH through phosphoenolpyruvate, pyruvate kinase, and lactate dehydrogenase (Barker *et al*., 1995). First, we performed a dose-response analysis to assess the inhibitory activity of the A1 lariat. The dose response curve showed the IC_{50} and K_i of the A1 lariat to be 193 μM and 5.95 μM, respectively (Figure 5.1a). Second, we examined the effects of increasing concentrations of ATP or substrate peptide on the inhibitory activity of the A1 lariat. Incubation of Abl kinase with the A1 lariat in the presence of increasing concentrations of ATP resulted in an increase in K_m for ATP, while not affecting V_{max} of the reaction, which is the characteristic of competitive inhibition, indicating that the A1 lariat inhibits kinase activity in an ATP dependent manner (Figure 5.1b). Incubation of Abl kinase with the A1 lariat in the presence of increasing concentrations of substrate peptide resulted in a decrease in V_{max} of the reaction, while not affecting K_m for substrate peptide, which is the characteristic of non-competitive inhibition, indicating that the A1 lariat inhibits kinase activity in a substrate-independent manner (Figure 5.1c).

Next, to verify whether the A1 lariat targets the myristate-binding site of Abl kinase, we carried out a fluorescence analysis of the binding of ligands (A1 lariat/myristic acid) to the Abl myristoyl pocket by titrating increasing amounts of ligands to the Abl-GNF2 complex. GNF2 is a myristate competitive small molecule inhibitor of Abl kinase (Adrian *et al*., 2006), which fluoresces at 407 nm upon binding to the protein. Myristic acid, included as a positive control, displaced GNF2 from the Abl-GNF2 complex with an IC_{50} of 12.5 ± 1.3 μM. The lariat was unable to displace GNF2, making IC_{50} calculations impossible, indicating that A1 does not bind to the myristate-binding pocket of the Abl kinase (Figure 5.1d).

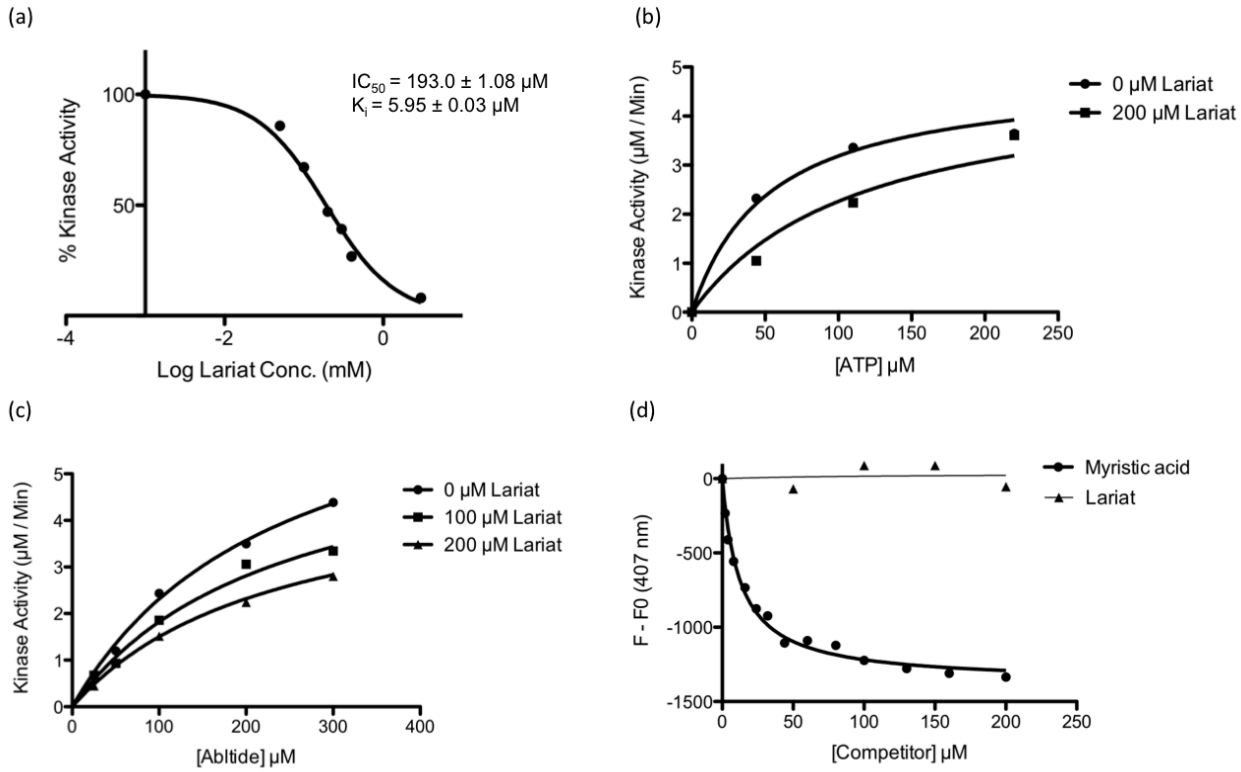

Figure 5.1. Steady-state kinetic analysis of Abl kinase inhibition by the synthetic A1 lariat: (a) Inhibitory activity of the A1 lariat. Recombinant c-Abl SH3-SH2-kinase was mixed with different concentrations of the A1 lariat, and kinase assays were performed using Abltide as a substrate. The values from individual samples were analyzed and plotted as a function of drug concentration to determine the IC_{50} of the A1 lariat. K_i was calculated from the IC_{50} value using the Cheng-Prusoff relationship (see methods). **(b)** Effect of increasing concentrations of ATP on the inhibitory activity of the A1 lariat. The curves represent calculated best fits to the Michaelis–Menton equation with a constant amount of Abltide and various amounts of ATP and the A1 lariat. **(c)** Effect of increasing concentrations of Abltide on the inhibitory activity of the A1 lariat. The curves represent calculated best fits to the Michaelis–Menton equation with a constant amount of ATP and various amounts of Abltide and the A1 lariat. **(d)** Fluorescence analysis of binding of the A1 lariat to Abl myristoyl pocket. Increasing amounts of ligands (A1 lariat or myristic acid) were titrated to Abl-GNF2 complex and the ability of the ligands to displace GNF2 from the Abl myristoyl pocket was examined by monitoring the fluorescence at 407 nm. The decrease in fluorescence at 407 nm was fit to the one-site competition binding equation for determining the IC_{50} value. All experiments were repeated at least twice and representative graphs are shown.

Together, the results from *in vitro* studies provide evidence that the A1 lariat is an ATP competitive inhibitor of Abl kinase. However, it cannot be concluded from these studies that the A1 lariat occupies the ATP binding pocket. This is because, in addition to ATP binding site inhibitors, allosteric inhibitors targeting a large additional cavity adjacent to the ATP binding pocket can still remain ATP competitive in kinetic analysis (Morphy, 2010). As the A1 lariat is comparatively larger than any typical type I/II kinase inhibitor, there are more chances for the lariat to target additional sites on the catalytic cleft outside the ATP binding site.

There are several explanations as to why the catalytic cleft, but not other epitopes of Abl kinase, is targeted by the lariat. First, the activation loop of Abl kinase is phosphorylated in yeast (data not shown), which causes the kinase to adopt an active conformation. In the active state, the catalytic cleft is wide open to accept Mg-ATP (Huse and Kuriyan, 2002; Nolen *et al*., 2004, Levinson *et al*., 2006), and this open conformation may favor the interaction of lariats with the catalytic cleft. Indeed, the preponderance of ATP-competitive small molecules over substrate-competitive/allosteric inhibitors is a consequence of using enzymatic assays to screen compound-libraries, which use highly active recombinant kinase domains, and maintain a low ATP concentration (Liu and Gray, 2006). Second, in order to compete with substrate proteins, lariat sequences should closely resemble kinase recognition motifs and adopt a "substrate-like" conformation, which may not be possible in the presence of a lactone constraint. In fact, most peptide inhibitors of kinases, which compete with substrate proteins, targeting proteins or docking sites are synthetic linear peptides that are rationally designed from kinase recognition motifs (Kaidanovich-Beilin and Eldar-Finkelman, 2006; Eldar-Finkelman and Eisenstein, 2009). Third, in addition to the screen against Abl SH1, the *Ssp-Ssp* R7 lariat library has also been used against LexA, which resulted in the isolation of two lariats that interacted near the autoproteolysis active site of LexA (Barreto *et al*., 2009). Results from these screens suggest that lariats isolated from this library could show a strong bias towards a particular epitope of a protein, which is located at or near the active site. Reasons for the bias could be that other epitopes may be masked by their interactions with endogenous yeast proteins, or the active site of a protein could possess certain epitopes that are more recognizable than others. Lariats that interact with less recognizable epitopes may be underrepresented and therefore missed during the selection. Increasing the size of a library or using a focused library during a screen may help to identify novel lariats that bind to other epitopes.

Previous reverse genetic screens have identified a number of constrained peptide inhibitors against defined targets, which were shown to be functional *in vivo* (Chattopadhyay *et al*., 2006; Nouvian *et al*., 2007; Guida *et al*., 2008; Brien *et al*., 2011). No rigorous *in vitro* analyses have been made to characterize their mechanism of action. By performing kinetic studies with the synthetic A1 lariat, we showed for the first time that a genetically selected lariat can remain functionally active *in vitro* and can inhibit the enzymatic activity of its target with a defined biochemical mechanism.

5.2. Generation and identification of higher affinity lariats

5.2.1 Site saturation mutagenesis of the A1 lariat

Optimizing the "drug like" properties of the lariats, such as affinity, specificity and solubility, should increase their potency as inhibitors of protein function. Therefore, we explored ways to modify such properties using a simple, robust and cost-effective protocol. In phage display and RNA aptamer screens, inhibitors often pass several rounds of selection, and therefore emerge with higher affinity (Cortese *et al*., 1996; Lorsch and Szostak, 1996). Affinity maturation of small molecules/synthetic peptides is a laborious process that often requires binding-site information, involving synthesis and screening of next-generation combinatorial chemical/peptide libraries. In the case of peptide aptamers, lead peptides are subjected to random mutagenesis, and tighter-binding variants are selected from mutagenic pools using more stringent Y2H reporter genes (Colas *et al*., 2000). Though this approach can generate higher affinity peptide aptamers, the importance of various side-chains on the inhibitor is not revealed by using this randomized process. Further, this approach has limitations such as biased mutational spectra and low mutation frequency. For example, Colas *et al*. were able to incorporate only two substitutions into a 20-mer Cdk2-interacting peptide aptamer, named Pep10, by adopting this approach. The higher affinity variant had a five-fold increase in affinity for Cdk2 over Pep10.

To improve the affinity of the A1 lariat, we first used a random mutagenesis approach. We amplified the noose region of the A1 lariat from pIN01-A1 following a mutagenic PCR protocol that can cause transitions and transversions by incorporating dPTP (2'-deoxy-P-nucleoside-5'-triphosphate) and 8-oxo-dGTP (8-oxo-7,8-dihydro-deoxyguanosine-triphosphate) into DNA, respectively. We then reintroduced the PCR products into the library vector to

construct a second-generation library consisting of 5 million members. Finally, we screened the library against Abl SH1 using yeast strains that harbored more stringent LexA operator reporter genes with different sensitivities (Colas *et al*., 2000). However, this approach only gave two point variants (ASGWQ**Q**LPFEY and ASGWQRLPF**G**Y), which had a less than two-fold increase in affinity for Abl SH1 relative to the A1 lariat (data not shown).

Since the random mutagenesis approach did not produce the desired results, and considering that the approach could not generate useful structure-activity relationship data for rational drug design, we sought to increase the affinity of the A1 lariat by first determining which amino acids are essential for its inhibition. To do this, we used site saturation mutagenesis (SSM), a beneficial method that is usually applied to residues in or near the active site of proteins during directed evolution (Parikh and Matsumura, 2005; Reetz *et al*., 2010). By employing SSM, we substituted each residue of the A1 lariat against all 20 possible amino acids at once, keeping other positions constant. We thus created nine small libraries containing 20 members each, for nine positions of the A1 lariat, and screened against Abl SH1 using the lariat Y2H interaction trap (Barreto *et al*., 2009). The results of the site-saturation analysis are summarized in Figure 5.2.

We did not get any substitutions at G1, W2, Q3 and L5 positions of the A1 lariat, indicating that these amino acids play an important role in contributing to Abl SH1-A1 interactions. At the fourth position, only 25% of the isolated sequences contain the wt residue arginine. Two different mutants, threonine (58%) and serine (17%), bearing hydroxyl side chains, account for the rest of the sequences. At the sixth position, there is a strong preference for aspartate (75%) over the wt residue proline (12.5%). Serine (12.5%) constitutes the rest of the sequences. At the seventh position, tryptophan (70%) often substitutes the wt residue phenylalanine (10%), and very few times tyrosine (10%) and histidine (10%) are seen.

Two positions, E8 and Y9 were fixed in the noose region of the *Ssp*-*Ssp* R7 lariat library during the primary screen to facilitate lariat formation. As we identified that E8 is not required to produce a lariat (Barreto *et al*., 2009), we randomized glutamate in the secondary screen, which gave rise to six new substitutions. Aspartate (19%) and asparagine (19%) are preferred at this position over the wt residue (14%). The last position of the lariat (Y9) can be substituted with tryptophan (10%) or phenylalanine (10%). However, based on the number of hits obtained, wt tyrosine (80%) is preferred at this position.

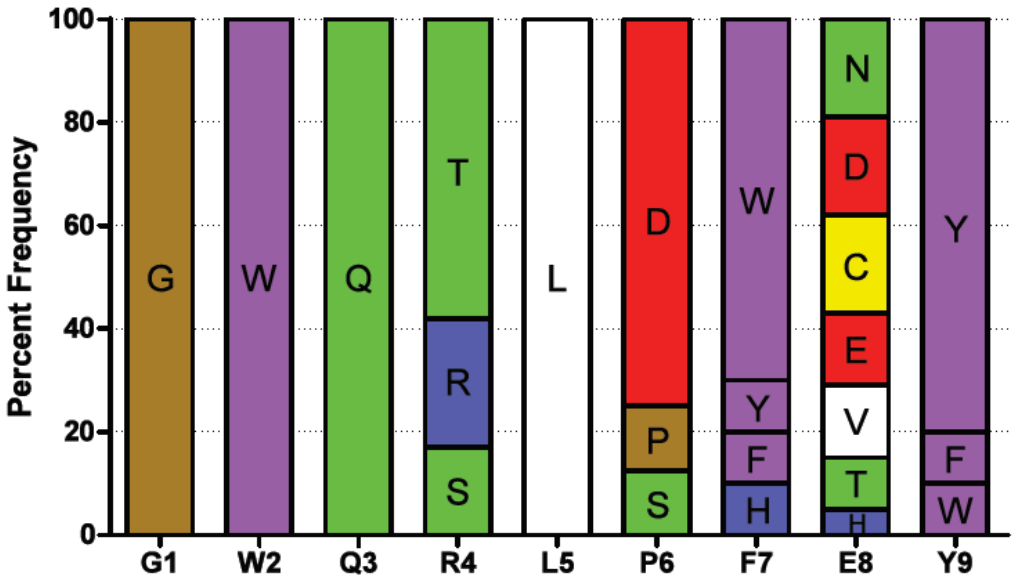

Figure 5.2. Saturation mutagenesis of the A1 lariat: Each position of the A1 lariat was saturated with all possible amino acids keeping other positions constant. Nine small libraries were thus created for nine positions of the A1 lariat and they were screened against the Abl SH1 bait. The prey plasmids were rescued from the hits and sequenced to identify the possible amino acid substitutions. The bars in the graph represent the percentage frequency of amino acids isolated from saturation mutagenesis screens for each position of the A1 lariat. Wild type residues of the A1 lariat are indicated at the bottom of the X-axis. Each amino acid is labeled by the one-letter code and standard amino acid colors are used in the graph.

5.2.2 Affinity maturation of the A1 lariat

Understanding the significance of various functional groups on the inhibitor scaffold is essential to optimize the molecule further. Unfortunately, generation of useful structure-activity relationship data, once hits are identified from large libraries of compounds, remains a major bottleneck in chemical genetics (Kritzer *et al*., 2009). An advantage of the peptide-based approach is that structure-activity relationship data can be generated rapidly and cost-effectively using mutagenesis.

We created a series of site-saturation mutants to identify which side chains of the A1 lariat are important for its function and how less important side chains can be modified to improve the properties of the A1 lariat. From the results of the site-saturation analysis, we reasoned that the lariats with R4T, P6D, F7W and E8N mutations would bind stronger to Abl SH1 relative to the A1 lariat. We thus designed a series of lariat constructs with one or more above-mentioned mutations and quantified their interactions with Abl SH1 using the Y2H based β-galactosidase assay. We also included F7Y mutation in the assay, as tryptophan (F7W)

could lead to a decrease in solubility and specificity of the lariat. The assay results are shown in Figure 5.3.

Among the five point variants tested (R4T, P6D, F7W, F7Y and E8N), three point variants (R4T, F7W and E8N) showed ~1.75 fold improvement, the P6D construct showed 1.25 fold improvement, and the F7Y construct did not show any improvement. Among the nine double variants (TG1-TG9) tested, the TG7 construct harboring P6D and E8N substitutions had the highest affinity and showed 4.6-fold improvement. In all cases, double variants had higher affinities than the corresponding single variants. Among the seven triple variants (TG10-TG16) tested, the TG10 construct harboring R4T, P6D and F7W substitutions had the highest affinity and showed 7-fold improvement. Notably, the affinity of the TG11 triple variant (R4T+P6D+F7Y) was lower than its corresponding double variant (TG1: R4T+P6D). In all other cases, triple variants had higher affinities than the corresponding single/double variants. The two quadruple variants, TG17 and TG18, with replacements in all the four possible positions of the lariat, showed 9-fold and 7-fold improvements, respectively.

Overall, we designed 18 third generation constructs (TG1-TG18) based on the SSM results and assayed them for binding to Abl SH1. We observed an improvement in affinity whenever an additional enhancing substitution was added to the A1 lariat. Of all the constructs tested, the TG17 (R4T+P6D+F7W+E8N) lariat had the highest affinity, followed by the TG18 (R4T+P6D+F7Y+E8N) and TG10 (R4T+P6D+F7W) lariats. The TG17 lariat showed 9-fold improvement in affinity relative to the A1 lariat, whereas the TG18 and TG10 lariats showed 7-fold improvement. The reasons for this enhancement in affinity could be multiple: (i) new hydrogen or ionic bonds could have been formed between the lariat and the target; (ii) the hydrophobic contact area at the lariat-target interface could have been increased; (iii) a better geometric fit with that of the binding site could have been achieved by the lariat; and (iv) the stability of the lariat and/or processing of the intein constructs could have been improved.

We next checked whether the lariat peptides were amenable to minimization without a significant loss in their affinity. Minimization of the lariats would be desirable for downstream applications as affinity reagents. We chose to delete the eighth position of the A1, TG17 and TG18 lariats, which is less important for Abl SH1-lariat interactions. However, the deletion completely abrogated the effects of A1, TG17 and TG18 lariats, indicating that all nine amino acids are required for the lariats to be functionally active (Figure 5.3).

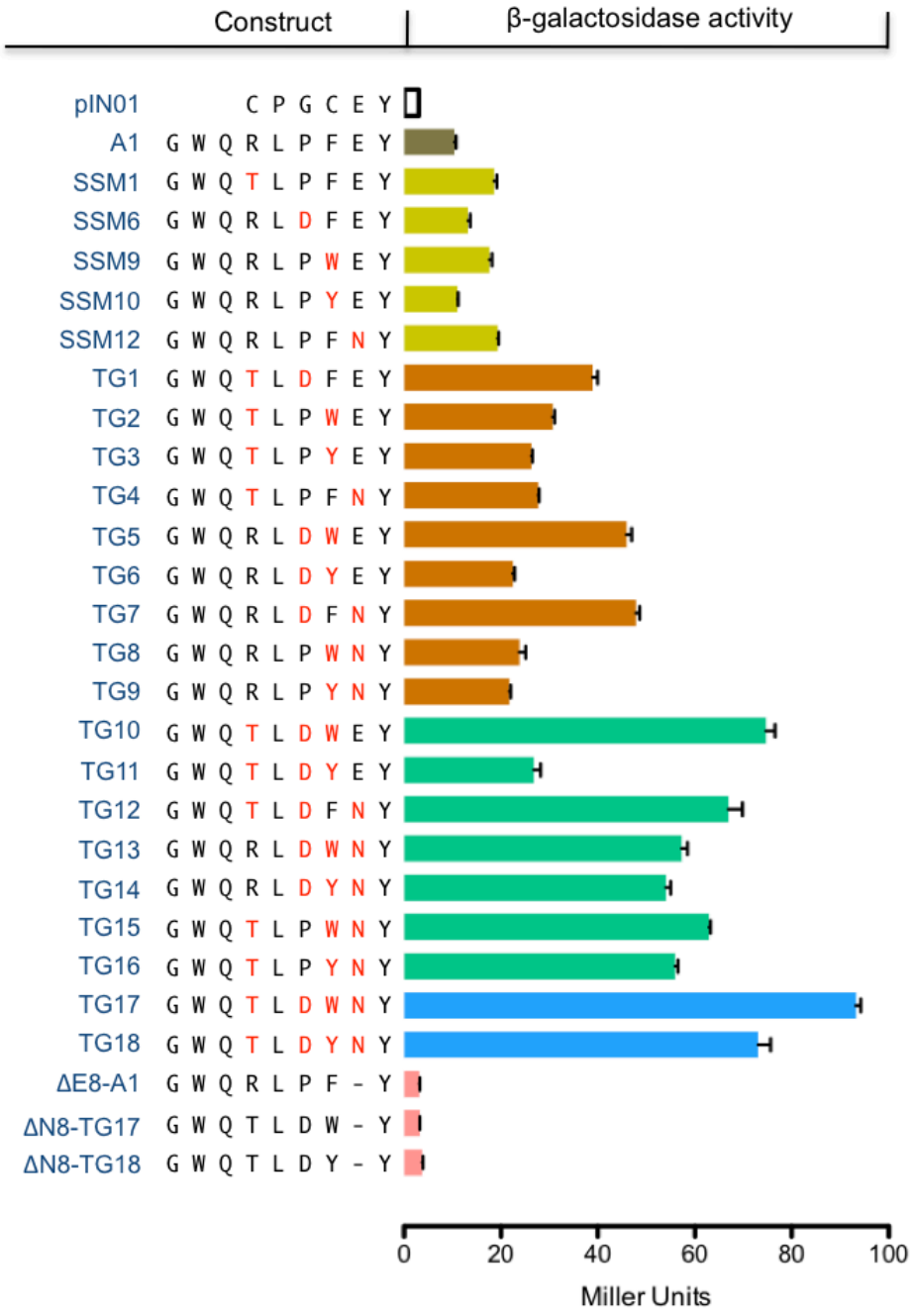

Figure 5.3. Affinity maturation of the A1 lariat: Lariat constructs with designed mutations were analyzed for their interactions with Abl SH1 using Y2H based β-galactosidase assay and expressed as Miller units. All interactions were examined three times starting with randomly selected independent clones. The bars represent mean ± SD for all experiments.

Taken together, we report here a new affinity maturation protocol consisting of two steps. In the first step, using SSM, we defined acceptable and tolerable substitutions at each position of the A1 lariat. In the second step, we designed specific mutations to the A1 lariat based on the SSM results and evolved higher affinity variants. The semi-rational affinity maturation protocol used in this study is advantageous over existing protocols in a number of ways. The new approach: (i) delineates important residues of the lariats, and generates useful structure-activity relationship data for drug design; (ii) explores the sequence space to the maximum extent, and minimizes the number of stop codons; (iii) has complete control over the position of randomization, and allows subset mutagenesis (e.g. introducing mainly positively charged residues); and (iv) is technically simple, robust and economical. The only disadvantage of this approach is that it is susceptible to biases arising from: (i) greater incorporation of one nucleotide than the other during oligonucleotide synthesis; and (ii) degeneration of triplets when they are translated into amino acids (Wong *et al*., 2006).

In summary, we show that the lariats are amenable to structure-activity relationship studies and optimization by delineating important residues of the A1 lariat and by improving the affinity of the A1 lariat, respectively. The ability to easily and rapidly generate useful data for rational drug design by mutagenesis should expand the usefulness of lariats as inhibitors of protein function. We also show that the affinity maturation protocol used in this study is more efficient than random mutagenesis. This new approach is also applicable to peptides isolated from phage display and peptide aptamer screens. Comparing the results from various affinity maturation experiments may help to answer questions such as how different lariats evolve, how many residues remain fixed or change frequently during evolution, do sequences that bind to a same kind of epitope eventually converge or diverge during evolution, do sequences evolve to resemble any naturally occurring interactors, and what kind of residues determine specificity, affinity, stability and processivity of the lariats?

5.3 Characterization of Abl SH1-interacting lariats

5.3.1 Analysis of the binding of peptides to Abl SH1

Considering the high conformational flexibility and low intracellular stability of linear peptides, genetic selection of constrained peptides is preferred over linear peptides (Horswill and Bencovic, 2005). In phage display and peptide aptamer screens, conformational constraint

is provided to peptides using disulphide bonds and scaffolding proteins, respectively (McConnell *et al*., 1994; Colas *et al*., 1996). A major disadvantage of disulphide bond-constrained peptides is that they are not stable under reducing conditions in cells (McLafferty *et al*., 1993). There are also several limitations in using scaffolding proteins to constrain peptides. Their stability, size, expression levels and intrinsic biological activity are of major concern (Abedi *et al*., 1998; Klevenz *et al*., 2002; Woodman *et al*., 2005). To overcome many limitations associated with scaffold proteins, lariats are constrained by a lactone bond using engineered intein domains.

To highlight the significance of lactone constraint and intein domains used in the lariat Y2H system, we cloned the noose regions of the A1, A2, TG17 and TG18 lariats into an inactive intein plasmid, which expresses a lariat precursor that does not undergo any steps in the intein-mediated cyclization reaction, and a linear peptide plasmid, which expresses a peptide whose C-terminus is not constrained by the I_N domain. Description and sequences of the constructs are shown in Figure 5.4(a) and 5.5(a). We then compared their binding affinities for Abl SH1 using the Y2H based β-galactosidase assay. The inactive A1 and A2 peptides retained their capacity to interact with Abl SH1 (Figure 5.4b), whereas the inactive TG17 and TG18 peptides had an approximately two-fold decrease in affinity for Abl SH1 relative to their corresponding lariat constructs (Figure 5.5b). The higher affinity of TG17 and TG18 lariats for Abl SH1 relative to their inactive versions indicates that the lariat structure is indeed required for these peptides to interact better with the target, highlighting the importance of lactone constraint for protein-peptide interactions. However, the lactone constraint may not be required for all peptides, particularly lead peptides, to interact with the target.

As shown in Figure 5.4b and 5.5b, the linear A1, A2, TG17 and TG18 peptides were unable to interact with Abl SH1, confirming the importance of intein domains used in the Y2H system. One reason that these linear peptides do not recognize the target may be their short half-lives in cells. The linear constructs used in our assays contain a free C-terminus, which may be open to degradation by cellular exoproteases (Horswill and Bencovic, 2005). Linear peptides may also be susceptible to proteosomal degradation. Previous studies have showed that only 5% of random unconstrained peptides fold into structures (Davidson and Sauer, 1994), and unstructured peptides are degraded by proteosomes because they are recognized as misfolded proteins (Baumeister and Lupas, 1997; Groll *et al*., 1997). Apart from their low

(a)

Construct	I_C	I_C-1	I_C+1	R_7	EY	I_N+1	I_N
A1 Lariat	Ssp I_C	Ala	Ser	GWQRLPF-EY		Cys	Ssp I_N
A1 Inactive	Ssp I_C	Ala	Ser	GWQRLPF-EY		Ala	Ssp I_N
A1 Linear	Ssp I_C	Ala	Ser	GWQRLPF-EY		Stp	-
A2 Lariat	Ssp I_C	Ala	Ser	GWHRLSE-EY		Cys	Ssp I_N
A2 Inactive	Ssp I_C	Ala	Ser	GWHRLSE-EY		Ala	Ssp I_N
A2 Linear	Ssp I_C	Ala	Ser	GWHRLSE-EY		Stp	-

(b)

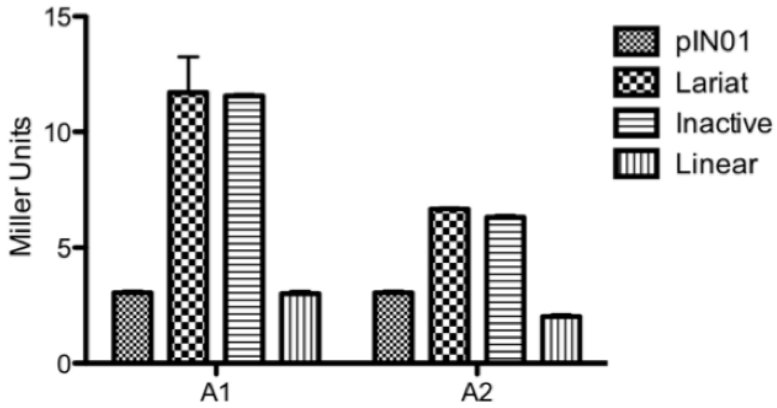

Figure 5.4. Y2H constructs and analysis: (a) Sequences of A1 and A2 lariat, inactive and linear peptide constructs. The lariats contain an Asn to Ala mutation at position I_C-1, which inhibits Asn side chain cyclization reaction and stops the reaction at the lariat intermediate. This mutation prevents the formation of a lactone cyclized peptide. The inactive constructs contain the same mutations as the lariat and a Cys to Ala mutation at position I_N+1. The Cys to Ala mutation blocks the N to S acyl shift and only produces a lariat precursor. The linear peptides contain a stop codon at the I_N+1 position. **(b)** Y2H analysis of the interaction of Abl SH1 with the above mentioned constructs and the pIN01 plasmid. pIN01 is a control plasmid that expresses an inactive intein with a CGPC peptide noose. The interactions were quantified using Y2H based β-galactosidase assay and expressed as Miller units. All interactions were examined three times starting with randomly selected independent clones. The bars represent mean ± SD for all experiments.

(a)

Construct	I_C	I_C-1	I_C+1	R_9	I_N+1	I_N
TG17 Lariat	Ssp I_C	Ala	Ser	GWQTLDWNY	Cys	Ssp I_N
TG17 Inactive	Ssp I_C	Ala	Ser	GWQTLDWNY	Ala	Ssp I_N
TG17 Linear	Ssp I_C	Ala	Ser	GWQTLDWNY	Stp	-
TG18 Lariat	Ssp I_C	Ala	Ser	GWQTLDYNY	Cys	Ssp I_N
TG18 Inactive	Ssp I_C	Ala	Ser	GWQTLDYNY	Ala	Ssp I_N
TG18 Linear	Ssp I_C	Ala	Ser	GWQTLDYNY	Stp	-

(b)

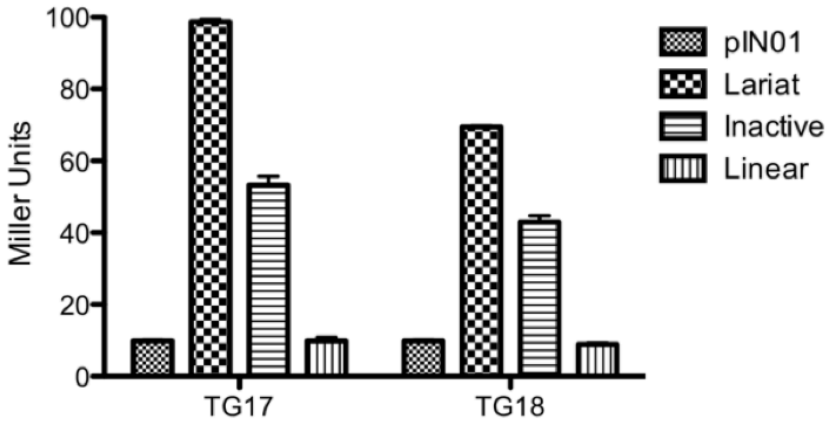

Figure 5.5. Y2H constructs and analysis: (a) Sequences of TG17 and TG18 lariat, inactive and linear peptide constructs. The lariats contain an Asn to Ala mutation at position I_C-1, which inhibits Asn side chain cyclization reaction and stops the reaction at the lariat intermediate. This mutation prevents the formation of a lactone cyclized peptide. The inactive constructs contain the same mutations as the lariat and a Cys to Ala mutation at position I_N+1. The Cys to Ala mutation blocks the N to S acyl shift and only produces a lariat precursor. The linear peptides contain a stop codon at the I_N+1 position. **(b)** Y2H analysis of the interaction of Abl SH1 with the above mentioned constructs and the pIN01 plasmid. pIN01 is a control plasmid that expresses an inactive intein with a CGPC peptide noose. The interactions were quantified using Y2H based β-galactosidase assay and expressed as Miller units. All interactions were examined three times starting with randomly selected independent clones. The bars represent mean ± SD for all experiments.

intracellular stability, linear peptides do not possess a conformational constraint that may be needed to recognize the target. In the case of inactive peptides, though the lactone constraint is absent, the peptide noose is still flanked by intein domains, which would impose a conformational constraint, and protect the noose region from exoproteases.

5.3.2 *In vitro* activity of the higher affinity peptides

To quantitate the inhibitory activity of the TG17 and TG18 lariats *in vitro*, we used the continuous spectroscopic kinase assay (Boerner *et al*., 1995). Truncated versions of the lariats were synthesized as mentioned in section 5.1.3 and tested against purified Abl kinase. Dose response curves showed the K_i of synthetic TG17 (A-[SGWQTLDWNY]) and TG18 (A-[SGWQTLDYNY]) lariats to be 804 nM and 2.41 μM, respectively, establishing a strong inhibition of Abl kinase activity (Figure 5.6). In agreement with Y2H results, the TG17 lariat exhibited a stronger efficacy than the TG18 lariat.

To examine the effect of lariat structure on Abl kinase inhibition, we evaluated the inhibitory activity of linear peptides corresponding to the TG17 and TG18 lariats. Dose response curves showed the K_i of synthetic TG17 (ASGWQTLDWNY) and TG18 (ASGWQTLDYNY) linear peptides to be 5.76 μM and 13.28 μM, respectively, indicating that the linear versions are about five to seven times less efficient than the lariat peptides at inhibiting the Abl kinase activity (Figure 5.6). This decrease in the inhibitory activity suggests that the linear peptides may not be adopting the optimal conformation needed to strongly interact with the target.

Our data confirm previous reports describing that genetically selected peptides show a decrease in their efficiency when assayed without a constraint. A synthetic linear peptide corresponding to the variable region of a Cdk2-interacting peptide aptamer showed a ~ 1000 fold decrease in its efficiency at inhibiting the kinase activity of Cdk2 (Cohen *et al*., 1998). In the case of a peptide aptamer that binds to ubiquitin ligase mouse double minute 2-protein (MDM2), the unconstrained peptide interacted ~ two fold less strongly with MDM2 than the constrained peptide (Brown *et al*., 2009). These results support the idea that the variable region of peptides is sufficient for activity and that the conformational constraint imposed on the variable region allows for a high-affinity interaction by lowering the entropic cost of binding. In contrast, there are some cases in which free peptides corresponding to the variable region of

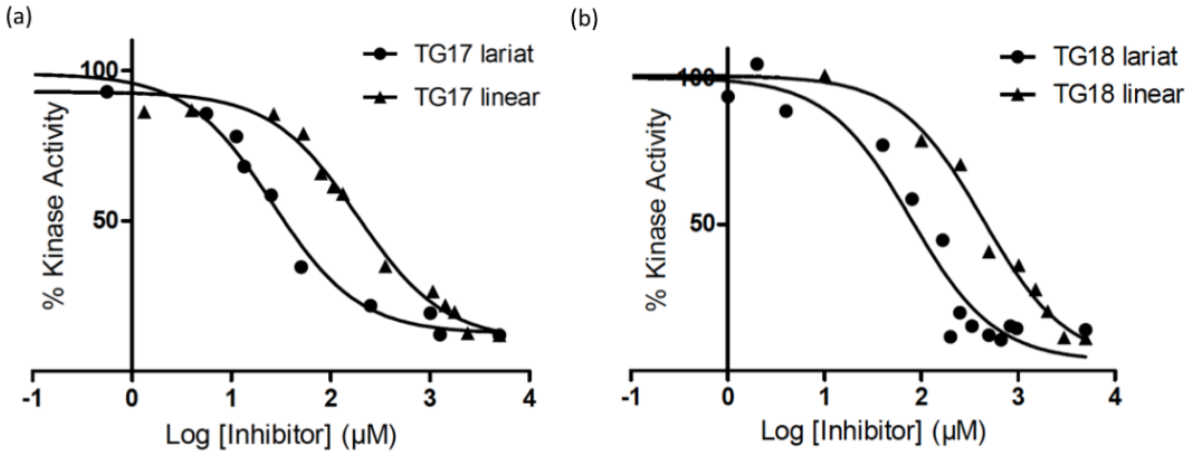

(C)

Construct	Lariat		Linear	
	IC_{50}* (μM)	K_i (μM)	IC_{50}* (μM)	K_i (μM)
TG17	26.06 ± 1.16	0.804 ± 0.04	186.64 ± 1.18	5.76 ± 0.036
TG18	78.16 ± 1.35	2.41 ± 0.042	430.53 ± 1.22	13.28 ± 0.037

* Biochemical IC_{50} for WT Abl SH3-SH2-SH1 in the presence of 2.2 mM ATP

Figure 5.6. *In vitro* activity of higher affinity peptides: Recombinant c-Abl SH3-SH2-kinase was mixed with different concentrations of the synthetic higher affinity peptides, and kinase assays were performed using Abltide as a substrate. The values from individual samples were analyzed and plotted as a function of inhibitor concentration to determine the IC_{50} values of the higher affinity peptides. Inhibitory constants (K_i) were calculated from the IC_{50} values using the Cheng-Prusoff relationship (see methods). **(a)** Dose-dependent inhibitory activity of TG17 lariat and linear peptides. **(b)** Dose-dependent inhibitory activity of TG18 lariat and linear peptides. **(c)** IC_{50} and K_i values of the higher affinity peptides derived from dose-response curves.

peptide aptamers retained their capacity to bind/inhibit the target (Schmidt *et al*., 2002; Martel *et al*., 2006; Nouvion *et al*., 2007), suggesting that the linear versions of genetically selected constrained peptides could also adopt a functional structure without a constraint.

5.3.3 *In vivo* activity of the lariats

Having demonstrated direct biochemical inhibition of Abl kinase activity, we proceeded to evaluate the *in vivo* inhibition of the Bcr-Abl kinase activity by the lariats. To do this, we subcloned the intein peptides into the murine stem cell virus vector and transiently transfected them into K562 cells that ectopically express the wild-type p210 Bcr-Abl oncoprotein. First, we confirmed the expression and processing of intein constructs using Western analysis with an antibody against the C-terminal FLAG tag. The A1 lariat plasmid released the FLAG tagged I_N domain, confirming the processing of inteins and production of the lariat (Figure 5.7a). Next, we determined the viability of the K562 cells by trypan blue exclusion to examine whether the lariats act against Bcr-Abl expressing cells. Expression of the lariats A1, TG17 and TG18 for 24 hours reduced the cell survival to 73%, 60% and 73%, respectively, relative to untreated cells that had 94% survival. Expression of the intein machinery alone reduced the cell survival to 86% relative to the untreated cells (Figure 5.7b). Finally, to confirm the inhibition of Bcr-Abl kinase activity by the lariats, we tested the effect of intracellular expression of the lariats on the phosphorylation status of Hck, a Src family kinase, which is constituently activated by Bcr-Abl for CML induction (Klejman *et al*., 2002). As shown in Figure 5.7c, there was a substantial inhibition of Hck phosphorylation in the cells transfected with lariats, establishing that the effects of the lariats on the viablity of the cells are indeed mediated via inhibition of Bcr-Abl kinase activity and are not because of off-target effects. Together, these *in vivo* studies clearly illustrate the potential of lariats as intracellular inhibitors of endogenous Bcr-Abl dependent signaling events.

Numerous studies have established the utility of various *trans* dominant agents such as small molecules, antibodies, synthetic peptides, peptide aptamers and monobodies in the manipulation of intracellular networks for research and therapeutic purposes (Barreto, 2010). We report here the first functional expression of lariats within mammalian cells, and demonstrate that lariats isolated and characterized using Y2H assays can be used as intracellular inhibitors. The ability of lariats to inhibit specific proteins, both *in vitro* and *in*

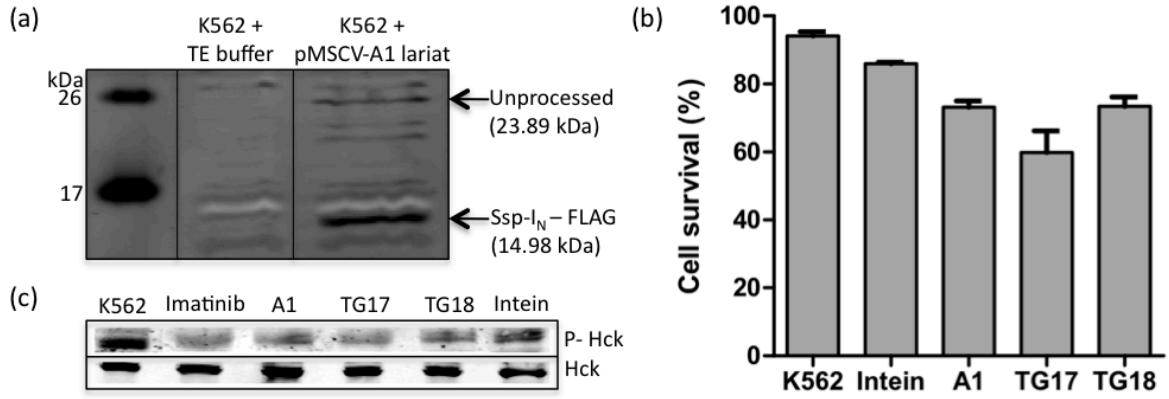

Figure 5.7. ***In vivo*** **activity of the lariats: (a)** Intein processing in K562 cells transfected with A1 lariat plasmid. Intein processing was detected by Western analysis using an anti-FLAG antibody. Calculated molecular weights of FLAG-tagged unprocessed intein construct and FLAG-tagged *Ssp*-I_N domain are 23.89 kDa and 14.98 kDa, respectively. **(b)** Effect of lariats on viability of K562 cells. Cells were transfected with lariat or intein plasmids and viability was assessed by tryphan blue exclusion after 24 hours. Intein plasmid has a CGPC peptide noose flanked by intein domains. Transfection efficiency was determined to be ~75% for all the plasmids by flow cytometry (not shown). **(c)** Effect of lariats and imatinib on the phosphorylation status of Hck in K562 cells. Cells treated with 1 μM imatinib or transfected with lariat or intein plasmids were lysed after 24 hours of treatment/transfection. Lysates were subjected to immunoblotting for detection of Hck phosphorylated at Tyr411 and total Hck.

vivo, suggests that they can be used as chemical genetic tools to study biochemical pathways, regulatory networks and cellular processes. More specifically, the anti-Abl lariats should prove valuable in the dissection of Bcr-Abl pathways, and to further investigate leukemogenesis. One major advantage in employing lariats for *in vivo* studies is that they can be delivered into cells using different approaches. In this study, we have used a retroviral vector to express lariats within cells. This method is valuable to control the expression of peptides in transfected cells, and to deliver peptides into target cells through viral infection. It is also possible to deliver lariats into cells with the help of protein transduction domains (Buerger and Groner, 2003) and cell-penetrating peptides (Saar *et al*., 2005).

5.3.4 Resistant mutation profile of the higher affinity lariats

In order to compare the affinity of the lariats TG17 and TG18 for drug resistant Abl kinase mutants, we performed site directed mutagenesis to create a series of mutant Abl SH1 baits and assayed them against the lariats using the Y2H based β-galactosidase assay. The lariats TG17 and TG18 interacted with all the Abl SH1 mutant baits, but with a lower affinity

compared to that of WT bait. The only exception to this is the H396P Abl SH1 bait for which the lariats displayed a ~2.5 fold higher affinity than for WT Abl SH1 (Figure 5.8).

We extrapolated the finding that the lariats bind to the catalytic cleft to reason out why the lariats had a change in affinity for drug resistant mutants. Thr315 is positioned on the surface of the ATP site, and an Ile mutation in that position can confer drug resistance via three different ways. The mutation: (i) leads to the loss of a hydrogen bond between Thr315 and the inhibitor; (ii) blocks the entry of the inhibitor into the back cleft and (iii) promotes conformational dynamics in the kinase domain (Azam *et al*., 2008). Mutation Y253F causes drug resistance by altering the distorted conformation of the phosphate-binding loop of the kinase. In addition, this mutation leads to the loss of direct binding between the drug and the side chain of tyrosine (Krishnamurthy and Maly, 2010). The decrease in affinity of the lariats for the T315I and Y253F mutants could be due to a change in the original conformation of the kinase and/or loss of bonded/steric interactions between the lariats and the target.

Mutation E355G is present in the catalytic loop of the kinase and confers drug resistance by indirectly altering the hydrophobic core of the catalytic cleft (Cowan-Jacob *et al*., 2004). The decrease in affinity of the lariats for the E355G mutant could be due to a change in the original shape/flexibility of the catalytic cleft required for lariat binding.

Mutations H396P and H396R are located in the activation loop of the kinase and cause resistance to drugs like imatinib and nilotinib by altering the Abl/c-Kit–like inactive conformation of the kinase, which is required for imatinib/nilotinib binding (Cowan-Jacob *et al*., 2004). The H396R mutation could favor the formation of the inactive Src/Cdk–like conformation (Bharathikumar and Geyer, unpublished work). As the affinity of the lariats is decreased for H396R Abl SH1 relative to WT Abl SH1, it appears that the lariats do not prefer the inactive Src/Cdk–like conformation of the kinase for binding.

Structural studies have shown that the H396P mutation causes Abl to adopt the active conformation from the original Abl/c-Kit like conformation (Young *et al*., 2006). The lariats interacted stronger with H396P Abl SH1 than WT Abl SH1, indicating that the lariats prefer the active conformation of the kinase for binding. This conformational preference could be a consequence of the lariats having been isolated using a yeast-based screen in which the kinases are highly active. In fact, Western analysis using a phosphospecific antibody that recognizes Abl phosphorylated at Tyr412 revealed that the activation loop of the LexA DBD-Abl SH1

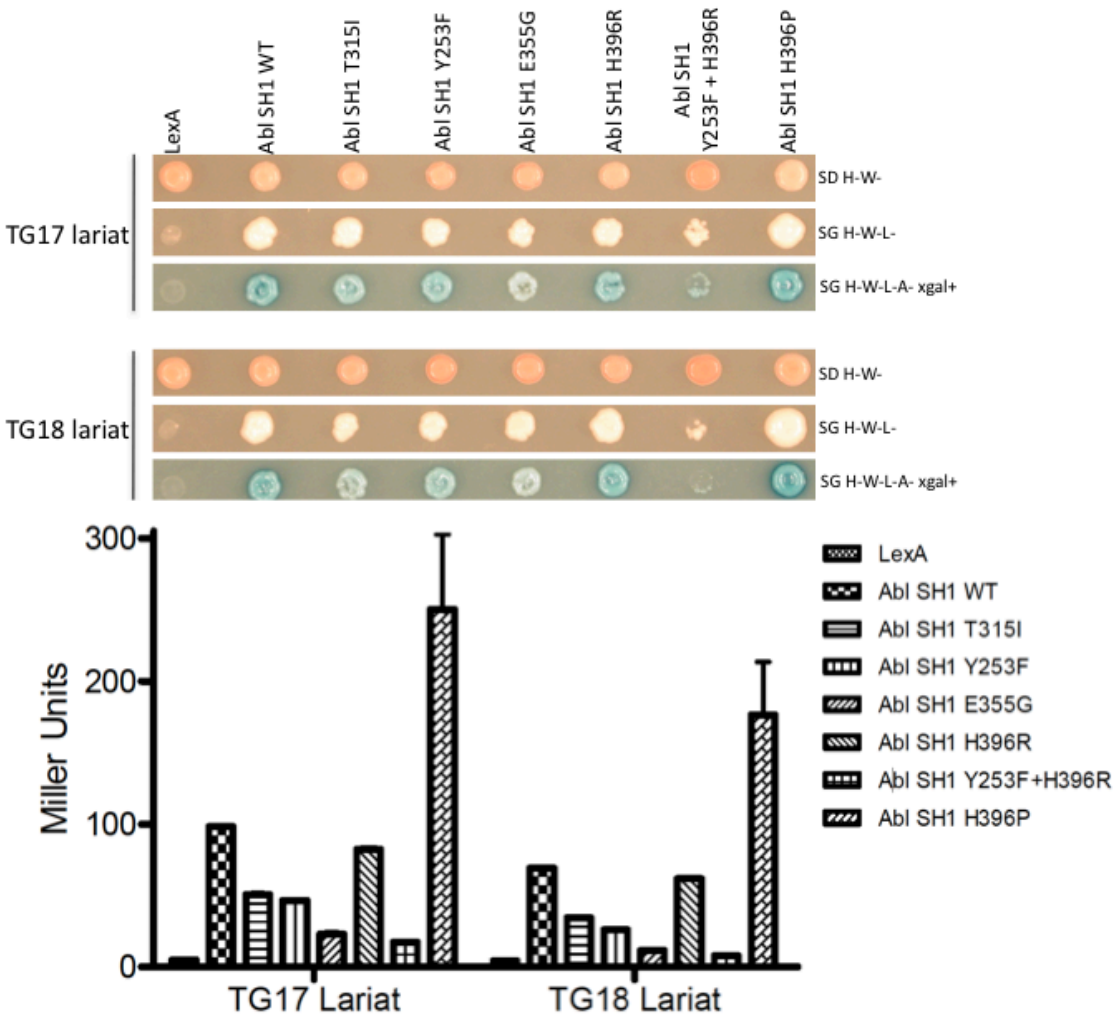

Figure 5.8. Resistant mutation profile of TG17 and TG18 lariats: (a) Y2H analysis of the interactions between Abl SH1 mutants and the lariats with two different selective media: (i) a less stringent synthetic galactose His^- Trp^- Leu^- media (SG H-W-L-), which selects for the activation of *LEU2* reporter gene, and (ii) a more stringent synthetic galactose His^- Trp^- Leu^- Ade^- $Xgal^+$ media (SG H-W-L-A-Xgal+), which selects for the activation of *LEU2*, *ADE2*, and *LacZ* reporter genes. SD H-W- represents yeast grown on nonselective synthetic dextrose His- Trp- media. **(b)** Interactions between Abl SH1 mutants and the lariats were quantified using Y2H based β-galactosidase assay and expressed as Miller units. All interactions were examined three times starting with randomly selected independent clones. The bars represent mean ± SD for all experiments. LexA bait was included as a negative control.

construct is predominantly phosphorylated in yeast (data not shown). Targeting the active conformation has at least two advantages: (i) the diseased state of the kinase is present in the active form; and (ii) the active conformation-specific inhibitors are only susceptible to mutations that directly impair drug binding. In contrast, inactive conformation-specific inhibitors are additionally susceptible to mutations that destabilize the specific inactive form and promote kinase activation (Johnson, 2009). Also, it is beneficial to further characterize active conformation-specific inhibitors because druggable allosteric sites of Abl kinase in its active form have not yet been analyzed, and such analysis could gain more insights into the design of highly selective drugs.

5.3.5 Selectivity profile of the TG17 lariat

In order to evaluate the kinase selectivity of higher affinity lariats, we assayed a panel of 200 kinases in the presence and absence of the synthetic TG17 lariat using an ATP site-dependent *in vitro* competition-binding assay (Kinex^{TM} Protein Kinase Microarray-200). Using this approach, the lariat was incubated with a biotinylated ATP probe on the protein kinase microarray. If the lariat binds to the kinase and directly or indirectly occludes the ATP binding pocket, then fewer probes can covalently bind to the ATP site. If the lariat does not bind to the kinase, there is no reduction in the binding of probes to the ATP site. The results were read out by quantifying the amount of ATP probe bound to the kinases using fluorescently labeled streptavidin conjugates.

The analysis revealed that the TG17 lariat possessed a selective profile, interacting with only 19 kinases among the Kinex^{TM} 200 diverse kinases panel at a concentration of 10 μM (Table 5.1). Kinases that had a relative binding score of less than 50% of the DMSO control were predicted as non-binders. The lariat had a slightly higher affinity for few off-targets in the panel than for the intended target. Few off-targets like Jak2 (Xie *et al*., 2001), Mek1/2 (Steelman *et al*., 2004) and Insulin-like growth factor 1 receptor (Lakshmikuttyamma *et al*., 2008), were indeed directly or indirectly activated by Bcr-Abl during the progression of the disease. Most notably, the lariat did not recognize any of the Src family kinases, which share a high structural similarity with Abl kinase in their active conformation (Young *et al*., 2006). In contrast, dasatinib binds to Abl kinase as well as to Src family kinases (Shah *et al*., 2004). A comprehensive analysis of selectivity using a competition-binding assay (Ambit Biosciences)

revealed that dasatinib interacted with 88 out of 317 kinases at 3 μM concentration (Karaman *et al*., 2008). The discrimination of Src family kinases by the TG17 lariat strongly suggests that the inhibitor might occupy less-conserved binding pockets in the kinase catalytic cleft.

Table 5.1: Kinome interaction profile of TG17 lariat at 10 μM concentration

Protein kinase	**Group**	**Family**	**Fold change in affinity relative to ABL1**
Mylk2	CAMK	Mylk	1.77
Plk1	Other	Plk	1.64
CK2a1	Other	CK2	1.41
Cdk7	CMGC	Cdk	1.34
Aurora C	Other	Aurora	1.21
Cdk5/P25	CMGC	Cdk	1.16
IGF1R	TK	InsR	1.14
VEGFR1	TK	VEGFR	1.11
Taok1	STE	STE20	1.06
CAMK2b	CAMK	CAMK3	1.04
Txk	TK	TEC	1.03
Mek1	STE	STE7	1.03
Abl1	**TK**	**Abl**	**1.00**
Mst4	STE	STE20	0.99
Rsk1	AGC	Rsk	0.93
Cdk6/CyclinD3	CMGC	Cdk	0.92
Cdk6/CyclinD1	CMGC	Cdk	0.91
Jak2	TK	Jak	0.90
Mek2	STE	STE7	0.87

6. Conclusions and Future Directions

The first step in the identification and characterization of new binding pockets in a therapeutically validated target is to screen for a new class of inhibitors that could potentially recognize novel druggable surfaces on the target. In an attempt to identify new allosteric drug binding pockets in the kinase catalytic cleft, we isolated lariat peptide inhibitors against Abl kinase, a drug target important in chronic myeloid leukemia and other disorders. Using *in vitro* kinetic and binding assays, we showed that a synthetic lariat, named A1, binds to the catalytic cleft that lies between the N- and C- lobes of the kinase catalytic domain, but not to the substrate peptide or the myristate binding region. To obtain tighter-binding variants of the A1 lariat, we developed an affinity maturation protocol consisting of two steps. In the first step, we defined acceptable and tolerable substitutions at each position of the A1 lariat using site-saturation mutagenesis (SSM). In the second step, we designed specific mutations to the A1 lariat based on the SSM results and evolved higher affinity variants. Synthetic and recombinant higher affinity lariats exhibited a strong inhibition of Abl kinase activity *in vitro* and Bcr-Abl kinase activity *in vivo*, respectively.

Finally, we evaluated the resistant mutation and selectivity profiles of the higher affinity lariats. While evaluating the resistant mutation profiles, we identified that the lariats bind specifically to the active state of kinase and possess the ability to differentiate closely related conformations of the kinase. By profiling a higher affinity lariat, named TG17, against a panel of 200 kinases, we identified that the lariat has a selective profile interacting with only 19 kinases. Selectivity analysis also indicated that the lariats do not recognize Src family kinases, which share a high structural similarity with Abl kinase in their active conformation. The discrimination of Hck, a Src family kinase, by anti Abl lariats was also confirmed by the lariat Y2H assay. Further, we were able to obtain lariats against Hck by designing mutations to the anti Abl lariats (Appendix 1). Once the structure of Abl kinase in complex with a lariat is solved, the information that we obtained from various mutagenesis screens could be useful to improve or to change the kinase selectivity profiles of small molecules.

Preliminary modeling studies showed that the TG17 lariat do not bind to the adenine-binding pocket (A-pocket) of Abl kinase. The lariat recognizes novel surfaces that lie adjacent to the A-pocket, while the catalytic cleft is in the active conformation. The lariat binds to the target through an unique entrance at the αC side (Appendices 2 and 3).

From the methodology perspective, we have demonstrated a number of things in this project. First, we show that a genetically selected lariat can remain functionally active *in vitro* and can inhibit the enzymatic activity of its target with a defined biochemical mechanism. Second, we confirm the processing of intein constructs and formation of the lariat in mammalian cells, and provide evidence that the lariats can function as intracellular inhibitors of endogenous signaling pathways and protein-protein interactions. Third, we demonstrate the potential of the lariat peptide approach in generating conformer specific affinity reagents. Taken together, we clearly illustrate that the lariats are powerful chemical genetic tools for performing reverse analysis of protein function.

Currently, we are performing biophysical experiments to confirm that the lariats do recognize allosteric sites in the kinase catalytic cleft. Once the allosteric recognition is confirmed, we would identify small molecules that disrupt Abl kinase-lariat interactions using peptide displacement screens. We are also involved in obtaining a NMR structure of the lariat, and a crystal structure of Abl kinase in complex with the lariat. These structures would provide information for the rational design of small molecules with improved properties, and for grafting the novel pharmacophores of the lariat onto existing small molecules using peptidomimetics. In addition to biophysical and structural studies, experiments to illustrate the power of lariat peptide technology in studying animal models of human disease are currently underway in our laboratory.

7. References

Adrian, F.J., Ding, Q., Sim, T., Velentza, A., Sloan, C., Liu, Y., Zhang, G., Hur, W., Ding, S., Manley, P.*, et al.* (2006). Allosteric inhibitors of Bcr-Abl dependent cell proliferation. Nat. Chem. Biol. *2*, 95-102.

Abedi, M.R., Caponigro, G., and Kamb, A. (1998). Green fluorescent protein as a scaffold for intracellular presentation of peptides. Nucleic Acids Res. *26*, 623-630.

Advani, A.S., and Pendergast, A.M. (2002). Bcr-Abl variants: biological and clinical aspects. Leuk. Res. *26*, 713-720.

Ausubel, F.M., Brent, R., and Kingston, R.E. (1988). Current Protocols in Molecular Biology (New York: John Wiley & Sons).

Ausubel, F.M., Brent, R., Kingston R.E., Moore, D.D., Seidman, J.G., Smith, J.A., and Struhl, K. (1997). Current Protocols in Molecular Biology (New York: John Wiley & Sons).

Azam, M., Seeliger, M.A., Gray, N.S., Kuriyan, J., and Daley, G.Q. (2008). Activation of tyrosine kinases by mutation of the gatekeeper threonine. Nat. Struct. Mol. Biol. *15*, 1109-1118.

Bardou, C., Borie, C., Bickle, M., Rudkin, B.B., and Colas, P. (2009). Peptide aptamers for small molecule drug discovery. Methods Mol. Biol. *535*, 373-388.

Barker, S.C., Kassel, D.B., Weigl, D., Huang, X., Luther, M.A., and Knight, W.B. (1995). Characterization of pp60c-Src tyrosine kinase activities using a continuous assay: autoactivation of the enzyme is an intermolecular autophosphorylation process. Biochemistry *34*, 14843-14851.

Barreto, K. (2010). A genetic screen to isolate “lariat” peptide inhibitors of protein function. Doctoral dissertation, University of Saskatchewan, Saskatoon.

Barreto, K., Bharathikumar, V.M., Ricardo, A., DeCoteau, J.F., Luo, Y., and Geyer, C.R. (2009). A genetic screen for isolating "lariat" peptide inhibitors of protein function. Chem. Biol. *16*, 1148-1157.

Baumeister, W., and Lupas, A. (1997). The proteasome. Curr. Opin. Struct. Biol. *7*, 273-278.

Bishop, A.C. (2004). A hot spot for protein kinase inhibitor sensitivity. Chem. Biol. *11*, 587-589.

Blume-Jensen, P., and Hunter, T. (2001). Oncogenic kinase signalling. Nature *411*, 355-365.

Boerner, R.J., Barker, S.C., and Knight, W.B. (1995). Kinetic mechanisms of the forward and reverse pp60c-Src tyrosine kinase reactions. Biochemistry *34*, 16419-16423.

Bogoyevitch, M.A., Barr, R.K., and Ketterman, A.J. (2005). Peptide inhibitors of protein kinases-discovery, characterisation and use. Biochim. Biophys. Acta *1754*, 79-99.

Borghouts, C., and Weiss, A. (2009). Production and purification of monomeric recombinant peptide aptamers: requirements for efficient intracellular uptake and target inhibition. In Peptides as drugs, B. Groner, ed. (Weinheim, Germany: Wiley-VCH), pp.145-186.

Brenke, R., Kozakov, D., Chuang, G.Y., Beglov, D., Hall, D., Landon, M.R., Mattos, C., and Vajda, S. (2009). Fragment-based identification of druggable 'hot spots' of proteins using Fourier domain correlation techniques. Bioinformatics *25*, 621-627.

Brien, G., Debaud, A.L., Bickle, M., Trescol-Biemont, M.C., Moncorge, O., Colas, P., and Bonnefoy-Berard, N. (2011). Characterization of peptide aptamers targeting Bfl-1 anti-apoptotic protein. Biochemistry *50*, 5120-5129.

Brown, C.J., Dastidar, S.G., See, H.Y., Coomber, D.W., Ortiz-Lombardia, M., Verma, C., and Lane, D.P. (2010). Rational design and biophysical characterization of thioredoxin-based aptamers: insights into peptide grafting. J. Mol. Biol. *395*, 871-883.

Brown, N.R., Noble, M.E., Endicott, J.A., and Johnson, L.N. (1999). The structural basis for specificity of substrate and recruitment peptides for cyclin-dependent kinases. Nat. Cell. Biol. *1*, 438-443.

Buerger, C., and Groner, B. (2003). Bifunctional recombinant proteins in cancer therapy: cell penetrating peptide aptamers as inhibitors of growth factor signaling. J. Cancer Res. Clin. Oncol. *129*, 669-675.

Buerger, C., Nagel-Wolfrum, K., Kunz, C., Wittig, I., Butz, K., Hoppe-Seyler, F., and Groner, B. (2003). Sequence-specific peptide aptamers, interacting with the intracellular domain of the epidermal growth factor receptor, interfere with Stat3 activation and inhibit the growth of tumor cells. J. Biol. Chem. *278*, 37610-37621.

Cattaneo, A., and Biocca, S. (1999). The selection of intracellular antibodies. Trends Biotechnol. *17*, 115-121.

Chattopadhyay, A., Tate, S.A., Beswick, R.W., Wagner, S.D., and Ko Ferrigno, P. (2006). A peptide aptamer to antagonize BCL-6 function. Oncogene *25*, 2223-2233.

Cherry, M., and Williams, D.H. (2004). Recent kinase and kinase inhibitor X-ray structures: mechanisms of inhibition and selectivity insights. Curr. Med. Chem. *11*, 663-673.

Cho, H.S., Mason, K., Ramyar, K.X., Stanley, A.M., Gabelli, S.B., Denney, D.W., Jr., and Leahy, D.J. (2003). Structure of the extracellular region of HER2 alone and in complex with the Herceptin Fab. Nature *421*, 756-760.

Christofk, H.R., Vander Heiden, M.G., Harris, M.H., Ramanathan, A., Gerszten, R.E., Wei, R., Fleming, M.D., Schreiber, S.L., and Cantley, L.C. (2008). The M2 splice isoform of pyruvate kinase is important for cancer metabolism and tumour growth. Nature *452*, 230-233.

Cohen, B.A., Colas, P., and Brent, R. (1998). An artificial cell-cycle inhibitor isolated from a combinatorial library. Proc. Natl. Acad. Sci. U. S. A. *95*, 14272-14277.

Cohen, M.S., Zhang, C., Shokat, K.M., and Taunton, J. (2005). Structural bioinformatics-based

design of selective, irreversible kinase inhibitors. Science *308*, 1318-1321.

Cohen, P. (2002). Protein kinases-the major drug targets of the twenty-first century? Nat. Rev. Drug Discov. *1*, 309-315.

Colas, P., Cohen, B., Jessen, T., Grishina, I., McCoy, J., and Brent, R. (1996). Genetic selection of peptide aptamers that recognize and inhibit cyclin-dependent kinase 2. Nature *380*, 548-550.

Colas, P., Cohen, B., Ko Ferrigno, P., Silver, P.A., and Brent, R. (2000). Targeted modification and transportation of cellular proteins. Proc. Natl. Acad. Sci. U. S. A. *97*, 13720-13725.

Coleman, R.G., Salzberg, A.C., and Cheng, A.C. (2006). Structure based identification of small molecule binding sites using a free energy model. J. Chem. Inf. Model. *46*, 2631-2637.

Cortese, R., Monaci, P., Luzzago, A., Santini, C., Bartoli, F., Cortese, I., Fortugno, P., Galfre, G., Nicosia, A., and Felici, F. (1996). Selection of biologically active peptides by phage display of random peptide libraries. Curr. Opin. Biotechnol. *7*, 616-621.

Cowan-Jacob, S.W., Guez, V., Fendrich, G., Griffin, J.D., Fabbro, D., Furet, P., Liebetanz, J., Mestan, J., and Manley, P.W. (2004). Imatinib (STI571) resistance in chronic myelogenous leukemia: molecular basis of the underlying mechanisms and potential strategies for treatment. Mini Rev. Med. Chem. *4*, 285-299.

Daley, G.Q., Van Etten, R.A., and Baltimore, D. (1990). Induction of chronic myelogenous leukemia in mice by the P210 Bcr/Abl gene of the Philadelphia chromosome. Science *247*, 824-830.

Davidson, A.R., and Sauer, R.T. (1994). Folded proteins occur frequently in libraries of random amino acid sequences. Proc. Natl. Acad. Sci. U. S. A. *91*, 2146-2150.

Davis, R.J. (1993). The mitogen-activated protein kinase signal transduction pathway. J. Biol. Chem. *268*, 14553-14556.

Dong, Q., Dougan, D.R., Gong, X., Halkowycz, P., Jin, B., Kanouni, T., O'Connell, S.M., Scorah, N., Shi, L., Wallace, M.B.*, et al.* (2011). Discovery of TAK-733, a potent and selective MEK allosteric site inhibitor for the treatment of cancer. Bioorg. Med. Chem. Lett. *21*, 1315-1319.

Dong, X., Stothard, P., Forsythe, I.J., and Wishart, D.S. (2004). PlasMapper: a web server for drawing and auto-annotating plasmid maps. Nucleic Acids Res. *32*, W660-664.

Elbing, K., and Brent, R. (2002). Current Protocols in Molecular Biology (New York: John Wiley & Sons).

Eldar-Finkelman, H., and Eisenstein, M. (2009). Peptide inhibitors targeting protein kinases. Curr. Pharm. Des. *15*, 2463-2470.

Fabbro, D., Ruetz, S., Buchdunger, E., Cowan-Jacob, S.W., Fendrich, G., Liebetanz, J., Mestan, J., O'Reilly, T., Traxler, P., Chaudhuri, B.*, et al.* (2002). Protein kinases as targets for anticancer agents: from inhibitors to useful drugs. Pharmacol. Ther. *93*, 79-98.

Faivre, S., Kroemer, G., and Raymond, E. (2006). Current development of mTOR inhibitors as anticancer agents. Nat. Rev. Drug Discov. *5*, 671-688.

Fischmann, T.O., Smith, C.K., Mayhood, T.W., Myers, J.E., Reichert, P., Mannarino, A., Carr, D., Zhu, H., Wong, J., Yang, R.S.*, et al.* (2009). Crystal structures of MEK1 binary and ternary complexes with nucleotides and inhibitors. Biochemistry *48*, 2661-2674.

Force, T., and Kolaja, K.L. (2011). Cardiotoxicity of kinase inhibitors: the prediction and translation of preclinical models to clinical outcomes. Nat. Rev. Drug Discov. *10*, 111-126.

Fuh, G., Wu, P., Liang, W.C., Ultsch, M., Lee, C.V., Moffat, B., and Wiesmann, C. (2006). Structure-function studies of two synthetic anti-vascular endothelial growth factor Fabs and comparison with the Avastin Fab. J. Biol. Chem. *281*, 6625-6631.

Futreal, P.A., Coin, L., Marshall, M., Down, T., Hubbard, T., Wooster, R., Rahman, N., and Stratton, M.R. (2004). A census of human cancer genes. Nat. Rev. Cancer *4*, 177-183.

Geiger, T.R., and Peeper, D.S. (2007). Critical role for TrkB kinase function in anoikis suppression, tumorigenesis, and metastasis. Cancer Res. *67*, 6221-6229.

Geyer, C.R., and Brent, R. (2000). Selection of genetic agents from random peptide aptamer expression libraries. Methods Enzymol. *328*, 171-208.

Gietz, R.D., and Schiestl, R.H. (2007). Frozen competent yeast cells that can be transformed with high efficiency using the LiAc/SS carrier DNA/PEG method. Nat. Protoc. *2*, 1-4.

Greenman, C., Stephens, P., Smith, R., Dalgliesh, G.L., Hunter, C., Bignell, G., Davies, H., Teague, J., Butler, A., Stevens, C.*, et al.* (2007). Patterns of somatic mutation in human cancer genomes. Nature *446*, 153-158.

Grimminger, F., Schermuly, R.T., and Ghofrani, H.A. (2010). Targeting non-malignant disorders with tyrosine kinase inhibitors. Nat. Rev. Drug Discov. *9*, 956-970.

Groll, M., Ditzel, L., Lowe, J., Stock, D., Bochtler, M., Bartunik, H.D., and Huber, R. (1997). Structure of 20S proteasome from yeast at 2.4 A resolution. Nature *386*, 463-471.

Guida, E., Bisso, A., Fenollar-Ferrer, C., Napoli, M., Anselmi, C., Girardini, J.E., Carloni, P., and Del Sal, G. (2008). Peptide aptamers targeting mutant p53 induce apoptosis in tumor cells. Cancer Res. *68*, 6550-6558.

Gumireddy, K., Baker, S.J., Cosenza, S.C., John, P., Kang, A.D., Robell, K.A., Reddy, M.V., and Reddy, E.P. (2005). A non-ATP-competitive inhibitor of BCR-ABL overrides imatinib resistance. Proc. Natl. Acad. Sci. U. S. A. *102*, 1992-1997.

Hanks, S.K., and Hunter, T. (1995). Protein kinases 6. The eukaryotic protein kinase superfamily: kinase (catalytic) domain structure and classification. Faseb J. *9*, 576-596.

Hantschel, O., and Superti-Furga, G. (2004). Regulation of the c-Abl and Bcr-Abl tyrosine kinases. Nat. Rev. Mol. Cell. Biol. *5*, 33-44.

Hantschel, O., Nagar, B., Guettler, S., Kretzschmar, J., Dorey, K., Kuriyan, J., and Superti-Furga, G. (2003). A myristoyl/phosphotyrosine switch regulates c-Abl. Cell *112*, 845-857.

Hardy, J.A., and Wells, J.A. (2004). Searching for new allosteric sites in enzymes. Curr. Opin. Struct. Biol. *14*, 706-715.

Hoffman, C.S., and Winston, F. (1987). A ten-minute DNA preparation from yeast efficiently releases autonomous plasmids for transformation of *Escherichia coli*. Gene *57*, 267-272.

Hoppe-Seyler, F., Crnkovic-Mertens, I., Denk, C., Fitscher, B.A., Klevenz, B., Tomai, E., and Butz, K. (2001). Peptide aptamers: new tools to study protein interactions. J. Steroid Biochem. Mol. Biol. *78*, 105-111.

Horswill, A.R., and Benkovic, S.J. (2005). Cyclic peptides, a chemical genetics tool for biologists. Cell Cycle *4*, 552-555.

Hu, Y., Fang, X., Dunham, S.M., Prada, C., Stachowiak, E.K., and Stachowiak, M.K. (2004). 90-kDa ribosomal S6 kinase is a direct target for the nuclear fibroblast growth factor receptor 1 (FGFR1): role in FGFR1 signaling. J. Biol. Chem. *279*, 29325-29335.

Hua, S.B., Qiu, M., Chan, E., Zhu, L., and Luo, Y. (1997). Minimum length of sequence homology required for *in vivo* cloning by homologous recombination in yeast. Plasmid *38*, 91-96.

Hubbard, S.R., and Till, J.H. (2000). Protein tyrosine kinase structure and function. Annu. Rev. Biochem. *69*, 373-398.

Huse, M., and Kuriyan, J. (2002). The conformational plasticity of protein kinases. Cell *109*, 275-282.

Isshiki, Y., Kohchi, Y., Iikura, H., Matsubara, Y., Asoh, K., Murata, T., Kohchi, M., Mizuguchi, E., Tsujii, S., Hattori, K.*, et al.* (2011). Design and synthesis of novel allosteric MEK inhibitor CH4987655 as an orally available anticancer agent. Bioorg. Med. Chem. Lett. *21*, 1795-1801.

Ivetac, A., and McCammon, J.A. (2010). Mapping the druggable allosteric space of G-protein coupled receptors: a fragment-based molecular dynamics approach. Chem. Biol. Drug Des. *76*, 201-217.

Jatiani, S.S., Cosenza, S.C., Reddy, M.V., Ha, J.H., Baker, S.J., Samanta, A.K., Olnes, M.J., Pfannes, L., Sloand, E.M., Arlinghaus, R.B.*, et al.* (2010). A non-ATP competitive dual inhibitor of JAK2 and BCR-ABL Kinases: elucidation of a novel therapeutic spectrum based on substrate competitive inhibition. Genes Cancer *1*, 331-345.

Johnson, L.N. (2009). Protein kinase inhibitors: contributions from structure to clinical compounds. Q. Rev. Biophys. *42*, 1-40.

Johnson, L.N., and Lewis, R.J. (2001). Structural basis for control by phosphorylation. Chem. Rev. *101*, 2209-2242.

Kaidanovich-Beilin, O., and Eldar-Finkelman, H. (2006). Peptides targeting protein kinases: strategies and implications. Physiology (Bethesda) *21*, 411-418.

Karaman, M.W., Herrgard, S., Treiber, D.K., Gallant, P., Atteridge, C.E., Campbell, B.T., Chan, K.W., Ciceri, P., Davis, M.I., Edeen, P.T.*, et al.* (2008). A quantitative analysis of kinase inhibitor selectivity. Nat. Biotechnol. *26*, 127-132.

Kerbel, R.S. (2008). Tumor angiogenesis. N. Engl. J. Med. *358*, 2039-2049.

Klejman, A., Schreiner, S.J., Nieborowska-Skorska, M., Slupianek, A., Wilson, M., Smithgall, T.E., and Skorski, T. (2002). The Src family kinase Hck couples BCR/ABL to STAT5 activation in myeloid leukemia cells. Embo J. *21*, 5766-5774.

Klevenz, B., Butz, K., and Hoppe-Seyler, F. (2002). Peptide aptamers: exchange of the thioredoxin-A scaffold by alternative platform proteins and its influence on target protein binding. Cell Mol. Life Sci. *59*, 1993-1998.

Koivunen, E., Wang, B., and Ruoslahti, E. (1994). Isolation of a highly specific ligand for the alpha 5 beta 1 integrin from a phage display library. J. Cell. Biol. *124*, 373-380.

Kolonin, M.G., and Finley, R.L., Jr. (1998). Targeting cyclin-dependent kinases in Drosophila with peptide aptamers. Proc. Natl. Acad. Sci. U. S. A. *95*, 14266-14271.

Kontopidis, G., McInnes, C., Pandalaneni, S.R., McNae, I., Gibson, D., Mezna, M., Thomas, M., Wood, G., Wang, S., Walkinshaw, M.D.*, et al.* (2006). Differential binding of inhibitors to active and inactive CDK2 provides insights for drug design. Chem. Biol. *13*, 201-211.

Krishnamurty, R., and Maly, D.J. (2010). Biochemical mechanisms of resistance to small-molecule protein kinase inhibitors. ACS Chem. Biol. *5*, 121-138.

Kritzer, J.A., Hamamichi, S., McCaffery, J.M., Santagata, S., Naumann, T.A., Caldwell, K.A., Caldwell, G.A., and Lindquist, S. (2009). Rapid selection of cyclic peptides that reduce alpha-synuclein toxicity in yeast and animal models. Nat. Chem. Biol. *5*, 655-663.

Kunz, C., Borghouts, C., Buerger, C., and Groner, B. (2006). Peptide aptamers with binding specificity for the intracellular domain of the ErbB2 receptor interfere with AKT signaling and sensitize breast cancer cells to Taxol. Mol. Cancer Res. *4*, 983-998.

Kwak, E.L., Sordella, R., Bell, D.W., Godin-Heymann, N., Okimoto, R.A., Brannigan, B.W., Harris, P.L., Driscoll, D.R., Fidias, P., Lynch, T.J.*, et al.* (2005). Irreversible inhibitors of the EGF receptor may circumvent acquired resistance to gefitinib. Proc. Natl. Acad. Sci. U. S. A. *102*, 7665-7670.

Laemmli, U.K. (1970). Cleavage of structural proteins during the assembly of the head of bacteriophage T4. Nature *227*, 680-685.

Lakshmikuttyamma, A., Pastural, E., Takahashi, N., Sawada, K., Sheridan, D.P., DeCoteau, J.F., and Geyer, C.R. (2008). Bcr-Abl induces autocrine IGF-1 signaling. Oncogene *27*, 3831-3844.

Landon, M.R., Lancia, D.R., Jr., Yu, J., Thiel, S.C., and Vajda, S. (2007). Identification of hot spots within druggable binding regions by computational solvent mapping of proteins. J. Med. Chem. *50*, 1231-1240.

Levinson, N.M., Kuchment, O., Shen, K., Young, M.A., Koldobskiy, M., Karplus, M., Cole, P.A., and Kuriyan, J. (2006). A Src-like inactive conformation in the Abl tyrosine kinase domain. PLoS Biol. *4*, e144.

Liao, J.J. (2007a). Molecular recognition of protein kinase binding pockets for design of potent and selective kinase inhibitors. J. Med. Chem. *50*, 409-424.

Liao, J.J. (2007b). Molecular targeting of protein kinases to optimize selectivity and resistance profiles of kinase inhibitors. Curr. Top. Med. Chem. *7*, 1332-1335.

Liao, J.J., and Andrews, R.C. (2007). Targeting protein multiple conformations: a structure based strategy for kinase drug design. Curr. Top. Med. Chem. *7*, 1394-1407.

Lindsley, C.W., Zhao, Z., Leister, W.H., Robinson, R.G., Barnett, S.F., Defeo-Jones, D., Jones, R.E., Hartman, G.D., Huff, J.R., Huber, H.E*., et al.* (2005). Allosteric Akt (PKB) inhibitors: discovery and SAR of isozyme selective inhibitors. Bioorg. Med. Chem. Lett. *15*, 761-764.

Liu, Y., and Gray, N.S. (2006). Rational design of inhibitors that bind to inactive kinase conformations. Nat. Chem. Biol. *2*, 358-364.

Liu, Y., Shah, K., Yang, F., Witucki, L., and Shokat, K.M. (1998). A molecular gate which controls unnatural ATP analogue recognition by the tyrosine kinase v-Src. Bioorg. Med. Chem. *6*, 1219-1226.

Lorsch, J.R., and Szostak, J.W. (1996). Chance and necessity in the selection of nucleic acid catalysts. Acc Chem. Res. *29*, 103-110.

Ma, H., Kunes, S., Schatz, P.J., and Botstein, D. (1987). Plasmid construction by homologous recombination in yeast. Gene *58*, 201-216.

Malumbres, M., and Barbacid, M. (2007). Cell cycle kinases in cancer. Curr. Opin. Genet. Dev. *17*, 60-65.

Manning, G., Whyte, D.B., Martinez, R., Hunter, T., and Sudarsanam, S. (2002). The protein kinase complement of the human genome. Science *298*, 1912-1934.

Martel, V., Filhol, O., Colas, P., and Cochet, C. (2006). p53-dependent inhibition of mammalian cell survival by a genetically selected peptide aptamer that targets the regulatory subunit of protein kinase CK2. Oncogene *25*, 7343-7353.

McConnell, S.J., Kendall, M.L., Reilly, T.M., and Hoess, R.H. (1994). Constrained peptide libraries as a tool for finding mimotopes. Gene *151*, 115-118.

McIntyre, K.W., Shuster, D.J., Gillooly, K.M., Dambach, D.M., Pattoli, M.A., Lu, P., Zhou, X.D., Qiu, Y., Zusi, F.C., and Burke, J.R. (2003). A highly selective inhibitor of I kappa B kinase, BMS-345541, blocks both joint inflammation and destruction in collagen-induced

arthritis in mice. Arthritis. Rheum. *48*, 2652-2659.

McLafferty, M.A., Kent, R.B., Ladner, R.C., and Markland, W. (1993). M13 bacteriophage displaying disulfide-constrained microproteins. Gene *128*, 29-36.

McWhirter, J.R., Galasso, D.L., and Wang, J.Y. (1993). A coiled-coil oligomerization domain of Bcr is essential for the transforming function of Bcr-Abl oncoproteins. Mol. Cell. Biol. *13*, 7587-7595.

Melnikova, I., and Golden, J. (2004). Targeting protein kinases. Nat. Rev. Drug Discov. *3*, 993-994.

Miller, R.A., Binkowski, B.F., and Belshaw, P.J. (2007). Ligand-regulated peptide aptamers that inhibit the 5'-AMP-activated protein kinase. J. Mol. Biol. *365*, 945-957.

Morphy, R. (2010). Selectively nonselective kinase inhibition: striking the right balance. J. Med. Chem. *53*, 1413-1437.

Muller, G. (2000). Peptidomimetics SH2 domain antagonists for targeting signal transduction. Topics Curr. Chem. *211*, 17-59.

Nagar, B., Hantschel, O., Young, M.A., Scheffzek, K., Veach, D., Bornmann, W., Clarkson, B., Superti-Furga, G., and Kuriyan, J. (2003). Structural basis for the autoinhibition of c-Abl tyrosine kinase. Cell *112*, 859-871.

Naumann, T.A., Savinov, S.N., and Benkovic, S.J. (2005). Engineering an affinity tag for genetically encoded cyclic peptides. Biotechnol. Bioeng. *92*, 820-830.

Noble, M.E., Endicott, J.A., and Johnson, L.N. (2004). Protein kinase inhibitors: insights into drug design from structure. Science *303*, 1800-1805.

Nolen, B., Taylor, S., and Ghosh, G. (2004). Regulation of protein kinases; controlling activity through activation segment conformation. Mol. Cell. *15*, 661-675.

Nouvion, A.L., Thibaut, J., Lohez, O.D., Venet, S., Colas, P., Gillet, G., and Lalle, P. (2007). Modulation of Nr-13 antideath activity by peptide aptamers. Oncogene *26*, 701-710.

O'Hare, T., Walters, D.K., Stoffregen, E.P., Jia, T., Manley, P.W., Mestan, J., Cowan-Jacob, S.W., Lee, F.Y., Heinrich, M.C., Deininger, M.W., *et al.* (2005). *In vitro* activity of Bcr-Abl inhibitors AMN107 and BMS-354825 against clinically relevant imatinib-resistant Abl kinase domain mutants. Cancer Res. *65*, 4500-4505.

Ohren, J.F., Chen, H., Pavlovsky, A., Whitehead, C., Zhang, E., Kuffa, P., Yan, C., McConnell, P., Spessard, C., Banotai, C., *et al.* (2004). Structures of human MAP kinase kinase 1 (MEK1) and MEK2 describe novel noncompetitive kinase inhibition. Nat. Struct. Mol. Biol. *11*, 1192-1197.

Okram, B., Nagle, A., Adrian, F.J., Lee, C., Ren, P., Wang, X., Sim, T., Xie, Y., Xia, G., Spraggon, G., *et al.* (2006). A general strategy for creating "inactive-conformation" Abl inhibitors. Chem. Biol. *13*, 779-786.

Parang, K., and Cole, P.A. (2002). Designing bisubstrate analog inhibitors for protein kinases. Pharmacol. Ther. *93*, 145-157.

Parang, K., and Sun, G. (2005). Protein kinase inhibitors in drug discovery. In Drug discovery handbook, S.C. Gad, ed. (Hoboken, NJ: John Wiley & Sons, Inc.), pp.1191–1258.

Parikh, M.R., and Matsumura, I. (2005). Site-saturation mutagenesis is more efficient than DNA shuffling for the directed evolution of beta-fucosidase from beta-galactosidase. J. Mol. Biol. *352*, 621-628.

Pendergast, A.M. (2002). The Abl family kinases: mechanisms of regulation and signaling. Adv. Cancer Res. *85*, 51-100.

Perez de Castro, I., de Carcer, G., and Malumbres, M. (2007). A census of mitotic cancer genes: new insights into tumor cell biology and cancer therapy. Carcinogenesis *28*, 899-912.

Reetz, M.T., Prasad, S., Carballeira, J.D., Gumulya, Y., and Bocola, M. (2010). Iterative saturation mutagenesis accelerates laboratory evolution of enzyme stereoselectivity: rigorous comparison with traditional methods. J. Am. Chem. Soc. *132*, 9144-9152.

Saar, K., Lindgren, M., Hansen, M., Eiriksdottir, E., Jiang, Y., Rosenthal-Aizman, K., Sassian, M., and Langel, U. (2005). Cell-penetrating peptides: a comparative membrane toxicity study. Anal. Biochem. *345*, 55-65.

Samanta, A., Perazzona, B., Chakraborty, S., Sun, X., Modi, H., Bhatia, R., Priebe, W., and Arlinghaus, R. (2011). Janus kinase 2 regulates Bcr-Abl signaling in chronic myeloid leukemia. Leukemia *25*, 463-472.

Schmidt, S., Diriong, S., Mery, J., Fabbrizio, E., and Debant, A. (2002). Identification of the first Rho-GEF inhibitor, TRIPalpha, which targets the RhoA-specific GEF domain of Trio. FEBS Lett. *523*, 35-42.

Scott, C.P., Abel-Santos, E., Jones, A.D., and Benkovic, S.J. (2001). Structural requirements for the biosynthesis of backbone cyclic peptide libraries. Chem. Biol. *8*, 801-815.

Scott, C.P., Abel-Santos, E., Wall, M., Wahnon, D.C., and Benkovic, S.J. (1999). Production of cyclic peptides and proteins *in vivo*. Proc. Natl. Acad. Sci. U. S. A. *96*, 13638-13643.

Seeliger, M.A., Young, M., Henderson, M.N., Pellicena, P., King, D.S., Falick, A.M., and Kuriyan, J. (2005). High yield bacterial expression of active c-Abl and c-Src tyrosine kinases. Protein Sci. *14*, 3135-3139.

Shah, N.P., Tran, C., Lee, F.Y., Chen, P., Norris, D., and Sawyers, C.L. (2004). Overriding imatinib resistance with a novel ABL kinase inhibitor. Science *305*, 399-401.

Smith, J.M., and Mayer, B.J. (2002). Abl: mechanisms of regulation and activation. Front. Biosci. *7*, d31-d42.

Sperandio, O., Miteva, M.A., Segers, K., Nicolaes, G.A., and Villoutreix, B.O. (2008). Screening outside the catalytic site: inhibition of macromolecular interactions through structure

based virtual ligand screening experiments. Open Biochem. J. *2*, 29-37.

Steelman, L.S., Pohnert, S.C., Shelton, J.G., Franklin, R.A., Bertrand, F.E., and McCubrey, J.A. (2004). JAK/STAT, Raf/MEK/ERK, PI3K/Akt and BCR-ABL in cell cycle progression and leukemogenesis. Leukemia *18*, 189-218.

Taylor, S.S., and Kornev, A.P. (2011). Protein kinases: evolution of dynamic regulatory proteins. Trends. Biochem. Sci. *36*, 65-77.

Tecle, H., Shao, J., Li, Y., Kothe, M., Kazmirski, S., Penzotti, J., Ding, Y.H., Ohren, J., Moshinsky, D., Coli, R.*, et al.* (2009). Beyond the MEK-pocket: can current MEK kinase inhibitors be utilized to synthesize novel type III NCKIs? Does the MEK-pocket exist in kinases other than MEK? Bioorg. Med. Chem. Lett. *19*, 226-229.

Vagner, J., Qu, H., and Hruby, V.J. (2008). Peptidomimetics, a synthetic tool of drug discovery. Curr. Opin. Chem. Biol. *12*, 292-296.

Vu, C.B. (2000). Recent advances in the design and synthesis of SH2 inhibitors of Src, Grb2 and ZAP-70. Curr. Med. Chem. *7*, 1081-1100.

Wang, J.Y. (2004). Controlling Abl: auto-inhibition and co-inhibition? Nat. Cell. Biol. *6*, 3-7.

Wang, J.Y., Wilcoxen, K.M., Nomoto, K., and Wu, S. (2007). Recent advances of MEK inhibitors and their clinical progress. Curr. Top. Med. Chem. *7*, 1364-1378.

Wei, G., Rafiyath, S., and Liu, D. (2010). First-line treatment for chronic myeloid leukemia: dasatinib, nilotinib, or imatinib. J. Hematol. Oncol. *3*, 47.

Weinstein, I.B., and Joe, A.K. (2006). Mechanisms of disease: Oncogene addiction-a rationale for molecular targeting in cancer therapy. Nat. Clin. Pract. Oncol. *3*, 448-457.

Wertman, K.F., Wyman, A.R., and Botstein, D. (1986). Host/vector interactions that affect the viability of recombinant phage lambda clones. Gene *49*, 253-262.

Wojcik, J., Hantschel, O., Grebien, F., Kaupe, I., Bennett, K.L., Barkinge, J., Jones, R.B., Koide, A., Superti-Furga, G., and Koide, S. (2010). A potent and highly specific FN3 monobody inhibitor of the Abl SH2 domain. Nat. Struct. Mol. Biol. *17*, 519-527.

Wong, T.S., Zhurina, D., and Schwaneberg, U. (2006). The diversity challenge in directed protein evolution. Comb. Chem. High Throughput. Screen. *9*, 271-288.

Woodman, R., Yeh, J.T., Laurenson, S., and Ko Ferrigno, P. (2005). Design and validation of a neutral protein scaffold for the presentation of peptide aptamers. J. Mol. Biol. *352*, 1118-1133.

Wu, S.Y., McNae, I., Kontopidis, G., McClue, S.J., McInnes, C., Stewart, K.J., Wang, S., Zheleva, D.I., Marriage, H., Lane, D.P.*, et al.* (2003). Discovery of a novel family of CDK inhibitors with the program LIDAEUS: structural basis for ligand induced disordering of the activation loop. Structure *11*, 399-410.

Xie, S., Wang, Y., Liu, J., Sun, T., Wilson, M.B., Smithgall, T.E., and Arlinghaus, R.B. (2001). Involvement of Jak2 tyrosine phosphorylation in Bcr-Abl transformation. Oncogene *20*, 6188-

6195.

Young, M.A., Shah, N.P., Chao, L.H., Seeliger, M., Milanov, Z.V., Biggs, W.H., 3rd, Treiber, D.K., Patel, H.K., Zarrinkar, P.P., Lockhart, D.J*., et al.* (2006). Structure of the kinase domain of an imatinib-resistant Abl mutant in complex with the Aurora kinase inhibitor VX-680. Cancer Res. *66*, 1007-1014.

Zhang, J., Adrian, F.J., Jahnke, W., Cowan-Jacob, S.W., Li, A.G., Iacob, R.E., Sim, T., Powers, J., Dierks, C., Sun, F*., et al.* (2010). Targeting Bcr-Abl by combining allosteric with ATP binding site inhibitors. Nature *463*, 501-506.

Zhang, J., Yang, P.L., and Gray, N.S. (2009). Targeting cancer with small molecule kinase inhibitors. Nat. Rev. Cancer *9*, 28-39.

Zhang, X., Subrahmanyam, R., Wong, R., Gross, A.W., and Ren, R. (2001). The NH_2 terminal coiled-coil domain and tyrosine 177 play important roles in induction of a myeloproliferative disease in mice by Bcr-Abl. Mol. Cell. Biol. *21*, 840-853.

8. Appendices

Appendix 1

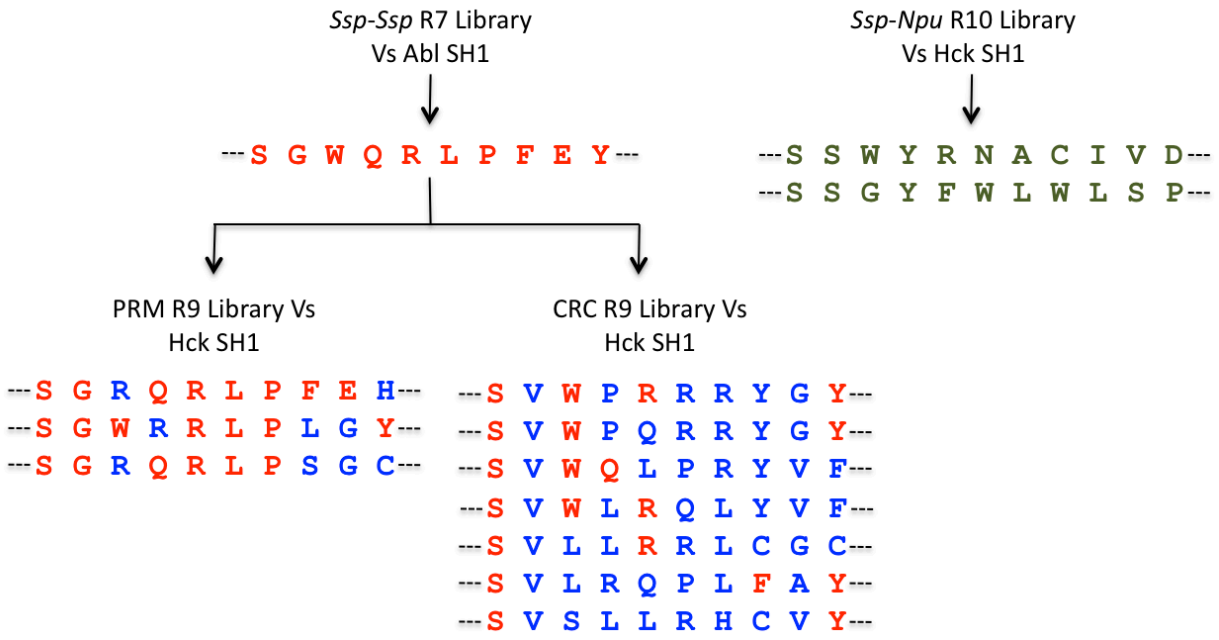

Lariat peptides against Hck SH1: The A1 lariat was isolated by screening a random 7-mer library (*Ssp-Ssp* R7) against Abl SH1. The noose region of the A1 lariat was subjected to PCR random mutagenesis and second position randomization to construct PRM R9 library and CRC R9 library, respectively. These second generation libraries were screened against Hck SH1 to obtain anti Hck lariats based on the A1 lariat. The WT residues of the A1 lariat are shown in red and the amino acid substitutions are shown in blue. A completely random 10-mer library (*Ssp-Npu* R10) was also screened against Hck SH1, which gave rise to two anti Hck lariats whose residues are shown in green.

Appendix 2

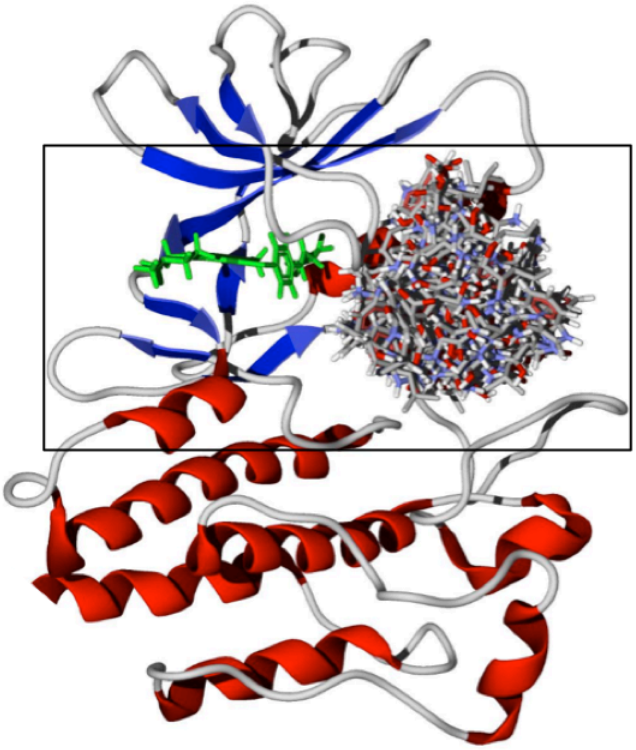

Binding mode of the TG17 lariat: The catalytic cleft of Abl kinase, which is indicated by a black rectangle in the figure, contains adenine, ribose, triphosphate and allosteric drug-binding pockets. The TG17 lariat predominantly occupies the allosteric region, while the catalytic cleft is in the active conformation. The kinase domain of Abl is shown in cartoon representation and the inhibitors are drawn as sticks. The N- and C- lobes of the kinase are colored blue and red, respectively. The top 15 "docked" conformations of the TG17 lariat obtained from modeling studies using three different programs are shown as tricolored sticks. VX-680 (colored green), a type I small molecule inhibitor, which occupies the adenine-binding pocket of Abl SH1 is also shown.

Appendix 3

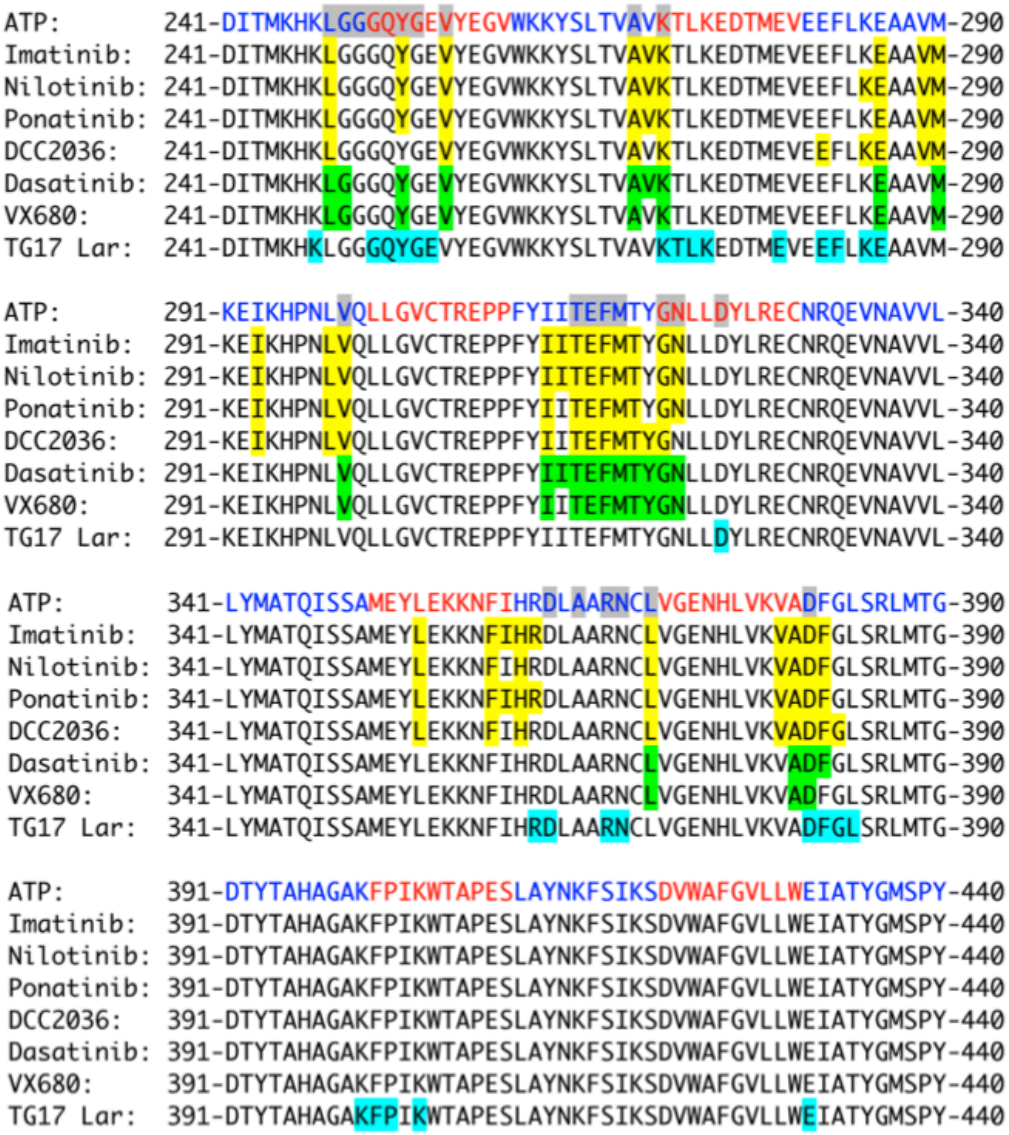

Abl SH1 residues that are involved in protein-ligand interactions: Eight different ligands that interact with the catalytic cleft of Abl SH1 are included in the figure. Imatinib, nilotinib, ponatinib and DCC2036 are type II small molecule inhibitors. Dasatinib and VX-680 are type I small molecule inhibitors. The residues that interact with ATP, type II inhibitors, type I inhibitors and the TG17 lariat are highlighted in grey, yellow, green, and cyan, respectively. The TG17 lariat binds predominantly to the allosteric region and has identified new residues for rational drug design, which have not been exploited by other type I or type II inhibitors. In the ATP binding pocket, the TG17 lariat makes contacts with residues that are involved in ribose and triphosphate binding but not with residues that are involved in adenine binding.